The role of lysosome alterations in bladder cancer progression

Camilla de Barros Santos

Université Pierre et Marie Curie

Ecole doctorale Complexité du Vivant - ED515
Department of Subcellular Structure and Cellular Dynamics - UMR144

Laboratory Molecular Mechanisms of Intracellular Transport

The role of lysosome alterations in bladder cancer progression

Camilla DE BARROS SANTOS

Doctoral Thesis in Cell Biology

Under the supervision of Dr. Bruno GOUD and Dr. Kristine SCHAUER
Presented and publicly defended on Thursday, September 28, 2017

Before the examining committee composed of:

Prof. Joëlle SOBCZAK-THEPOT	Université Pierre et Marie Curie	President
Dr. Cécile GAUTHIER-ROUVIERE	CRBM	Reviewer
Dr. Guillaume MONTAGNAC	Institut Gustave Roussy	Reviewer
Dr. Ana-Maria LENNON-DUMENIL	Institut Curie	Examiner
Dr. Yves ALLORY	Université Paris Est Créteil	Examiner
Dr. Bruno GOUD	Institut Curie	Thesis Director
Dr. Kristine SCHAUER	Institut Curie	Thesis Director

Abstract

Cancer is a multifactorial disease defined by a rapid development of abnormal cells. Malignant cells acquire competitive advantages for growth and proliferation through a big spectrum of genetic and epigenetic changes leading to major changes in the transcriptome and proteome profiles and thus to alterations in multiple signaling pathways, intracellular trafficking and metabolism. Although many cellular pathways have been studied in the context of cancer, including signaling, migration, loss of apical-basal cell-polarity and cell adhesion, little is known about cancer-related alterations on the sub-cellular, organelle level. This PhD thesis aimed to identify alterations in intracellular compartments and to study how these changes correlate with cancer progression. In classical culture, the systematic study on the organization and relative positioning of organelles is challenging because of the strong morphological cell-to-cell variations. To overcome this problem, we used innovative micro-patterning technique in combination with quantitative, probabilistic mapping of cell organelles. Using a systematic analysis of different cell lines representing different stages of bladder cancer, we identified several changes in the positioning of organelles. The most striking phenotype was revealed by lysosomes, whose distribution was more peripheral in cells representing higher grades of bladder cancer. This suggested that lysosome positioning could be potentially relevant in cancer progression. Therefore, we aimed to characterize the impact of lysosome alteration on cell behavior in transformed cells. We found that changes in lysosome positioning played a role on bladder cancer cell invasion. Indeed, anterograde transport of lysosomes correlate with 3D invasion behavior, contrary to retrograde transport that correlated with decreased cell invasion. Finally, we studied about the molecular mechanisms by which lysosome alterations impact cell invasion.

Keywords: Lysosome positioning, Bladder cancer, Invasion, Micropatterning, Density maps

Résumé

Le cancer est une maladie multifactorielle définie par un développement rapide de cellules anormales. Les cellules malignes acquièrent des avantages compétitifs qui permettent une croissance et prolifération anormales, grâce à un large spectre de changements génétiques et épigénétiques conduisant à des changements majeurs dans les profils de transcriptome et protéome et ainsi des modifications dans des voies de signalisation, le trafic intracellulaire et le métabolisme. Des nombreuses voies cellulaires ont été étudiées dans le contexte du cancer, y compris la signalisation, la migration, la perte de la polarité cellulaire apico-basale et l'adhésion cellulaire, cependant très peu est connu sur les altérations au niveau des organelles. Cette thèse a comme objectif d'identifier des altérations dans les compartiments intracellulaires et d'étudier leurs corrélations avec la progression du cancer. Dans la culture cellulaire classique, l'étude systématique de l'organisation du positionnement relatif des organelles est difficile en raison des fortes hétérogénéités morphologiques des cellules. Pour contourner ce problème, nous avons utilisé l'innovante technique des micro-patrons combinée à des cartes de densité des organelles. Après une analyse systématique de différentes lignées cellulaires représentant différents grades du cancer de la vessie, nous avons identifié des changements dans le positionnement de plusieurs organelles. Le changement de position le plus important a été observé pour les lysosomes, dont la distribution était plus périphérique dans les cellules représentant des grades plus avancées du cancer de la vessie. Ceci suggère que le positionnement des lysosomes pourrait être potentiellement important dans la progression du cancer. Par conséquent, nous avons cherché à caractériser l'impact de l'altération des lysosomes sur le comportement des cellules transformées. Nous avons constaté que les changements dans le positionnement des lysosomes jouent un rôle dans l'invasion des cellules cancéreuses de la vessie. En effet, le transport antérograde des lysosomes est en corrélation avec l'invasion 3D, contrairement au transport rétrograde qui corrèle avec une diminution de l'invasion cellulaire. Enfin, nous avons étudié les mécanismes moléculaires par lesquels les altérations du lysosome ont un impact sur l'invasion cellulaire.

Mots-clés: Positionnement des lysosomes, Cancer de la vessie, Invasion, Micro-patrons, Cartes de densité

Remerciements

J’aimerais tout d’abord remercier les membres de mon jury pour avoir accepté d’évaluer mon travail : Joëlle Sobczak-Thépot qui a accepté de présider ma soutenance de thèse, Cécile Gauthier-Rouvière et Guillaume Montagnac qui ont eu la lourde tâche d’être rapporteurs de ce travail et Ana-Maria Lennon-Duménil et Yves Allory qui ont accepté d’être examinateurs de ma thèse.

Ensuite, je remercie énormément Bruno Goud de m’avoir accueilli au sein de son équipe depuis plus de 4 ans et Kristine Schauer de m’avoir directement encadré durant tout ce projet. Au-delà des discussions scientifiques, je vous remercie aussi pour votre compréhension et soutien dans des moments difficiles pendant ces dernières années. Je remercie aussi la Capes – Ciência sem Fronteiras, pour le financement de cette thèse pendant 4 ans et l’Ecole Doctorale “Complexité du Vivant” d’avoir retenu ma candidature.

Je tiens à remercier mes collaborateurs : François Radvanyi, Danijela Vignjevic et Youmna Attie qui m’ont permis d’avancer dans mon projet de thèse. Ainsi que les membres de mon comité de thèse, Edgar Gomes et Marie-Helène Verlhac, pour les discussions enrichissantes. Un grand merci également aux membres de la plataforme d’imagerie, spécialement Patricia Le Baccon.

Je remercie aussi les tous membres de l’équipe Goud, nos discussions hebdomadaires m’ont permis d’enrichir mes connaissances scientifiques et m’ont beaucoup aidé à progresser dans mon projet. J’aimerais en particulier remercier Anahí et Amal pour nos discussions, Stéphanie pour la confiance que tu m’as accordé dans des projets où nous avons travaillé ensemble et Sabine qui a toujours été là pour m’écouter, m’accueillir et m’aider. Je n’ai pas assez de mots pour remercier Bruno Latgé pour tout son soutien, aide et compagnie ; partager cette thèse avec toi c’est un plaisir et un confort énorme. Un grand merci spécial à Alex, Guillaume et Hugo pour toujours m’accueillir dans votre bureau avec votre bonne humeur qui détend l’atmosphère.

Merci aussi aux membres de l’ADIC et du YRLS (2016), avec qui j’ai pu développer ma passion pour l’organisation d’évènements et construire des amitiés extraordinaires. Je suis extrêmement chanceuse d’avoir connu, grâce à l’ADIC, Imène, Léa et spécialement Melissa avec qui j’ai partagé mes plus grandes joies et déceptions pendant ma thèse. Je suis à toujours reconnaissante pour votre amitié, encouragements, soutien et nos discussions scientifiques et philosophiques. Un grand merci à Arthur pour son amitié et partage, mes journées d’été à Vavin n’auront pas été les mêmes sans toi.

Je tiens à remercier ma “famille française” : Luciana, Douglas, Nathália, Julia, Renata, Danilo et Iara, je suis chanceuse de vous avoir près de moi dans toutes les étapes de ma vie ici. Un merci spécial à Iara, c’est grâce à toi que je suis là aujourd’hui. Merci aussi à Marie-Pierre, Milena et Jeanne, vous m’avez accueilli comme partie de votre famille et c’est aussi grâce à vous que Paris est devenu chez moi.

Finalement, je remercie énormément ma famille qui m’a toujours encouragé, malgré la distance. Je sais que je peux compter sur vous dans tous les moments et qu’auprès de vous je trouverai toujours confort et affection. Je suis très reconnaissante pour tout ce que vous avez fait pour moi. Je dédie cette thèse à mon grand-père, l’homme le plus intègre et digne que j’ai jamais connu. Il sera pour toujours marqué sur moi.

Table of Contents

Index of figures and tables

List of abbreviations

Arl8b	ADP Ribosylation Factor Like GTPase 8B
BicD2	Bicaudal D homolog 2
CTRL	Control
DAPI	4',6-Diamidine-2'-phenylindole dihydrochloride
EGF	Epithelial growth factor
EGFR	Epithelial growth factor receptor
EMT	Epithelial mesenchymal transition
ER	Endoplasmic reticulum
FGFR3	Fibroblast growth factor receptor 3
G1	Grade 1
G2	Grade 2
G3	Grade 3
GM130	Golgi matrix protein 130kDa
HA	Human influenza hemagglutinin
HEPES	4-(2-hydroxyethyl)-1-piperazineethanesulfonic acid
KIF	Kinesin superfamily
Lamp1	Lysosomal-associated membrane protein 1
LC3	Microtubule-associated protein 1A/1B-light chain 3
MCS	Membrane contact sites
MIBC	Muscle-invasive bladder cancers
MMP	Matrix metalloproteinases
mRNA	Messenger RNA
mTOR	Mechanistic target of rapamycin
NMIBC	Non muscle-invasive bladder cancers
ORP1L	Oxysterol-binding protein-related protein 1L
PLA	Proximity ligation assay
PTP1B	Tyrosine-protein phosphatase non-receptor type 1
RNF26	Ring finger protein 26
RPMI	Roswell Park Memorial Institute
siRNA	Small interfering RNA
T1	Stage 1
T2	Stage 2
T3	Stage 3
T4	Stage 4
Ta	Non-invasive papillary carcinoma

INTRODUCTION

1. Cancer

The World Health Organization (WHO) defines cancer as a disease caused by abnormal growth and spread of cells that can affect any part of the body. Cancer is responsible for around 16% of deaths in the world, and metastasis are the major cause of death associated with cancer (WHO, 2017).

Cancer is a multifactorial disease, triggered by interaction of genetic, epigenetic and extrinsic factors. As the human organism is constantly exposed to agents that can cause damages to DNA, many factors can trigger a cancer, such as tobacco, alcohol, ultraviolet rays and some viruses (like hepatitis B and human papilloma virus) (Ho et al., 2012a; WHO, 2017). Moreover, intrinsic factors, like reactive oxygen species (ROS) formed during the metabolism of oxygen, ageing and hereditary genes are also promoters of cancer (Tubiana, 2008).

1.1. Hallmarks of cancer

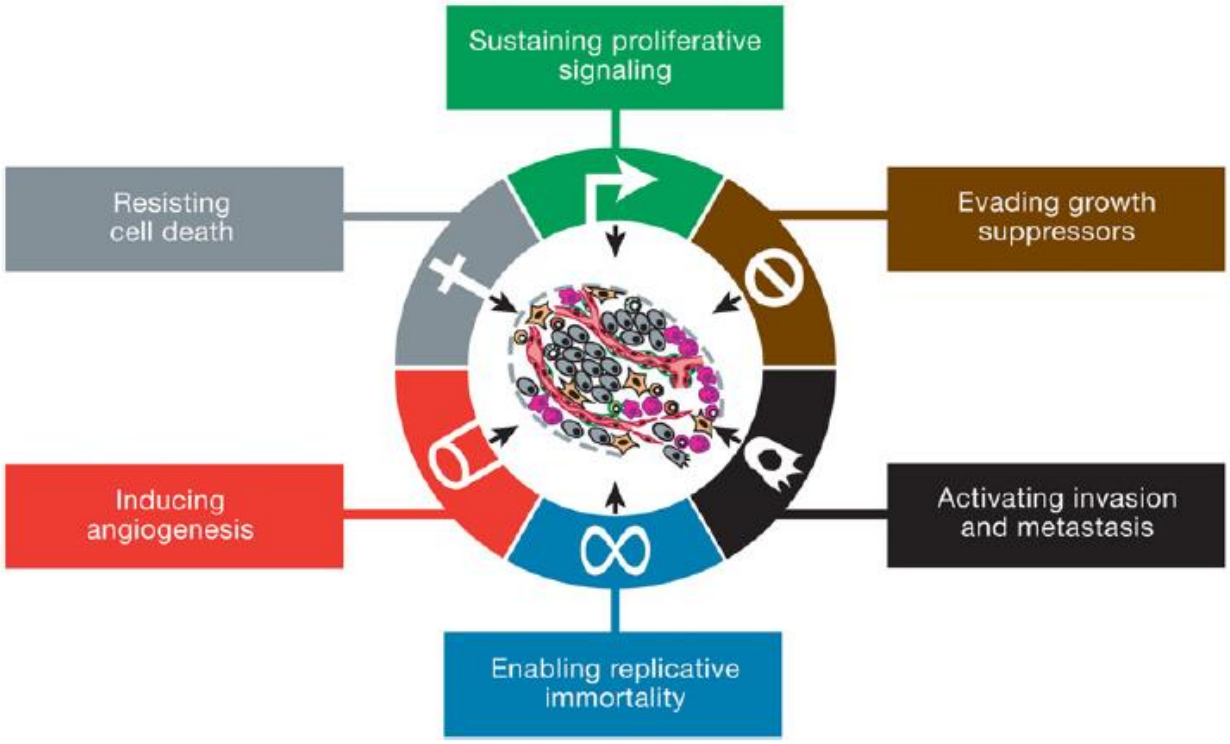

Figure 1: The Hallmarks of Cancer The 6 original hallmarks of cancer proposed by Hanahan and Weinberg in 2000.

During cancer, normal cells progressively acquire several functional characteristics until they become tumor cells, also known as neoplastic cells. In 2000, Hanahan and Weinberg have defined the six hallmarks of cancer: self-sufficiency in growth signals, insensitivity to anti-growth signals, evading apoptosis, limitless replicative potential, sustained angiogenesis and tissue invasion and metastasis (Hanahan and Weinberg, 2000) (Figure 1). These hallmarks are complementary capabilities that enable normal cells to undergo tumor growth and metastatic dissemination, when cells spread to distant organs.

1.1.1. Self-sufficiency in growth signals

Transformed cells have acquired competitive advantages for cell proliferation and growth. Growth factors are major players in proliferative signaling. Cancer cells can either abnormally produce growth factor receptors, or stimulate neighbor cells from the adjacent stroma to supply growth factors (Cheng et al., 2008). For instance, epidermal growth factor (EGF) binds its receptor EGFR at the plasma membrane and stimulates cell growth. In physiological conditions, it is implicated, for instance, in embryonic development and wound healing. However, in cancer this pathway is frequently deregulated (Calvo and Rowinsky, 2004).

1.1.2. Insensitivity to anti-growth signals

In order to proliferate and disseminate to secondary sites, cancer cells inactivate tumor suppressor genes and resist cell death (Hanahan and Weinberg, 2011). The tumor suppressor genes, also known as antioncogenes, act by limiting cell growth and proliferation in normal cells, however cancer cells acquire the ability to inactivate them. Well known tumor suppressor genes are retinoblastoma-associated (RB) and tumor-protein 53 (TP53). In normal cells, RB negatively regulates cell growth from extracellular signals, whereas TP53 inhibits cell growth due to cellular stress, such as genome damage and oxygenation defects (Hanahan and Weinberg, 2011). Contrary, cancer cells acquire selective growth advantage when oncogenes are activated by mutations (Vogelstein et al., 2013). These genes are promotors of cancer.

1.1.3. Evading apoptosis

In addition, transformed cells have to overcome the programmed cell death, apoptosis. In physical conditions, apoptosis is triggered in response to stress, such as nutrient deprivation and hypoxia, whereas in cancer, the cells suppress pro-apoptotic signals (Hanahan and Weinberg, 2011). For instance, the tumor suppressor TP53 is also a pro-apoptotic regulator.

The loss of this gene results in cells insensitive to apoptosis stimuli (Koff et al., 2015). Interestingly, is has been reported that apoptosis can favor cancer by killing less-suited clones for cancer dissemination (Labi and Erlacher, 2015).

1.1.4. Limitless replicative potential

Normal cells undergo a limited number of cell divisions and growth cycles. This is because telomeres, which are responsible to protect the ends of chromosomes, shorten after each division, limiting the number of cell divisions (Greider and Blackburn, 1985). Cell division is restricted during senescence, a non-proliferative state, in which the cells are still viable. Cancer cells undergo a transition called immortalization, in which they acquire the potential to replicate unlimitedly (Hanahan and Weinberg, 2011). In cancer cells, the telomerase, an enzyme that repeatedly adds segments to the end of telomeres (Greider and Blackburn, 1989), provides immortality characteristics to these cells (Blasco, 2005).

1.1.5. Sustained angiogenesis

Cancer cells require, as normal cells, the presence of nutrients and oxygen provided by blood vessels. Thus, in order to fulfill the metabolic needs for increased proliferation, tumor cells promote angiogenesis, where pre-existing blood vessels form new vessels (Hanahan and Weinberg, 2000, 2011). Furthermore, cancer cells can adopt other forms of vascularization, like hijacking of existing vessels, or *de novo* formation of new bloods vessels (Fouad and Aanei, 2017). This tumor-associated neovascular network is continuously developed, from the microscopic premalignant phase until tumor growth.

1.1.6. Tissue invasion and metastasis

Finally, cancer cells are characterized by escape from their original location and spread into tissues of the entire body. First, cancer cells undergo local invasion by breaching the basement membrane, a barrier that surrounds almost all tissues. Then, cells perform intravasation, defined by breaching the blood or lymphatic vessels and reaching the circulation. Next, cells may extravasate from the vessels, and colonize a secondary organ where they form the secondary tumor (Hanahan and Weinberg, 2000, 2011). Epithelial cancer cells often colonize adjacent tissues. Moreover, many secondary tumors are developed in bone marrow and liver tissues, probably due to their highly permeable vessels that facilitate cancer cell extravasation (Fouad and Aanei, 2017).

In 2011, Hanahan and Weinberg have proposed two enabling characteristics that favor cancer cells to acquire cancer hallmarks: genomic instability and tumor-promoting inflammation (Hanahan and Weinberg, 2011). Genomic instability allows cancer cells to acquire selective advantages, enabling the genetic alterations that drive cell transformation and tumor progression. The genetic mutations are classified in: i) deletions, that always target tumor suppressors, ii) amplifications, in which the product of an oncogene is abnormally increased, and iii) translocations that fuse two genes to form an oncogene (Vogelstein et al., 2013). Tumor-promoting inflammation contributes to cancer development by providing growth and proangiogenic factors and by helping the remodeling of the extracellular matrix (Grivennikov et al., 2010). Thus, immune cells and the inflammation signaling support hallmark capabilities (Hanahan and Weinberg, 2011).

Moreover, Hanahan and Weinberg have described two emerging hallmarks of cancer. The first one is the ability to reprogram and modify cell metabolism in order to support neoplastic proliferation. Normal cells consume glucose through glycolysis that occurs in the cytosol, and then the pyruvate (the product of glycolysis) is oxidated in the mitochondria. Under anaerobic conditions, the glycolysis is favored in order to spare oxygen that is consumed during mitochondrial respiration. Cancer cells reprogram their metabolism and energetic production by consuming high rates of glucose through glycolysis, even in the presence of oxygen (Hanahan and Weinberg, 2011; Warburg, 1956). This phenotype is known as Warburg effect and is also called as aerobic glycolysis. The second emerging hallmark is the capacity of cancer cells to evade immunological destruction, either by avoiding detection by immune cells, or by limiting the immunological killing (Hanahan and Weinberg, 2011).

Recently, the hallmarks described by Hanahan and Weinberg in 2000 and 2011 have been revisited. Fouad and Aanei pointed out that the initial hallmarks of cancer are also shared by some benign tumors (Fouad and Aanei, 2017), for instance, endometrial cells from the benign endometriosis that are capable to invade new tissues while maintaining their benign histological appearance (Wilbur et al., 2017). Additionally, they have proposed a new model of seven hallmarks of cancer: 1) selective growth and proliferative advantage that merges the first and second original hallmarks; 2) altered stress response favoring overall survival, a merge of the third and fourth hallmarks. The following four hallmarks have been conserved: 3) vascularization; 4) invasion and metastasis and 5) metabolic rewriting. Finally, they have proposed 7) abetting microenvironment as a new hallmark that considers the stroma as an active contributor to tumor growth (Fouad and Aanei, 2017).

1.1.7. Tumor environment

The stroma is the connective tissue that surrounds epithelial tissues. It is colonized by several cell types, including, fibroblasts, immune cells, and vessels made of endothelial cells. The tumor-associated stroma (Figure. 2) is mostly responsible for the heterogeneity within tumors, because of the cell-cell communication between cancer and stromal cells (Fouad and Aanei, 2017; Hanahan and Weinberg, 2011). The endothelial cells of blood vessels participate in angiogenesis. The pericytes, which are mesenchymal cells related to muscle cells, act with the endothelial cells to synthesize the basement membrane of the vessels (Hanahan and Weinberg, 2000, 2011). The immune cells found in the stroma, such as macrophages and lymphocytes, can contribute to tumor growth (DeNardo et al., 2008). Cancer associated fibroblasts are an important type of mesenchymal cells. These cells favor proliferation (Bhowmick et al., 2004), angiogenesis (Fukumura et al., 1998) and invasion (Dumont et al., 2013). Additionally, mesenchymal stem and progenitor cells can be found in the stroma. These cells have the ability to differentiate into specialized cells from the tumor associated stroma. They are recruited from the adjacent bone marrow to ensure the formation of the different stroma cell types (Bergfeld and DeClerck, 2010). Moreover, cancer stem cells are found in the tumor-associated stroma. These cells often qshare markers with stem cells of the tissue of origin (Cho and Clarke, 2008). They are responsible for the heterogeneity of several aspects of cancer cells, for instance differentiation, proliferation and invasiveness (Hanahan and Weinberg, 2011).

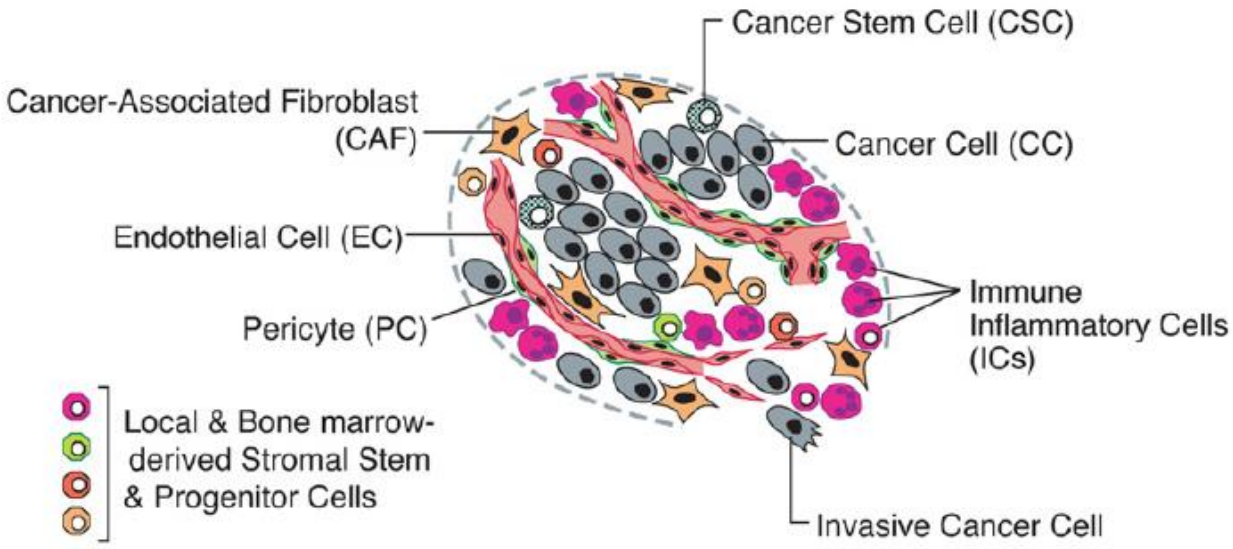

Figure 2: The tumor microenvironment A large variety of cells present in the tumor associated stroma. Cancer associated fibroblasts (CAF) and immune inflammatory cells (ICs) participate in the remodeling of the extracellular matrix. Endothelial cells (EC) and pericytes (PC) are implicated in the angiogenesis process. Stromal and cancer stem cells are also present in the tumor microenvironment. Adapted from Hanahan and Weinberg 2011.

2. Bladder cancer

Bladder cancer is the 9th most common cancer worldwide and represent 4% of cancer-related deaths (Ferlay et al., 2015). It is the 7th most common in men worldwide, whereas in women it is less common (17th) (Burger et al., 2013). Bladder cancer is very heterogeneous and occurs mainly in patients after the age of 65 (Ferlay et al., 2015). Genetic factors and extrinsic factors, like consumption of tobacco and alcohol constitute the main risks for the development of bladder cancers (Benhamou et al., 2016; Ferlay et al., 2015).

2.1. Classification of bladder cancers

Several classifications have been established to characterized bladder cancer, showing high heterogeneity, that depend on invasion (staging), morphology (grading) and genetics (molecular characteristics). The 1973 WHO system classifies tumors according to three grades of increasingly aggressive behavior, grades 1, 2 and 3, based on morphological criteria. The grades of cancer mean how much cancer cells look similar to non-transformed cells, 1 being the most similar to normal cells and 3 the most de-differentiated. Bladder cancer progresses along two pathways: the papillary cancers from the Ta pathway, which has a low-grade malignant potential (grades G1/G2), but high rates of recurrence, and the flat lesions from the Carcinoma *in situ* (Cis) pathway that always have high-grade (G3) of malignity (Humphrey et al., 2016).

Bladder cancers are also classified according to their invasion phenotype: Non-muscle-invasive bladder cancers (NMIBC) represents 80% of new diagnosed cases. Furthermore, NMIBC of low grades present high rate of recurrence (around 50%), and 20% of higher-grades NMIBC progress to muscle-invasive bladder cancers (MIBC). MIBC are associated with poor prognosis, with 50% of death cases within 5 years of cystectomy, the chirurgical removal of bladder (Benhamou et al., 2016; Knowles, 2008). Moreover, the stages represent the degree of invasion of bladder cancers (Figure 3). According to the Union for International Cancer Control TNM system, the NMIBC are divided into three stages: the papillary Ta and Tis stage (also called Cis, in which cells form non-invasive flat tumors, are restricted to the urothelial layer), and stage T1 that represents cells who have breached the basement membrane. MIBC are classified in stage T2, in which the invasion reaches the muscle tissue; the T3 stage classifies the invasion of the adipose tissue and the T4 stage with the dissemination to nearby organs (Benhamou et al., 2016; Ho et al., 2012a).

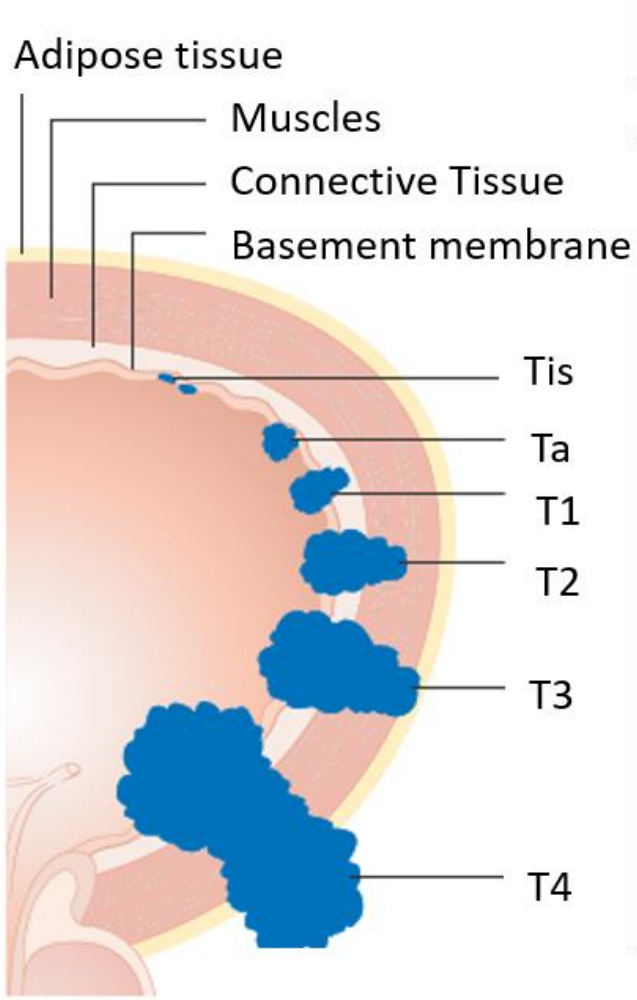

Figure 3: Representation of the different stages of bladder cancer progression. The NMIBC stages: Tis flat tumor, papillary Ta and T1. And the MIBC T2 to T4. Adapted from Cancer Research UK

Bladder cancer heterogeneity is due to the presence of different mutations. The fibroblast growth factor receptor 3 (FGFR3) acts as an oncogene in bladder cancer (Cappellen et al., 1999; van Rhijn et al., 2001). Indeed, activating mutations of the gene encoding this receptor is the most common genetic alteration in papillary NMIBC, especially in low-grades tumors (Billerey et al., 2001; Knowles, 2008). Additionally, large scale transcriptomic data demonstrated that the epidermal growth factor receptor (EGFR) pathway is associated with a subtype of bladder cancers, the basal-like subgroup, that represents 23,5% of MIBC. In these basal-like tumors the epidermal growth factor receptor (EGFR) pathway is overexpressed. In addition, 75% of the basal-like analyzed tumors were mutated for TP53.

Moreover, it was shown that the basal-like phenotype is associated with squamous differentiation, high grades and stages of bladder cancer progression, leading to poor survival (Rebouissou et al., 2014). Luminal-like MIBC subgroup are characterized by peroxisome proliferator activator receptor (PPAR - a transcription factor implicated in cell differentiation and metabolism) overexpression and FGFR3 mutations, which suggest that these cells originate from papillary NMIBC (Choi et al., 2014) (Figure 4).

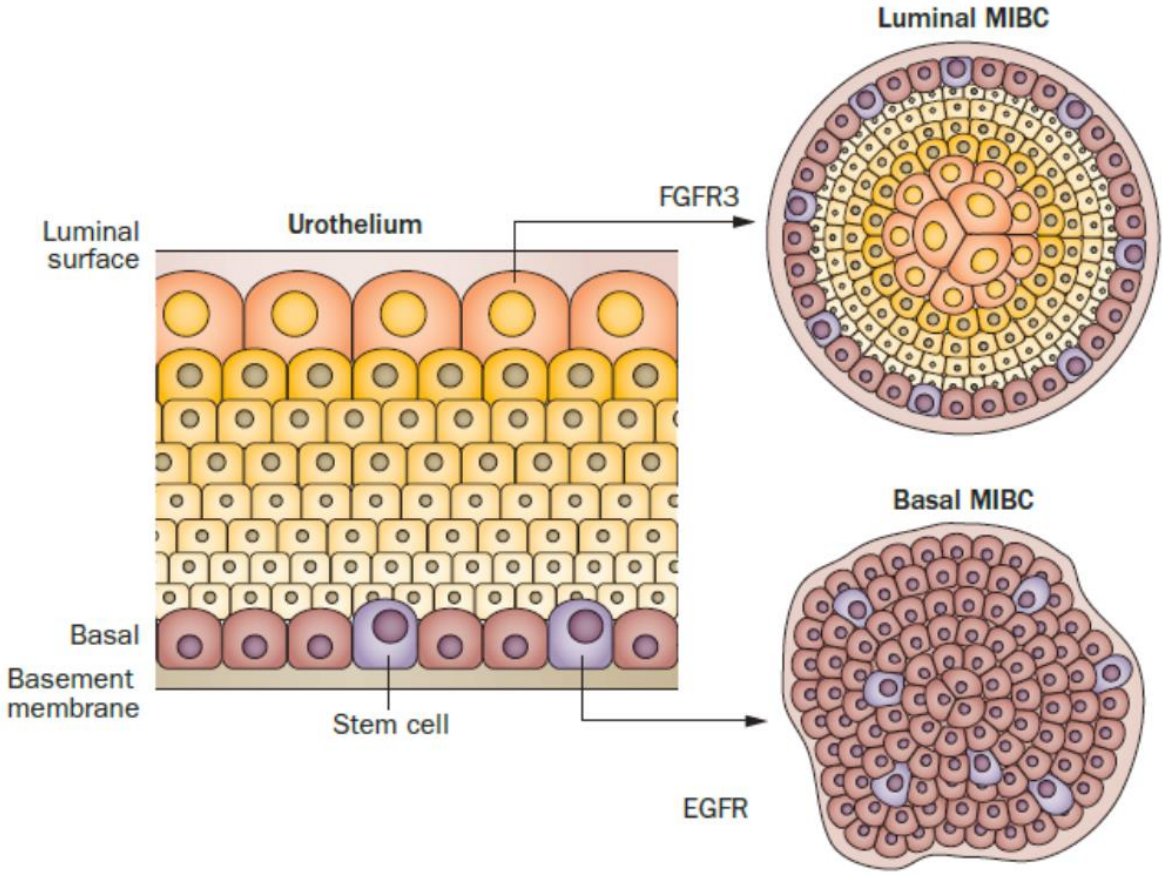

Figure 4: Differences between MIBC origins. Basal-like MIBC (lower) is mutated to EGFR and present a disorganized differentiation, whereas luminal-like MIBC (upper) are frequently mutated for FGFR3 and present a less disorganized phenotype. Adapted from Choi et al. 2014.

2.2. Deregulated trafficking pathways in bladder cancer cells

Growing evidence indicates that key regulators of intracellular trafficking, for instance small GTPases, play an important role in cancer. Abnormalities in the architecture of trafficking pathways lead to aberrations in the transport and sorting activities of the cell, for instance

defective transport of growth factor receptors or aberrant recycling of adhesion molecules. In addition, the disorganization of trafficking compartments such as endosomes impact signaling pathways, as growing evidence indicate that growth factor-mediated signaling persists throughout the intracellular journey of growth factor receptors. Several studies have highlighted a role for several GTP-ases of the Rab family in human cancers (Amillet et al., 2006; Bravo-Cordero et al., 2007; Gebhardt et al., 2005; Lankat-Buttgereit et al., 1994; Wheeler et al., 2015). Rab proteins are key regulators of intracellular trafficking, controlling the formation of transport carriers from donor membranes, their movement along cytoskeletal tracks and their tethering/fusion with target membranes. Rab proteins are themselves under a strict control by a complex regulatory network of proteins that includes guanine nucleotide exchange factors (GEFs), GTPase activating proteins (GAPs) and guanine nucleotide dissociation inhibitors (GDI). In their active form Rab GTPases interact with a diverse range of effector proteins, such as molecular motors, lipid kinases, tethering factors and scaffolding proteins (Stenmark, 2009).

A transcriptome study from our laboratory has demonstrated that many genes encoding Rab proteins as well as their regulators and effectors were deregulated in bladder cancer (Ho et al., 2012a). Interestingly, changes in gene expression often correlated with tumour progression along one of the pathways, the papillary low grade pathway (Ta pathway) or the carcinoma *in situ* (Cis) pathway. The genes encoding Rab27 or its regulators and effectors were deregulated in both pathways. Rab23 gene was specifically deregulated in tumors from the Cis pathway. Contrary, for the Ta pathway, no genes encoding Rab proteins or their regulators and effectors were found that were specifically deregulated. Furthermore, Ho and collaborators found that genes encoding Rab11 and Rab20 were associated with urothelial cell differentiation.

3. Intracellular changes during cancer disease

Cancer cells present genetic and epigenetic modification, but also display morphological alterations in their subcellular organization. In healthy tissues, the apical-basal polarity is essential for normal physiological function of epithelial cells and the tissue integrity. The maintenance of this polarity is regulated by cell intrinsic factors, like protein trafficking and cytoskeleton, and by extrinsic factors, like the cell-cell, mainly mediated by cadherins, and cell-matrix interactions mediated by integrins (Muthuswamy and Xue, 2012; Wodarz and Näthke, 2007) (Figure 5). The genetic and epigenetic changes that occur during cancer development lead to major changes in the transcriptome and proteome profiles of cells and thus to alterations in multiple signaling pathways and intracellular trafficking. This leads to morphological changes that provide competitive advantages during cancer spread.

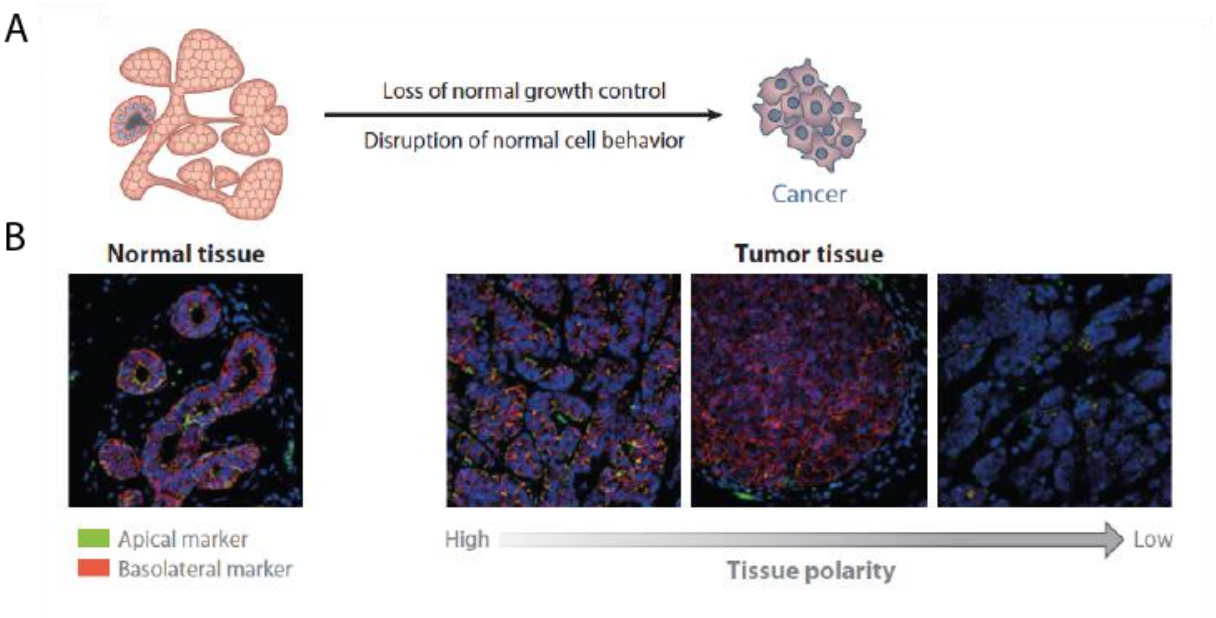

Figure 5: Disruption of normal cell behavior of cancer cells. A. Loss of normal growth and disruption of normal cell behavior are characteristics of malignant cells. **B.** Organized pattern of normal human breast cancer tissue evidenced by apical (in green) and basolateral markers (in red). The DAPI stains the nucleus (in blue). Gradual loss of apical marker staining in breast cancer tissues. Adapted from Muthuswamy and Xue 2012.

3.1. Epithelial-mesenchymal transition

The epithelial-mesenchymal transition (EMT) is the most studied example of changes in cell morphology. EMT is a physiological process in embryogenesis during development and in would healing, during which epithelial cells acquire, partially or totally, mesenchymal characteristics, such as fibroblast-like shape, changes of cell-cell adhesions (Peinado et al., 2004) (Figure 6) and loss of apical-basal polarity (Thiery and Sleeman, 2006). The concept of EMT has been introduced to cancer because cancer cells dedifferentiate from epithelial pattern, which facilitate cell migration. During EMT, the cells have an increased expression of proteases, which favors the degradation of the extracellular matrix and thus increase cell escape (Thiery et al., 2009).

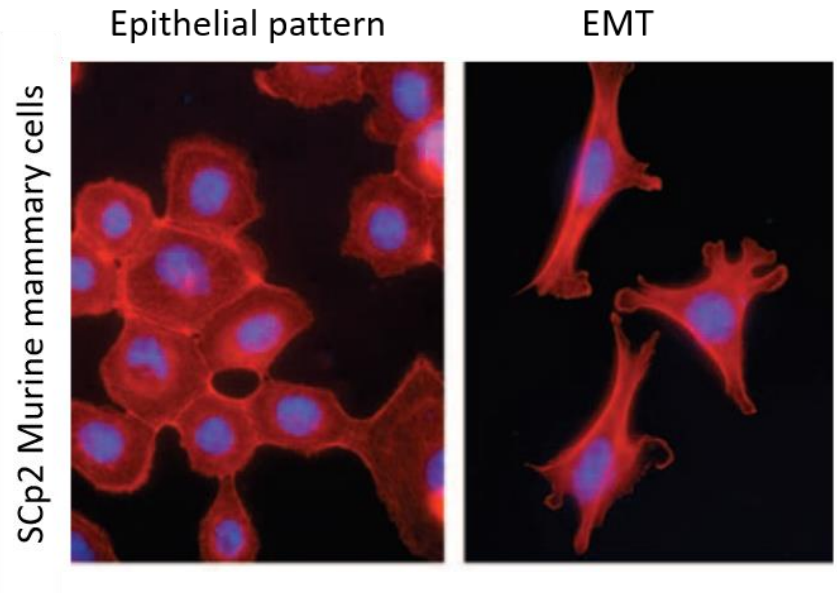

Figure 6: Morphological changes during EMT. Murine mammary cells stained for actin with Phalloidin (in red) and for nucleus with Dapi (in blue). Cells treated with MMP3 to induce EMT (right). Loss their cell-cell contacts and have an elongated shape in comparison to control situation (left). Adapted from Thiery and Sleeman 2006.

The EMT requires changes in cadherin expression (van Roy, 2014). Cadherin superfamily plays a crucial role in cell morphology because it is the major player implicated in cell-cell interactions, which impacts baso-lateral polarity (Harris and Tepass, 2010). Cadherins are type-1 transmembrane receptors that mediate cell-cell adhesion localized in domains of the membrane enriched in cholesterol (Causeret et al., 2005). The extracellular domain of cadherins forms cellular junctions by binding cadherins from adjacent cells, while the

cytoplasmic tail interacts with catenins in the cytoplasm (Harris and Tepass, 2010). The catenin-cadherin complex binds to the cytoskeleton to mediate its remodeling, which impacts cell shape and trafficking of proteins (Harris and Tepass, 2010; Odenthal et al., 2016). Several types of cadherins exist, the E-, N- and P- cadherins. E-cadherin is exclusively expressed in epithelial cells (van Roy, 2014). N-cadherin is found in mesenchymal cells (van Roy, 2014) and their mediated contacts are transient (Theveneau and Mayor, 2012). P-cadherin overlaps with E-cadherin in epithelial cells, however is also found in mesenchymal cells. Both E and P-cadherins play a role in intercellular force transmission of epithelial cells (Bazellières et al., 2015). Abnormal cadherin function is a common characteristic of cancers (Harris and Tepass, 2010; van Roy, 2014). Because E-cadherin is a major player in epithelial cell-cell interaction, it acts as growth and invasion suppressor (van Roy, 2014). Therefore, E-cadherin loss is a common feature of epithelial cancers and is used to diagnosis and prognosis. E-cadherin expression is associated with positive prognosis (van Roy, 2014). N-cadherin expression is often associated with a poor prognosis (van Roy, 2014). During EMT, a switch between E and N-cadherin is required (van Roy, 2014). Moreover, P-cadherin is frequently associated with increased migration and invasion (Plutoni et al., 2016).

During EMT, cells modify their polarization. Three complexes regulate cell polarity in mammalian cells: the protease-activated receptor (PAR) and the atypical protein kinase C (aPKC) complex, Crumbs complex and Scribble complex (Muthuswamy and Xue, 2012). The deregulation of these complexes have been implicated in malignant transformation by leading to a loss of apical-basal polarity (Muthuswamy and Xue, 2012; Wodarz and Näthke, 2007).

The mutation of transforming growth factor β (TGFβ) has been implicated in EMT and inhibition of apoptosis (Valdés et al., 2002). These morphological and functional changes favor the survival, dissemination and metastatic spread of cancer cells (Hanahan and Weinberg, 2011; Thiery et al., 2009; Wodarz and Näthke, 2007).

Once metastatic mesenchymal-like cells reach the secondary organ, they can undergo mesenchymal-epithelial transition (MET). This transition allows the differentiation in specialized epithelial cells to properly colonize the 3D complex structure of the secondary site (Clark and Vignjevic, 2015; Thiery et al., 2009).

3.2. Mesenchymal-amoeboid transition

Cancer cells can undergo mesenchymal-amoeboid transition (MAT). These cells change from an elongated to a round irregular cellular shape and become highly contractile, which allows the cells to squeeze through narrow spaces in the stroma (Friedl and Alexander, 2011; Liu et al., 2015). In this transition, Rac activity is often decreased, whereas Rho is activated and mediates actin contractility (Friedl and Alexander, 2011). This transition can be led by loss of protease activity and decrease in binding between cells and extracellular matrix (Friedl and Alexander, 2011; Friedl and Wolf, 2003). The absence of focal adhesions lead to loss of cortical membrane tensions that result in round cellular shape and acceleration of cell migration (Liu et al., 2015). Additionally, the amoeboid transition can occur in cells migrating collectively in a β1 independent manner, this process is called collective-amoeboid transition (CAT) (Friedl and Wolf, 2003).

Alterations in intracellular compartments in cancer

Changes in cancer cell shape due to alterations in cell polarity and adhesion are well characterized (Friedl and Wolf, 2003). However, the morphological alterations observed in cancer cells are not well-defined on the subcellular, organelle level. On the subcellular level, few alterations have been characterized in cancer cells, for example: abnormal nuclear size and shape (Zink et al., 2004a); augmented secretion of lysosomes, in prostate cancer cells (Steffan et al., 2014); increased energy production in mitochondria due to crosstalk with tumor associated stroma (Wallace, 2012); elevation of reactive oxygen species after activation of peroxisome proliferator activator receptors (Keller et al., 2000) and Golgi apparatus fragmentation (Petrosyan, 2015).

3.3. Nucleus

The nucleus is a membrane-enclosed organelle that contains most of the cellular DNA. The nuclear morphology is currently used for diagnosis of cancer (Zink et al., 2004a). Indeed, alterations in nuclear size, shape, margins and numbers are often observed in tumor cells (Baba and Câtoi, 2007; Dey, 2010). During cancer dissemination, cells have to change their shape to pass through narrow spaces in the extracellular environment. The nucleus is the biggest organelle in cells and is stiffer than the cytoskeleton (Friedl et al., 2011). Nuclei deformation was observed in cells migrating under confinement *in vitro* (Denais et al., 2016; Raab et al., 2016). Cells migrating through narrow spaces presented leakage of nuclear proteins to the cytoplasm, which indicates disruption of the nuclear membrane. Thus, the deformability capacity of nuclei is a limitation to cell migration.

3.4. Mitochondria

Mitochondria are organelles originated from symbiotic bacteria that are responsible for cell respiration and energy production but also for the generation of reactive oxygen species (ROS) and initiation of apoptosis (Wallace, 2012). Alterations in function and number of mitochondria have been implicated in cancer (Wallace, 2012; Warburg, 1956; Zong et al., 2016). To provide more energy to cancer cells, abnormal glycolysis occur in mitochondrial membranes even during aerobic conditions, which is known as Warburg effect (Baba and Câtoi, 2007; Warburg, 1956). The accumulation of mitochondria, in kidney cancers, provoked high rates of respiration and sustained proliferation (Hasumi et al., 2012). The ROS produced by mitochondrial activity causes cell toxicity that can initiate apoptosis. In cancer cells with inhibited apoptosis, ROS accumulation can contribute to malignant transformation (Wallace, 2012).

Interestingly, the mitonchondrial metabolism can influence the tumor associated stroma. Cancer cells secret H_2O_2, which induces degradation of mitochondria of the fibroblasts that leads to increased glycolytic metabolism. The increased glycolysis generates secretion of acids, such as lactate and ketones, to the extracellular space. Cancer cells use these acids for energy production, favoring cancer progression (Wallace, 2012).

The mitochondria are not part of the vesicular cellular trafficking, thus these organelles adapt their shape and distribution within the cytoplasm to efficiently distribute their metabolites (Daniele et al., 2014). In epithelial migrating cancer cells, the anterograde localization

(between nucleus and leading edge) of mitochondria correlates with increase in velocity and directional persistence (Desai et al., 2013).

3.5. Peroxisomes

Peroxisomes are organelles responsible for the reduction of hydrogen peroxide and the catabolism of fatty acids. Oxidation of long chain fatty acids in peroxisomes shorten these lipids that will be next metabolized by the mitochondria (Lodhi and Semenkovich, 2014). Peroxisomes have the ability to increase their number and size in response to the accumulation of fatty acids (Delille et al., 2006). The nuclear transcription factors peroxisome proliferator-activated receptors (PPARs) are responsible for the highly dynamic proliferation of this organelle. The increase in number of peroxisomes results in increase of ROS production and it was reported that these proliferators can initiate or promote cancer development (Keller et al., 2000).

Interestingly, PPARγ (one of three isoforms) has been implicated in the induction of differentiation of normal human urothelial cells (Varley et al., 2004). Moreover, PPARγ gene was amplified in 15% of luminal muscle-invasive bladder cancers, which suggests a role in bladder cancer promotion (Choi et al., 2014).

3.6. Golgi apparatus

The Golgi apparatus is an essential organelle that consists of interconnected flattened cisternae. It is a key player in protein glycosylation, trafficking and sorting along the biosynthetic/secretory pathway. In cancer cells this organelle is often fragmented (Chia et al., 2012; Petrosyan et al., 2014) and poorly developed (Baba and Câtoi, 2007). Pertubation in Golgi morphology leads to aberrant glycosylation, which impact protein folding and stability (Petrosyan et al., 2014). The gene encoding Golgi phosphoprotein 3 (GOLPH3) was reported to be an oncogene (Scott et al., 2009). Oncogenic GOLPH3 regulates cell size, abnormal production of growth factors (Scott et al., 2009) and is implicated in aberrant glycosylation and secretion of matrix metalloproteinases (Rizzo et al., 2017).

Several Rab proteins are localized at the Golgi apparatus (Petrosyan, 2015). The deregulation of these proteins have been reported in cancer, for instance Rab6a interact with giantin, a Golgi matrix protein, in normal conditions. However, it was reported that in prostate

cancer cells, Rab6a interacts with myosin II, an actin associated motor protein, which leads to Golgi disassembly and deregulated trafficking (Petrosyan et al., 2014). Moreover, Rab proteins often associate with kinesins to transport proteins sorted from Golgi. Interestingly, it has been shown that depletion of several kinases that are found down-regulated in cancers induce Golgi fragmentation and defects in glycan biosynthesis and protein secretion (Chia et al., 2012).

3.7. Endoplasmic reticulum

Endoplasmic reticulum (ER) is an organelle that forms an interconnected cisternae network that is continuous with the nuclear membrane. It is the major organelle responsible for protein folding and translocation (Yadav et al., 2014). ER stress leads to unfolded or misfolded proteins. The accumulation of unfolded proteins triggers apoptosis to avoid cells with defective ER (Yadav et al., 2014). In cancer cells, ER stress can contribute to cell survival (Mollereau, 2013). Cancer cells induce hyperactivation of ER protein folding and transport to support cell survival and proliferation (Lee, 2007). During cancer progression, a reduction of the ER is associated with an increase of free ribosomes (Baba and Câtoi, 2007).

4. Lysosomes and lysosome-related organelles

Lysosomes were first described by Christian de Duve and collaborators as acidic granules containing hydrolases (De Duve et al., 1955). These organelles are surrounded by a phospholipid bilayer membrane and contain over 60 different types of soluble hydrolases that require an acidic pH (4.5-5) for maturation and optimal activity (Kallunki et al., 2013). These hydrolases can degrade several substrates, such as proteins, carbohydrates, lipids and nucleic acids (Fennelly and Amaravadi, 2017; Hämälistö and Jäättelä, 2016).

To prevent the degradation of the lysosomal membrane by hydrolases, lysosomal membrane proteins are heavily glycosylated. Around 50% of the lysosomal membrane is composed of the transmembrane lysosome-associated membrane protein 1 and 2 (LAMP1 and LAMP2). Other important lysosomal membrane proteins are the tetraspanin transmembrane CD63 (also known as LAMP3), lysosome integral membrane protein 1 and 2 (LIMP1 and LIMP2) and vacuolar H+-adenosine triphosphatase (V-ATPase) (Kallunki et al., 2013; Solomon and Muro, 2017). The V-ATPase is responsible for the acidification of the lysosomes, by gradually pumping protons into the lysosomal lumen until pH 5 to 4.5 (Hämälistö and Jäättelä, 2016).

In addition to conventional lysosomes, whose function is degradation, cells contain many lysosome-related organelles. Late endosomes share many molecular markers of lysosomes, but have several cellular functions (see below). In cytotoxic T cells and osteoclasts, all lysosomes are secretory, whereas in mast cells lysosome-related organelles co-exist with conventional lysosomes. The melanosomes of melanocytes, and Weibel-Palade bodies from endothelial cells are specialized lysosome related organelles (Luzio et al., 2014). The exocytosis of secretory lysosomes-related organelles is mediated by Ca^{2+} and soluble NSF attachment receptor (SNAREs) that are major regulators of membrane fusion (Rodríguez et al., 1997).

An emerging role of lysosomes and lysosome-related organelles (for simplicity lysosomes will be used hereafter) has been proposed in cancer. During malignant transition, the secretion of lysosomal proteases is increased in prostate cancer (Dykes et al., 2016; Steffan et al., 2010). Lysosome-related functions, such as autophagy and exosome secretion, have been shown to be deregulated in breast cancer (Rashed et al., 2017; Hare and Harvey, 2017; Hendrix and De Wever, 2013). Interestingly, proteins and mechanisms implicated in lysosome positioning have been reported to be deregulated during prostate cancer both *in vitro* and *in vivo* (Dykes et al., 2016; Steffan et al., 2009, 2010). Moreover, lysosome positioning has been recently shown to be implicated in EMT-mediated tumor invasion

(Dykes et al., 2017). Interestingly, a large scale screening has reported lysosome associated membrane protein 1 (Lamp1) as an important biomarker associated with bladder cancer (Duriez et al., 2017). Lamp1 expression is increased in urine samples from patients with bladder cancers as compared to control samples.

4.1. Lysosome biogenesis

Several pathways have been shown to participate in lysosomal biogenesis: the endocytic pathway; the secretory route for the delivery of enzymes from the Golgi apparatus; and fusion events with late or recycling endosomes (Braulke and Bonifacino, 2009; Klumperman and Raposo, 2014; Luzio et al., 2014) (Figure 7).

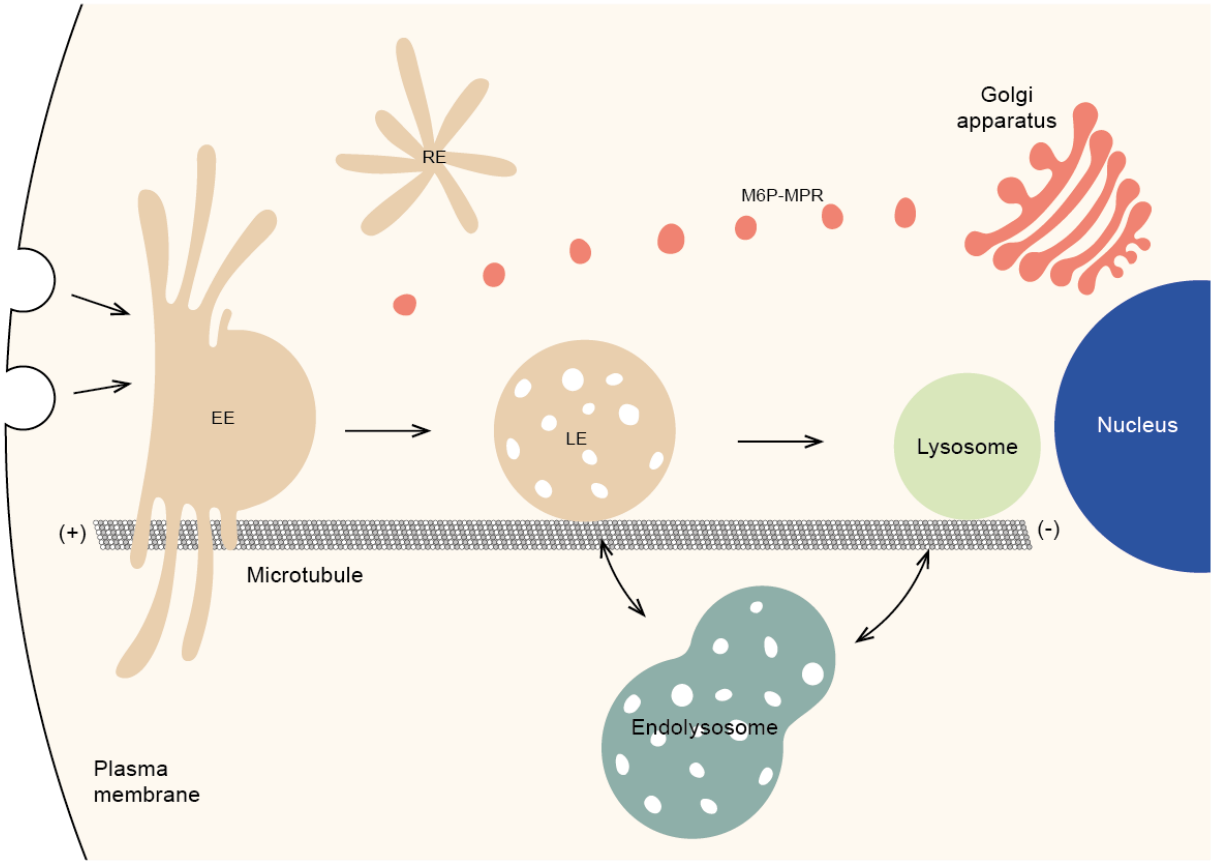

Figure 7. Lysosomal biogenesis. *The endocytic pathway*: Maturation from early endosomes (EE) to late endosomes (LE) and finally lysosomes. *The secretory pathway*: Newly synthetized proteins are tagged with mannose 6 phosphate (M6P) and transported to EE. Upon acidification the proteins are delivered to the lysosomes. *Endolysosome*: Late endosomes and lysosomes can fuse, to exchange proteins, forming the hybrid organelle endolysosome.

4.1.1. Endosomal maturation pathway

Lysosomes derive from early and late endosomes through maturation. The early endosomes are composed of a globular region and of tubular extensions. The tubular structures form the recycling endosomes that recycle molecules (e.g. transferrin and its receptor) to the plasma membrane. Early endosomes are enriched in Rab5 (Huotari and Helenius, 2011; Klumperman and Raposo, 2014). The maturation of the sorting endosomes to late endosomes initiates with the switch of Rab5 to Rab7 (Rink et al., 2005). Rab7 drives the transport of late endosomes along microtubules towards the perinuclear region (Bucci et al., 2000; Jordens et al., 2001). Late endosomes contain several intraluminal vesicles that represent incorporations of endosomal membranes via ESCRT (endosomal sorting complex required for transport) complexes. Because of the presence of intraluminal vesicles, the late endosomes are also called multivesicular bodies (Huotari and Helenius, 2011; Klumperman and Raposo, 2014). Through this endosomal maturation pathway, late endosomes deliver endocytosed cargos, such as integrins and growth factor receptors, to the lysosomes for degradation (Huotari and Helenius, 2011; Klumperman and Raposo, 2014).

4.1.2. Delivery of lysosomal enzymes by the secretory pathway

Lysosomal hydrolases are synthetized as proenzymes in the endoplasmic reticulum and delivered to lysosomes trough the Golgi apparatus. The best-studied pathway for the secretion from the Golgi apparatus to lysosomes relies on the mannose-6-phosphate receptor (MPR). The prohydrolases are tagged with mannose-6-phospate (M6P) residues in the Golgi, then the M6P residues bind specifically to MPRs in the *trans* Golgi network (TGN). The complex MPRs-M6P-hydrolase exits the TGN through clathrin-coat intermediates and fuses with early endosomes. Then, upon acidification in late endosomes, the complex is dissociated and the hydrolases are released into the lumen of late endosomes, where the hydrolases become active due to the acidic pH (Braulke and Bonifacino, 2009; Kallunki et al., 2013). Although MPRs represent an important pathway in lysosomal biogenesis, they are not present in mature lysosomes (Braulke and Bonifacino, 2009; Luzio et al., 2014), instead they are recycled back to the Golgi apparatus (Wang et al., 2014).

4.1.3. Fusion with late endosomes

Additionally, fusion events have been proposed to be important for lysosomal biogenesis. The formation of the hybrid endolysosome from the fusion of lysosomes with late endosomes

has been proposed to allow the exchange of proteins from both organelles (Klumperman and Raposo 2014; Luzio et al. 2014).

4.2. Lysosomal Functions

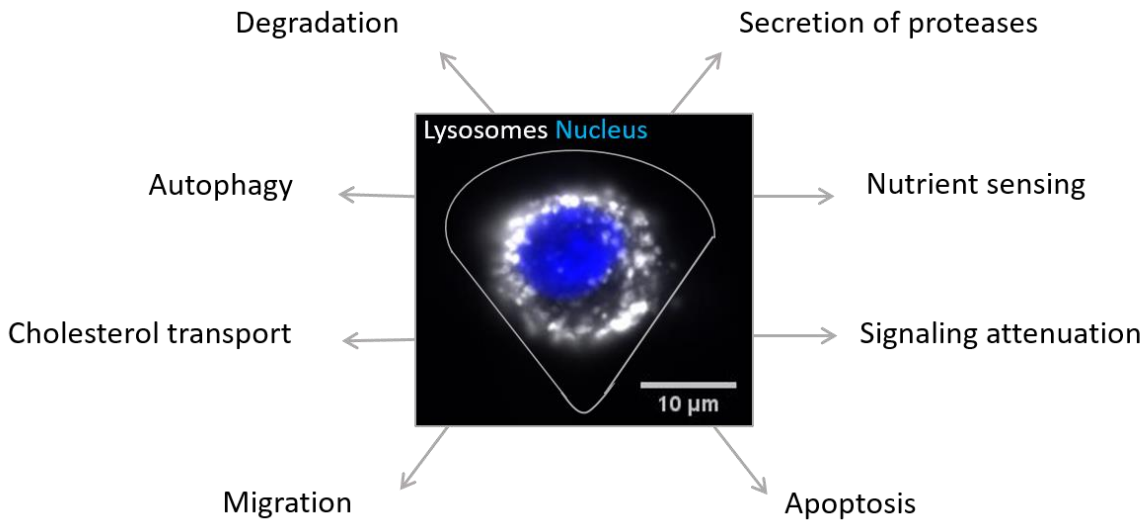

Figure 8: Functions of lysosomes.

4.2.1. Role of lysosomes in cellular catabolism

4.2.1.1. Degradation

The major function of lysosomes is to degrade macromolecules through the action of the lysosomal hydrolases. These enzymes are classified by the substrate they degrade, such as: proteases (proteins), phosphatases (phosphoric acid residues), nucleases (nucleic acids), glycosidases (sugars), lipases (lipids) and sulfatases (sulfate esters) (Braulke and Bonifacino, 2009). The most studied lysosomal hydrolases belong to the family of cathepsin proteases, because of their implication in several cancers (Kallunki et al., 2013). The proteins and receptors entering the endosomal system by endocytosis (e.g. integrins) are degraded by cathepsins and recycled to the cytosol for metabolical reuse (Klumperman and Raposo, 2014; Solomon and Muro, 2017).

The secretion of lysosomal proteases has been implicated in cancer (Dykes et al., 2017; Kallunki et al., 2013; Machado et al., 2015; Steffan et al., 2014). The secretion of cathepsin D is increased in most solid cancers, and cathepsin B overexpression is widely found in most types of cancers and in the tumor-associated stroma. The secreted cathepsins participate in the degradation of the extracellular matrix, which favors cell invasion, tumor growth and angiogenesis (Fennelly and Amaravadi, 2017; Kallunki et al., 2013). In prostate cancer, cells depleted for Rab7, the lysosomes are translocated to the cell periphery, which increases the secretion of cathepsin B (Steffan et al., 2014). Also in prostate cancer cells, it was reported that Arl8b, present on peripheral lysosomes, is necessary for secretion of proteases, matrigel degradation, tumor growth and invasion (Dykes et al., 2016). Small GTPase Rab7 and Arl8b key regulators of lysosome transport (see below). Furthermore, exacerbated lysosomal exocytosis of hydrolases increases the invasiveness phenotype of sarcoma cells (Machado et al., 2015). Moreover, enhanced secretion of lysosomes leads to acidification of the extracellular milieu that is a common feature of the tumor microenvironment and has been implicated in enhanced tumor invasion (Steffan et al., 2009). On the contrary, the release of cathepsins into the cytosol, upon destabilization of lysosomal membrane, can trigger apoptosis and impairs cancer progression (Kallunki et al., 2013).

4.2.1.2. Autophagy

Autophagy is a lysosomal-related multistep recycling process in which cytosolic components are recognized and isolated, then delivered to lysosomes for degradation (Galluzzi et al., 2017; Nakamura and Yoshimori, 2017). This process happens at a basal level, however it is accelerated by cellular stress such as starvation, organelle damage and pathogen infection (Galluzzi et al., 2017; Nakamura and Yoshimori, 2017). Autophagy is classified as: i) microautophagy, a process that occurs in yeast and plants, where the cytosolic components for degradation are sequestered by invaginations of the vacuole membrane; ii) chaperone-mediated autophagy, in which cytosolic soluble molecules are delivered to lysosomes for degradation via protein-translocation complex, instead of membrane invaginations; iii) and macroautophagy, the best characterized process of autophagy, where large amounts of cytosol, and even whole organelles, are sequestered to subsequently being degraded and reclycled (Galluzzi et al., 2017). Macroautophagy initiates by the formation of the phagophore, a double membrane structure that surrounds the intracellular component. Then, this membrane expands forming the enclosed autophagosome (Fennelly and Amaravadi, 2017; Galluzzi et al., 2017; Klionsky et al., 2012). Finally, autophagophore fuses with lysosome forming the autolysosome, where the degradation of the sequestered material occurs. Then, the molecules are recycled for metabolical reuse (Galluzzi et al., 2017).

The role of autophagy in cancer is not clear. Autophagy has been described as a mechanism to support cancer cell survival in hostile environment. Indeed, when cells are exposed to starvation, such as in tumor environment, in order to compensate the nutrient deprivation, they initiate autophagy (Mathew et al., 2007). The activation of mTORC1 signaling lead to breast tumor progression and poor survival (Hare and Harvey, 2017). On the contrary, autophagy has been suggested as a tumor suppressor mechanism. For instance, impairment of autophagy causes oxidative stress, DNA damage, genome instability and inflammation, which can drive cancer initiation and progression (Mathew et al., 2009; White, 2015)

4.2.2. Lysosomes function as platform of signaling molecules

Transcription factor EB (TFEB) acts as the major regulator of lysosomal biogenesis and autophagy, thus cellular catabolism. Non-active TFEB is highly phosphorylated and is localized at the lysosomal membrane. However, under in low nutrition condition and requirement of degradation of macromolecules, TFEB becomes dephosphorylated and is translocated to the nucleus, where it activates the transcription of lysosomal and autophagy-related genes, initiating the synthesis of lysosomal hydrolases and lysosomal membrane proteins as well as autophagy (Luzio et al., 2014; Settembre et al., 2012). Indeed, during starvation, mammalian target of Rapamycin complex 1 (mTORC1) is present in the lysosomal membrane and is inactivated, which triggers activation of autophagy. On the contrary, when cells have high amounts of nutrients, mTORC1 limits lysosomal biogenesis by keeping TFEB inactive at the lysosomal membrane (Fennelly and Amaravadi, 2017; Hämälistö and Jäättelä, 2016; Luzio et al., 2014).

4.2.3. Attenuation of signaling

The degradation of signaling receptors by lysosomes is important to attenuate receptor-mediated signaling. When lysosomal degradation is delayed, for instance due to slower transport of activated receptors from early endosomes to late endosomes, the signaling from the receptors is activated for longer periods. In the case of the epithelial growth factor receptor (EGFR), the activation of the mitogen-activated protein kinase (MAPK) pathway is sustained, when its degradation is delayed. MAPK activation induces transcription factors implicated in cell proliferation and survival (Taub et al., 2007).

4.2.4. Cholesterol transport

Besides their main function as degradative compartment, lysosomes are also implicated in cholesterol transport. The oxysterol-binding protein related 1 (ORP1L) is a cholesterol sensor present at lysosomes. This protein promotes interaction between lysosomes and endoplasmic reticulum under low cholesterol conditions to allow transfer of cholesterol from lysosomes to endoplasmic reticulum (Rocha et al., 2009). An important disease related to deregulated lysosomal homeostasis of cholesterol is Niemman Pick disease type C (NPC). In physiological conditions, NPC2 binds to cholesterol in lysosomes and delivers it to NPC1 that will transfer it to a cytosolic cholesterol-binding protein. In this disease, both NPC 1 and 2 can be mutated, although mutation of NPC1 is more common (around 95% of cases). The mutations impair the sorting of cholesterol out of lysosomes (Maxfield, 2014).

4.2.5. Migration and invasion

Lysosomes have been implicated in cell migration, by fast recycling of activated α5β1 integrins from the leading edge towards the plasma membrane at the cell rear of migrating cells (Dozynkiewicz et al., 2012). Additionally, peripheral lysosomes positive for the p14-MP1 complex (MAPK kinase 1 partner MP1 and its endosomal adaptor protein 14) promote turnover of focal adhesions (FAs) required for migration. P14-MP1 positive lysosomes dissociate the integrins from the Ras GTPase-activating-like protein (IQGAP1), a scaffold protein (Schiefermeier et al., 2014). Moreover, BORC (biogenesis of lysosomes-related organelles complex 1 related complex) recruits the small GTPase ADP-rybosylation factor like protein 8b (Arl8b) that is specifically localized at lysosomes and mediates peripheral lysosomal movement. It has been observed that BORC knock-out cells present a clustered lysosomal pool at the cell center and a severely impaired cell spreading and migration phenotype (Pu et al., 2015). The authors hypothesize that peripheral lysosomes are required for integrin dynamics. Furthermore, silencing of the Rab7 leads to slower cell migration, due to an accumulation of β1 integrins at the leading edges of migrating lung cancer cells (Margiotta et al., 2017). In addition, it was reported that Rab27-mediated protease release cleaves integrin at the cell rear, in order to allow cell detachment and support cell dynamics (Singh et al., 2012).

During invasion, in addition to cell migration, proteolysis of adjacent extracellular matrix is required. Matrix metalloproteinases (MMPs) are key players in extracellular substrate degradation (Friedl and Wolf, 2003). MT1-MMP (MMP14) is manly located at lysosomes (Steffen et al., 2008). MT1-MMP positive lysosomes move biderectionally along microtubules

regulated by KIF5B and p150^{Glued} (Marchesin et al., 2015). These lysosomes accumulate in invadopodia membranes (Poincloux et al., 2009) were they secrete MT1-MMP to promote pericellular proteolysis (Monteiro et al., 2013), which favors cancer cell invasion (Hotary et al., 2003). Following local exocytosis, MT1-MMP are rapidly internalized and delivered to lysosomes to mediate fast recycling to the plasma membrane (Macpherson et al., 2014).

4.2.6. Exosome secretion

In some cases, multivesicular bodies, organelles that are tightly related to lysosomes, can secret intraluminal vesicles to the extracellular environment, which are called exosomes. Exosomes are small vesicles (30-100 nm) that carry proteins, lipids and RNA to the extracellular milieu and mediate cell-to-cell communication (Klumperman and Raposo, 2014; Simons and Raposo, 2009). Due to their endosomal origin, exosomes contain proteins found in endosomes, such as Rab proteins and integrins. However, these vesicles are specifically enriched in some proteins that are considered as exosomal markers, such as flotillin and CD63. Moreover, exosomes are enriched in cholesterol, sphingolipds and fatty-acyl chains. The most distinct function of exosomes is cell-cell communication, for instance exosomes can transport messenger RNA (mRNA) (Valadi et al., 2007). In addition, exosomes are implicated in regulation of coagulation after release from platelets (Simons and Raposo, 2009).

Exosomes are implicated in tumor progression by releasing proteomic material, which can travel through circulation and create a metastatic niche (H Rashed et al., 2017). Additionally, exosomes carry pre-angiogenic factors, and are implicated in cancer-associated fibroblast differentiation (Rashed et al., 2017; Klumperman and Raposo, 2014). Moreover, small GTPase Rab27a that regulates the docking of MVE with the plasma membrane regulates exosomal secretion in mammary carcinoma *in vivo*, which favor tumor progression and metastasis (Bobrie et al., 2012).

4.2.7. Apoptosis

Lysosomal membrane permeabilization can trigger apoptosis, an important regulator of tissue homeostasis, through leakage of hydrolases into the cytosol. These hydrolases can permeabilize the mitochondrial membrane, liberating cytochrome c that will activate the caspase cascade. Additionally, upon lysosomal membrane permeabilization, some cathepsins trigger cell death in a caspase-independent manner via necroptosis, a form of programmed necrosis (Fennelly and Amaravadi, 2017; Piao and Amaravadi, 2015).

4.3. Molecular regulators of lysosomal positioning

Lysosomes are scattered around the entire cellular cytoplasm but sometimes can also be found concentrated at the perinuclear region or at the cell periphery. This organelle moves bidirectionally using the cellular microtubule network: the anterograde (centrifugal) transport implicates the kinesins, molecular motor proteins that drive cargos towards the plus-end of microtubules (which in non-polarized cells are localized at cell periphery), whereas the retrograde (centripetal) transport is driven by dynein towards the minus-end of microtubules (Bonifacino and Neefjes, 2017; Pu et al., 2016) (Figure 9).

The implications of lysosome positioning in cancer cells is an emerging field. For instance, it was shown that lysosomes are distributed to the cell periphery due to acidification of the microenvironment in tumors (Glunde et al., 2003; Steffan et al., 2009). These peripheral lysosomes induce filopodia formation and tumor invasion, in breast cancer cells (Glunde et al., 2003). In prostate cancer cells, peripheral lysosomes in response to acidic pH secrete more cathepsin B, which increases tumor invasion (Steffan et al., 2010).

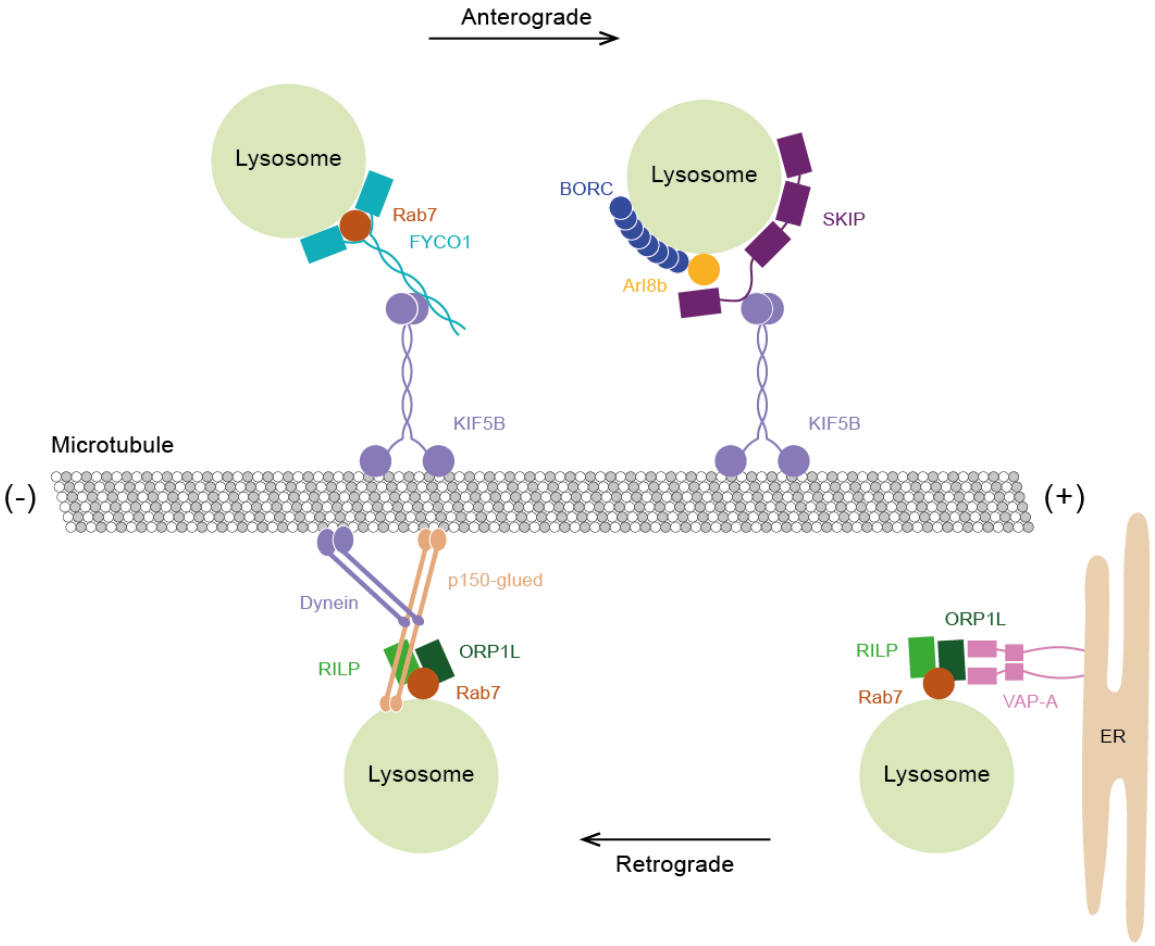

Figure 9: Main regulators of lysosome trafficking. (top) Anterograde transport regulated by Rab7-FYCO1 and BORC-Arlb8b-SKIP interaction. Both complexes recruit KIF5B to transport the lysosomes to the cell periphery. (bottom) Retrograde transport mainly regulated by Rab7-RILP complex. Rab7-RILP and ORP1L associate and recruit the dynactin subunit p150^{Glued} that mediates the dynactin transport. Under low cholesterol conditions, this association is impaired because ORP1L interacts with the ER protein VAP-A. Adapted from Pu et al. 2016

4.3.1. Motor proteins

4.3.1.1. Kinesins

Kinesins are microtubule-dependent motor proteins that use ATP hydrolysis to walk along microtubules. Several kinesin proteins (KIFs) have been implicated in the anterograde movement of lysosomes, for instance KIF5B (kinesin-1) (Rosa-Ferreira and Munro, 2011; Tanaka et al., 1998), KIF3A (kinesin-2) (Vihervaara et al. 2011), KIF1Bβ and KIF1A (kinesin-

3) (Guardia et al., 2016). These kinesins have been shown to drive lysosomes towards the plus-end of microtubules. Particularly KIF5B seems to play an important role in lysosomal anterograde transport. The depletion of this protein results in lysosomes clustering at the cell center (Rosa-Ferreira and Munro, 2011; Tanaka et al., 1998).

4.3.1.2. Dynein

The retrograde (centripetal) transport of lysosomes is driven by dynein in a dynactin-dependent manner. Dynein and dynactin are both multisubunit complexes. The linking of dynein to lysosomes depends on intermediate proteins and cargo adaptors, like BICD2 (bicaudal D homolog 2 protein) that stabilizes the dynein-dynactin interaction and mediates the linkage of cargos, such as intracellular compartments (Reck-Peterson, 2015). Moreover, $p150^{Glued}$, a dynactin subunit was shown to form a complex with regulators of lysosomal trafficking to mediate anterograde transport of this organelle (Rocha et al., 2009).

4.3.2. Upstream regulation of motor proteins by small GTPases

4.3.2.1. Arl8b

The small GTPase ADP-rybosylation factor like protein 8b (Arl8b) is an Arf-like protein, specifically localized at lysosomes. Arl8b is specifically recruited from the cytosol to the lysosomes by BORC (Pu et al., 2015). BORC is an octameric complex (composed of BLOS1, BLOS2, BLOS3, snapin, KXD1, MEF2BNB, myrlysin, lypersin and diaskedin) that associates to the cytosolic face of the lysosomal membrane.

Once on the lysosomal membrane, Arl8b recruits SifA and kinesin-interacting protein (SKIP) to lysosomes, through its RUN domain (Rosa-Ferreira and Munro, 2011). The Arl8b-SKIP complex recruits the kinesin-1 heavy chain KIF5B to lysosomes that are moved towards the cell periphery (Guardia et al., 2016; Rosa-Ferreira and Munro, 2011). Moreover, Arl8 can additionally recruit KIF1Bβ and KIF1A, proteins from kinesin-3 family, for centrifugal movement of lysosomes (Guardia et al., 2016). Arl8b is implicated in lysosomal trafficking, through its effector Vsp41, a subunit of the tethering HOPS complex (Garg et al., 2011).

Arl8b was recently implicated in cancer progression. The knock-down of Arl8b, in prostate cancer cells, prevents the anterograde transport of lysosomes, which decreases the secretion of proteases (Dykes et al., 2016), and reverses the invasive phenotype of cells

undergone EMT (Dykes et al., 2017). Moreover, depleted Arl8b cells do not grow as xenograft tumors in vivo (Dykes et al., 2016).

4.3.2.2. Rab7a

Rab7a regulates traffic from late endosomes to lysosomes. Rab7a recruits Rab7-interacting lysosomal protein (RILP), a cytosolic protein, by an interaction with RILP C-terminal region. The N-terminal region of RILP binds to the dynactin/p150^{Glued} subunit (Jordens et al., 2001). Thus, Rab7 promotes centripetal movement of lysosomes and a central lysosome positioning. The formation of the Rab7-RILP-p150^{Glued} complex is regulated by cholesterol levels, because it is only maintained under high levels of cholesterol through ORP1L, a cholesterol sensor. In low cholesterol conditions, ORP1L binds to VAP (vesicle-associated membrane protein), an endoplasmic reticulum protein and does not support the recruitment of dynactin/p150^{Glued} complex on lysosomes. Therefore, lysosomes are found at the cell center at high cholesterol levels and at the cell periphery at low cholesterol levels (Rocha et al., 2009). Although Rab7a is mostly responsible for retrograde transport of lysosomes, it can also participate in the anterograde transport through its other effector, FYCO1 (FYVE- and coiled-coil-domain-containing protein). FYCO1 is a motor adaptor that binds plus-end kinesins to distribute lysosomes to cell periphery (Raiborg et al., 2015). This interaction is dependent on the neuronal ER protein, protrudin, which transfers KIF5B to FYCO1 on lysosomes. Consequently, peripheral lysosomes fuse with the plasma membrane inducing protrusion formation in neuronal cells (Raiborg et al., 2015). Moreover, it was reported that ORP1L can also recruit kinesin-2, KIF3A, a plus-end directed motor protein that mediates centrifugal lysosome distribution (Vihervaara et al., 2011). Additionally, Rab7a interacts with other cytoskeleton components, such as vimentin, a protein member of intermediate filaments, and with the small GTPase Rac1, a key regulator of the actin cytoskeleton (Margiotta et al., 2017).

Steffan and collaborators (Steffan et al., 2010) have demonstrated, in vitro, that depletion of Rab7 leads to peripheral lysosome positioning, augmentation of cathepsin B secretion and increase of invasion, in prostate cancer cells. Conversely, when RILP is overexpressed the lysosomes are clustered at the perinuclear region and the invasion is decreased, which indicates that lysosome positioning plays a role in cancer invasion (Steffan et al., 2010). Additionally, they have provided evidence that Rab7 is a tumor suppressor, *in vivo*. Tumors derived from Rab7-silenced cells grow larger due to increased proliferation and invasion of cancer cells, and decreased apoptotic rates (Steffan et al., 2014). Furthermore, Rab7 silencing reduced cell-cell contact, which increased cell motility and invasion in melanoma

cells (Alonso-Curbelo et al., 2014), although cell proliferation was decreased in these cells. Conversely, Rab7 knock-down drecresed the recycling of MT1-MMP to the plasma membrane, which negatively impacted fibrosarcoma migration and invasion (Williams and Coppolino, 2011).

4.3.2.3. Rab27

Rab27 has two isoforms, Rab27a and Rab27b, that share 71% of amino-acid identity and are encoded by different genes (Ramalho et al., 2001). These proteins regulate secretion of exosomes from the multivesicular bodies/late endosomes (Ostrowski et al., 2010).

Rab27 localizes on lysosome-related organelles and late endosomes/multivesicular bodies and regulates the exocytosis of exosomes once secreted (Hendrix and De Wever, 2013). This protein participate in exocytosis by mediating fusion of secretory lysosomes with the plasma membrane (Neeft et al., 2005; Wu et al., 2001). Rab27 participates in exocytosis by mediating fusion of secretory lysosomes with the plasma membrane (Neeft et al., 2005; Wu et al., 2001). Both Rab27 isoforms are required for efficient secretion of exosomes in HeLa cells (Ostrowski et al., 2010). Silencing of both Rab27 isoforms reduced the number of exosomes, but did not change their protein content. However, the depletion of Rab27 a and b causes different phenotypes: Rab27a knock-down leads to bigger multivesicular bodies that are less motile than the control, whereas multivesicular bodies depleted for Rab27b clustered at the perinuclear region (Ostrowski et al., 2010). Interestingly, it has been reported that Rab27a inhibition reduces the secretion of a soluble nonexosome-associated molecule *in vivo*, the matrix metalloproteinase 9 (MMP9) (Bobrie et al., 2012).

Depletion of Rab27 expression has been shown to increase invasion of colorectal cancers (Dong et al., 2015). Contrary, inhibition of Rab27a significantly reduces secretion of exosomes and non-exosome-associated proteins, which consequently impairs the growth of metastatic mammary adenocarcinoma 4T1 in mice, and reduces its ability to metastasize. Although, the growth and spreading of the nonmetastatic mammary tumor type, TS/A, were not impaired by Rab27a inhibition (Bobrie et al., 2012). Depletion of Rab27a impared invadopodia formation and pericellular proteoslysis in head and neck carcinoma cells (Hoshino et al., 2013). Additionally, it has been shown that Rab27b overexpression is implicated in the increase of invasion, proliferation and acidification of extra-cellular matrix *in vitro*, and increased tumor volume and weight *in vivo* (Hendrix and De Wever, 2013). Interestingly, in bladder cancer, the deregulation of Rab27 and its interacting proteins are associated with muscle-invasive tumors in both Ta and Cis pathways, and could be linked to the loss of differentiation markers of these tumors (Ho et al., 2012a). Thus, the deregulated

expression of Rab27 suggests an alteration in lysosome-related organelles in bladder tumors. Indeed, Rab27 silencing was implicated with reduction of exosome secretion, and consequently invasion in grade 3 bladder cancer cells (Ostenfeld et al., 2014).

4.3.3. Other proteins

In addition to Rab7 and Rab27, other GTPases have been implicated in retrograde lysosome positioning, such as the Golgi localized Rab34 (Wang and Hong, 2002). This Rab protein interacts with RILP mediating dynein binding at the lysosome. Since Rab34 is mostly localized at the Golgi apparatus, this interaction suggests a close apposition of Golgi and lysosomal membranes (Pu et al., 2016). Furthermore, the overexpression of Rho and its effector ROCK results in peripheral lysosome distribution (Nishimura et al., 2002).

In addition to small GTPases, other proteins mediate retrograde lysosomal transport. The depletion of lysosomal transmembrane domain of LAMP1 and LAMP2 impairs the transport of lysosomes towards the microtubule organizing center, which is driven by dynein-dynactin, in a Rab7-independent manner (Huynh et al., 2007; Krzewski et al., 2013). Notably, the dynactin subunit $p150^{Glued}$ was less expressed in LAMP1 depleted cells (Krzewski et al., 2013), even though Rab7-RILP recruitment was not impaired (Huynh et al., 2007; Krzewski et al., 2013). Furthermore, the Ca^{+2}-sensor ALG-2 links the lysosomes to dynein-dynactin in response to changes in Ca^{+2} levels (Li et al., 2016).

4.3.4. Cellular regulation of lysosomal positioning

Several intracellular process play a role in lysosome positioning, such as acidification (Heuser, 1989; Steffan et al., 2009), autophagy/signaling (Korolchuk et al., 2011), membrane contact with other organelles (Jongsma et al., 2016; Raiborg et al., 2015; Rocha et al., 2009) and nutrient sensing (Korolchuk et al., 2011; Rocha et al., 2009).

4.3.4.1. pH

The cytoplasmic pH (pHi) interferes with lysosome positioning. When the cytosolic pH is acidic, the lysosomes move toward the cell periphery. On the contrary, alkalization by ammonium chloride, drives the lysosomes to the cell center through microtubules (Heuser, 1989). Although acidification of cytoplasm drives the lysosomes to cell periphery, it was reported that these peripheral lysosomes have a more alkaline intraluminal pH. The author's

hypothesis that this less acidic luminal pH is an impairment for the maturation of lysosomes, which mostly happens at the perinuclear region (Johnson et al., 2016).

4.3.4.2. Autophagy

Autophagy has been implicated in intracellular distribution of lysosomes. mTORC1 is activated upon translocation from cytoplasm to the lysosomal membrane, which inhibits autophagy signaling (Pu et al., 2016). Anterograde lysosome transport mediated by Arl8b and kinesin-3 family (KIF1Bβ and KIF2) increases mTORC1-lysosome association, and mTORC1 activation. Contrary, the depletion of these proteins cluster lysosomes at the cell center, which facilitates the fusion with autophagosomes (Korolchuk et al., 2011).

4.3.4.3. Membrane contact sites

Recent studies correlate the intracellular distribution of lysosomes and lysosome dynamics with membrane contact sites between lysosomes and the endoplasmic reticulum (Friedman et al., 2013; Jongsma et al., 2016; Raiborg et al., 2015; Rocha et al., 2009; Vihervaara et al., 2011). Membrane contact sites are zones of close apposition between membranes of two different organelles (10-20 nm), with no fusion, in order to exchange lipids and Ca^{2+} (Holthuis and Levine, 2005). Interestingly, the extension of contact site between endoplasmic reticulum and the endosomal vesicles seems to depend on their maturation. Indeed, early endosomes form tight, but less extended membrane contact sites than recycling endosomes. Moreover, late endosomes and lysosomes are almost completely bound by endoplasmic reticulum membranes (Friedman et al., 2013), which suggests that membrane contact sites could play a role in lysosome maturation.

4.3.5. Ubiquitination

Recently, an ubiquitinase was shown to act as a scaffold for lysosomes at the cell center. The endoplasmic reticulum protein RNF26 mediates ubiquitin ligation and recruits sequestosome 1 (SQSTM1), a ubiquitin biding protein to the endoplasmic reticulum membrane. This complex attracts lysosomes that stay retained at the perinuclear region, probably to complete their maturation, as shown by extracellular dye endocyosis and delivery to lysosomes as well as EGFR degradation (Jongsma et al., 2016). The deubiquitinase protein, USP15, dissociates the ubiquitin ligation and releases the lysosomes for fast transport to the cell periphery (Jongsma et al., 2016).

5. Cell migration and invasion

Cell migration and invasion are physiological processes, which cells use to move and penetrate into tissues. Invasion and migration are processes based on complex mechanisms that require highly adaptive capacity of cells. This adaptive response of invading cells is called plasticity. Cellular plasticity is critical for morphological changes during transitions, for instance epithelial mesenchymal transition (Krakhmal et al., 2015; Thiery et al., 2009). The transitions are tightly linked to cell movement because during migration and invasion cells have to constantly adapt to changes in microenvironment substrate, change their shape and stiffness and communicate with the neighbor cells (Friedl and Wolf, 2003). Invasion is the penetration of tissue barriers that requires proteolysis of extracellular substrate, in addition to migration and adhesion (Krakhmal et al., 2015). These processes occur in physiological conditions, for instance during embryogenic development and wound healing. However, migration and invasion are hallmarks of cancer disease (Hanahan and Weinberg, 2000). During metastasis, cancer cells detach from the primary tumor and the tumor-associated stroma and move towards the lymphatic and blood vessels where they reach the circulation and distant organs (Krakhmal et al., 2015).

5.1. Steps of single cell migration and invasion

Single cells can detach from the collective cell cluster and undergo individual cell migration and invasion. Individual cell movement is coordinated within the cell body. The cell movement occurs in a synchronized, contractile and pulsatile manner, which allow the cell to adhere, generate traction force and glide (Friedl and Alexander, 2011) (Figure 10A).

The model of cell migration proposed by Friedl and Alexander in 2003 consists of five steps: 1) The initial propulsion and elongation of the membrane protrusions are driven by actin cytoskeleton. The small GTPases Cdc42 and Rac1 control the assembly of signaling proteins and actin filaments at membrane protrusions called pseudopods. 2) The pseudopods are responsible for the extracellular matrix recognition and binding through recruited of integrins that bind to the extracellular matrix and form the focal adhesions (Friedl and Alexander, 2011; Odenthal et al., 2016). The focal adhesions are regions of cluster of integrins in close apposition between the cellular membrane and the substrate (~20nm) (Friedl and Alexander, 2011; Friedl and Wolf, 2003). 3) Soluble proteases are secreted for focalized proteolysis of the extracellular matrix. 4) Actin contractility at the cell rear generates forces of traction for the final step, 5) the cellular rear-end retraction.

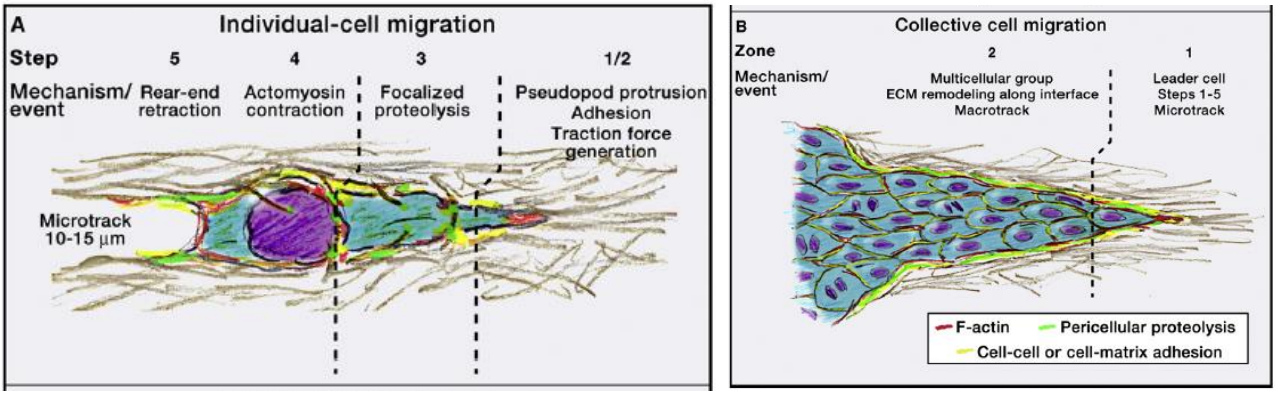

Figure 10: Cell migration and invasion. A. the 5 steps model of individual cell migration that requires change in cell shape, recruitment of integrins and contractility and proteolysis during invasion. **B.** Collective cell migration from the path-generating cells and cells from the inner and trailing cells. Adapted from Friedl and Alexander 2011.

The first barrier that epithelial cancer cells have to cross during invasion is the basement membrane. This membrane surrounds nearly all tissues, providing structural support and protection. It is mainly composed of self-assembled collagen type IV and laminins. The breaching of the basement membrane involves: i) proteolytic degradation by MMPs; ii) displacement of basement membrane by mechanical forces and iii) abnormal synthesis of basement membranes components around tumors (Glentis et al.).

Once the basement membrane is breached, the invasive cells reach the stroma. The stroma is composed of extracellular matrix and some cell types, such as fibroblasts and immune cells (Clark and Vignjevic, 2015) (Figure 11). The most abundant component of the extracellular matrix is collagen type I. During cancer, the stroma becomes stiffer due to changes in collagen. The amount of this protein increases, their fibers become straighter and aligned in parallel with the tumor edge (Conklin et al., 2011). The reorganization of the stroma is mainly mediated by cancer-associated fibroblasts (CAFs) that secret extracellular matrix, enzymes for the proteolysis of the stroma (for instance MMPs) and growth factors (Attieh and Vignjevic, 2016; Clark and Vignjevic, 2015). Cancer-associated fibroblasts also exert mechanical forces by widening pores in the extracellular matrix, which favors cell movement (Attieh and Vignjevic, 2016). Indeed, it was reported that CAFs form junctions with cancer cells to mediate force transmission and favor collective cell migration (Labernadie et al., 2017).

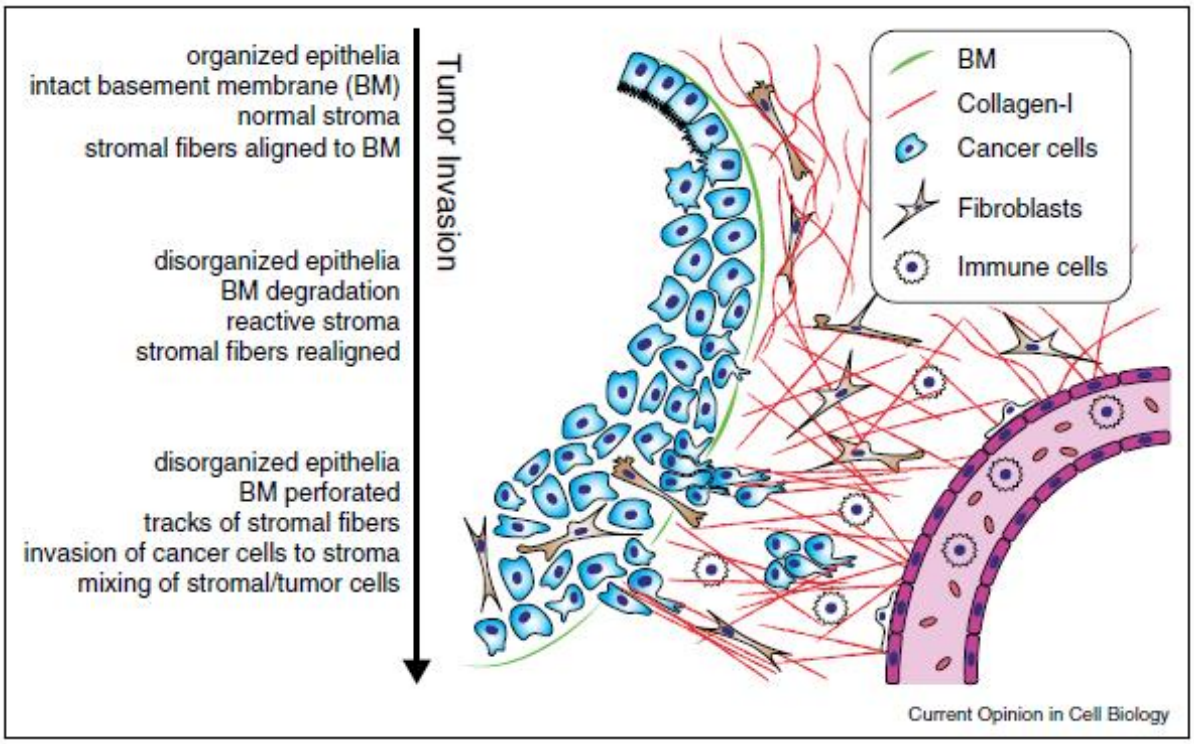

Figure 11: Tumor invasion. First, the cells proliferate without invading, next changes in tumor cells present changes in cell shape. Then, the tumor-associated stroma becomes active and help the cancer cells to breach the basement membrane and undergo invasion. Adapted from Clark and Vignjevic 2015.

5.1.1. Main players of migration and invasion

Small GTPase proteins from Rho family, Rho, Rac and Cdc42, are crucial to cell migration, because they control the actin cytoskeleton and regulate focal adhesion formation (Friedl and Alexander, 2011; Parri and Chiarugi, 2010; Qadir et al., 2015). Cdc42 regulate the assembly of complexes of proteins to mediate actin polymerization and membrane protusion formation. Cancer cells often overexpres Cdc42, which leads to increased cell migration and invasion (Qadir et al., 2015). RhoA and its effector Rho-associated serine/threonine kinase (ROCK), mediate stress fibers assembly and contraction to generate forces during migration. The contraction of actin is mainly regulated by myosin II. While Rac proteins regulate actin polymerization at membrane protusions (Parri and Chiarugi, 2010). Increased expression of these proteins are commonly associated with cancer invasion and progression (Porter et al., 2016).

The cluster of integrins form focal adhesions that are essential for mechanosignaling and force generation during migration (Friedl et al., 2011). Integrin receptors are the major proteins responsible for the adhesion and crosstalk between cells and the extracellular matrix. They are heterodimers formed by α and β subunits. The association of 1 of the 9 β subunits with the 24 types of α subunits are responsible for the variety of specific binding with different substrates (Alberts et al., 2002). Thus, the integrin clusters present in a specific focal adhesion depend on the extracellular matrix substrate. For instance, α2β1 integrins bind to collagen (Maaser et al., 1999), while α5β1 and αvβ3 integrins bind to fibronectin (Cukierman et al., 2001; Leavesley et al., 1992) and α6β1 and α6β4 bind laminin (Rabinovitz and Mercurio, 1997). After endocytosis integrins can either be recycled to the plasma membrane or be degraded. For instance, in cancer cells, cell survival and proliferation signaling receptors are often fast recycled to the plasma membrane, instead of being degraded. This support cell migration and cancer progression (Goldenring, 2013). Moreover, integrins can engage or impair growth factors through signaling crosstalk (Ivaska and Heino, 2011). Recently, it was shown that clathrin-coated pits support cell migration in 3D by providing an anchorage site to collagen (Elkhatib et al., 2017). These structures are engaged by integrins and accumulate on collagen fibers.

The matrix metalloproteinases (MMP) are the major proteases responsible for extracellular matrix degradation and remodeling. These proteases are secreted as soluble proenzymes that are activated in contact with the extracellular matrix. They are recruited to the cell surface by integrins. For instance, the collagenase MMP1 binds α2β1 integrins (Dumin et al., 2001), the gelatinase MMP2 binds αvβ3 (Brooks et al., 1998), and the collagenase membrane-type metalloproteinase-1 (MT-MMP1, also know as MMP14) binds to β1 and β3 integrins (Gálvez et al., 2002). Moreover, the MMPs regulate extracellular growth factors (e.g. epidermal, hepatocyte and fibroblast growth factors) by activating (Mu et al., 2002), inactivating (Dean et al., 2008) or degrading (Sounni et al., 2010) these components.

5.1.2. Mesenchymal migration and invasion

Mesenchymal migration is the movement of mesenchymal cells and cells undergone EMT. This migration is considered as a slow migration process (0.1-2 μm/min) and is characterized by the five steps model. It. Cells that undergo this process have a fibroblast-like, spindle-shaped morphology. This type of migration is manly found in cells from connective tissue tumours, such as fibrosarcomas and gliomas. EMT is characteristic for poorly differentiated

epithelial tumors (Friedl and Wolf, 2003). In these cells, cell-cell E-cadherin junctions are weaken or lost, whereas the activity of integrins and proteases are retained (Krakhmal et al., 2015; Thiery et al., 2009).

5.1.3. Ameoboid migration

Amoeboid migration requires less adhesion from the cell. In this process, cells behave like the amoeba *Dictyostelium discoideum*, which is characterized by cycles of expansion and contraction, high deformability and low adhesion to the extracellular matrix. The amoeboid migration can be fast or slow (0.1-20 µm/min), and instead of degrading, cells circumnavigate the extracellular matrix. Amoeboid migration is common for lymphoma, myeloic leukaemia and lung carcinoma cells (Friedl and Wolf, 2003).

5.2. Collective migration and invasion

Cells move collectively forming strands, clusters or streams. In physiological conditions, collective cell movement occurs during embryological development, development of glands and ducts of mammary tissue angiogenesis and wound healing. In tumors, two forms of collective movement are found: 1) the protruding sheets that stay attached to the primary tumor promoting a local invasion; and 2) cells clusters that detach from the primary tumor to invade the interstitial tissue (Friedl and Alexander, 2011; Krakhmal et al., 2015). Collective cell movement requires cell-cell adhesion to synchronize movements of the neighboring cells that form the multicellular contractile body. Thus, cadherin-mediated adhesion is essential to collective migration. Intercellular force transmission is generated by cadherin and cortical actin dependent cell-cell junctions (Harris and Tepass, 2010; Hegerfeldt et al., 2002), while integrins generate traction forces through binding to extracellular matrix. The inner and trailing cells of the contractile body move passively, dragged by the leading cells, called path-generating cells (Figure 10B). The path-generating cells promote migration traction via pseudopods and proteolysis of adjacent extracellular matrix (Friedl and Alexander, 2011; Friedl and Wolf, 2003).

6. Geometrical confinement as a tool to study cells under normalized conditions

The observation of early abnormalities in cell architecture could be a potent tool to identify and characterize cancer progression. However, systematic studies on the organization and relative positioning of intracellular organelles are difficult because, on the one hand, *in vivo* approaches are limited by the access of the samples, and on the other hand, *in vitro* cultured cells display a strong morphological cell-to-cell variation (Figure 12). *In situ* cells are confined within a microenvironment and are highly sensitive to mechanical forces and geometrical organization (Théry, 2010) (Figure 12). In classical *in vitro* cultures, these parameters are abrogated. Cell-cell variation occurs due to differences in cell-matrix adhesion, cell-cell contact, and dynamic shape changes during migration (Friedl and Alexander, 2011; Krakhmal et al., 2015). To overtake this difficulty, a new approach has been developed in our laboratory that combines normalization of single cells by bioengineered micropatterned surfaces with a mathematical method based on kernel density estimation (KDE) that allows to distinguish differences in cell organization in normalized cells (Schauer et al., 2010a).

6.1. Normalization of cell adhesion by micropatterning

Innovative micropatterning technique is employed to normalize the adhesion geometry of cells by bioengineered micropatterned surfaces (Théry et al., 2006a). Micropatterning represents a minimal cell culture system, where cells adhere to micro-fabricated surfaces coated with extracellular matrix proteins, such as fibronectin or collagen, that forces cells to adopt a given, defined shape, reducing cell-to-cell variation and mimicking cell confinement in tissues (Gumbiner, 1996; Théry, 2010). This technique was introduced in cell biology 50 years ago (Carter, 1967) and and has recently became widely popular in biomedical research (Théry, 2010). Micropatterning methods have been used to study, for instance, the role of cell adhesion and cell-cell interactions in cell polarity (Desai et al., 2009; Théry et al., 2006b).

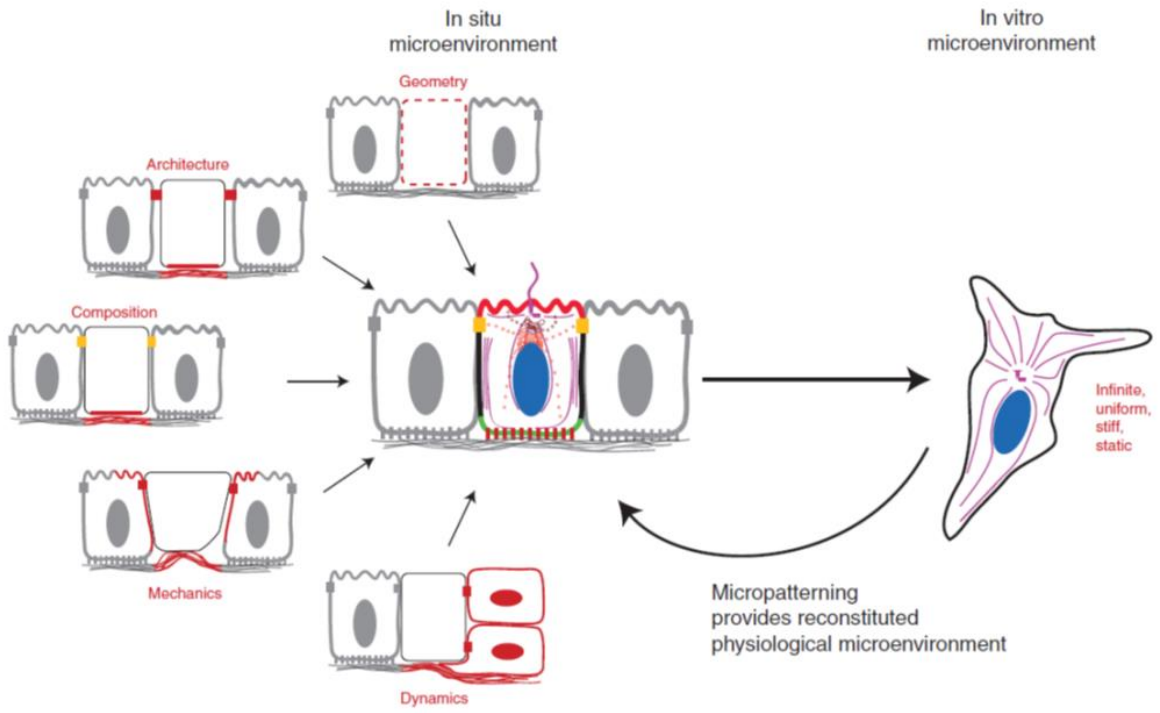

Figure 12: The cell microenvironment in situ and in vitro. (left) *In situ* cells respond to several parameters of the microenvironment mainly imposed by adjacent cells (in gray), while cells in classical *in vitro* culture (right) loose mechanical and chemical cues. Micropatterning provides some of these parameters to reconstruct a tissue-like organization. Reproduced from Théry 2010.

6.1.1. Control of the internal cell organization

Micropatterns adhesive regions allow the control of intracellular organization. Asymmetrical micropattern shapes present an adhesive and a non-adhesive area (Figure 13A). This asymmetry leads to anisotropic distribution of adhesion proteins, such as integrins, and a polarized arrangement of both actin and microtubule cytoskeletons (Théry et al., 2006a). Cortical actin accumulates at the adhesive regions, whereas F-actin forms stress fibers in non-adhesive areas. The adenomatous polyposis coli (APC) protein participates in the connection between actin and microtubules (Näthke et al., 1996) and is distributed at adhesive areas. Microtubules stop growing when they reach APC enriched regions, while they continue to grow in non-adhesive areas (Figure 13B). Additionally, intracellular compartments have a defined localization at the subcellular level. Golgi apparatus and centrosome are found close to the cell center, while the nucleus is off-centered towards non-adhesive region (Théry et al., 2006a). Moreover, early endosomes, lysosomes and ER exit sites are spatially organized in crossbow-shaped micropatterns (Schauer et al., 2010a)

(Figure 13C). Thus, the micropatterning technology enables the study of the average cellular architecture by cell normalization.

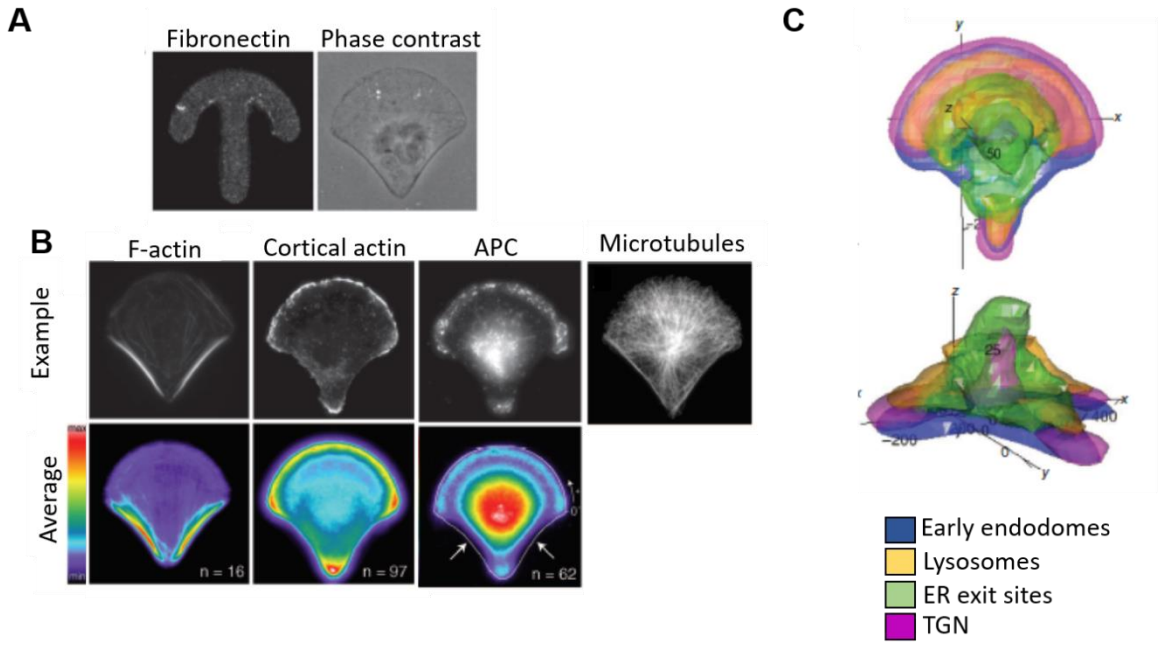

Figure 13: Control of intracellular organization. A.[1] Crossbow-shaped micropattern stained for fibronectin and representative cell visualized in phase contrast microscopy. **B.**[1] (top) Representative cell stained for F-actin, cortactin, APC and microtubules. (bottom) average intensity projections of tens of cells. **C.**[2] 50% contour density map (of the kernel density estimation) showing stable intracellular organization of early endosomes, lysosomes, ER exit sites and TGN in tens of cells. Adapted from 1. Théry et al. 2006 2. Schauer et al. 2010

Although micropatterning mimics geometrical constains that are encountered in tissue, this artificial system lacks control of other parameters, for instance the dynamics and composition of the microenvironment (Théry, 2010). Cells are highly responsive to their microenvironment, but these parameters cannot be taken into account when culturing cells on adhesive micropatterns.

6.2. Quantification of cell organization by density mapping

Organelles are intimately linked to the cytoskeleton and are highly dynamic, thus their intracellular distribution varies constantly in unconstrained cells (Schauer et al., 2010a). The micropatterning method allows normalization of cell shape (Théry et al., 2006a). Fluorescent images of tens of cells can be superposed and parameters, such as average and maximum intensity projections can be used to study intracellular distribution of structures. However, this analysis does not take into account the 3 dimensional distribution of the intracellular compartments, which limits their quantitative comparison between different conditions (Duong et al., 2012). Therefore, a computational approach that is based on kernel density estimation (KDE) has been developed in our laboratory. This quantitative method provides a three-dimensional (3D) density map that reveals the average intracellular distribution of compartments and allows systematic study and quantitative comparison of the organization of intracellular compartments (Schauer et al., 2010a).

In brief, 3D images of several cells, in which organelles are stained by fluorescence, are acquired. These images are segmented with a specific profile for each studied compartment providing the coordinates of each segmented structure. All coordinates are aligned using the fluorescent staining of the micropattern. A Gaussian function (kernel) is centered at each segmented structure (coordinate) and summed forming a cloud of densities that represents the probability of organelle positioning throughout the cell. This calculation thus provides a three-dimensional density map in which several probability contours can be visualized. These contours represent the smallest area in which a given percentage of organelles can be found, for example the 50% contour defines the smallest region where 50% of the fluorescently stained organelles are located (Figure 14A). The statistical error for density estimation is virtually unchanged after 20-50 cells (Schauer et al., 2010a) (Figure 14B-C).

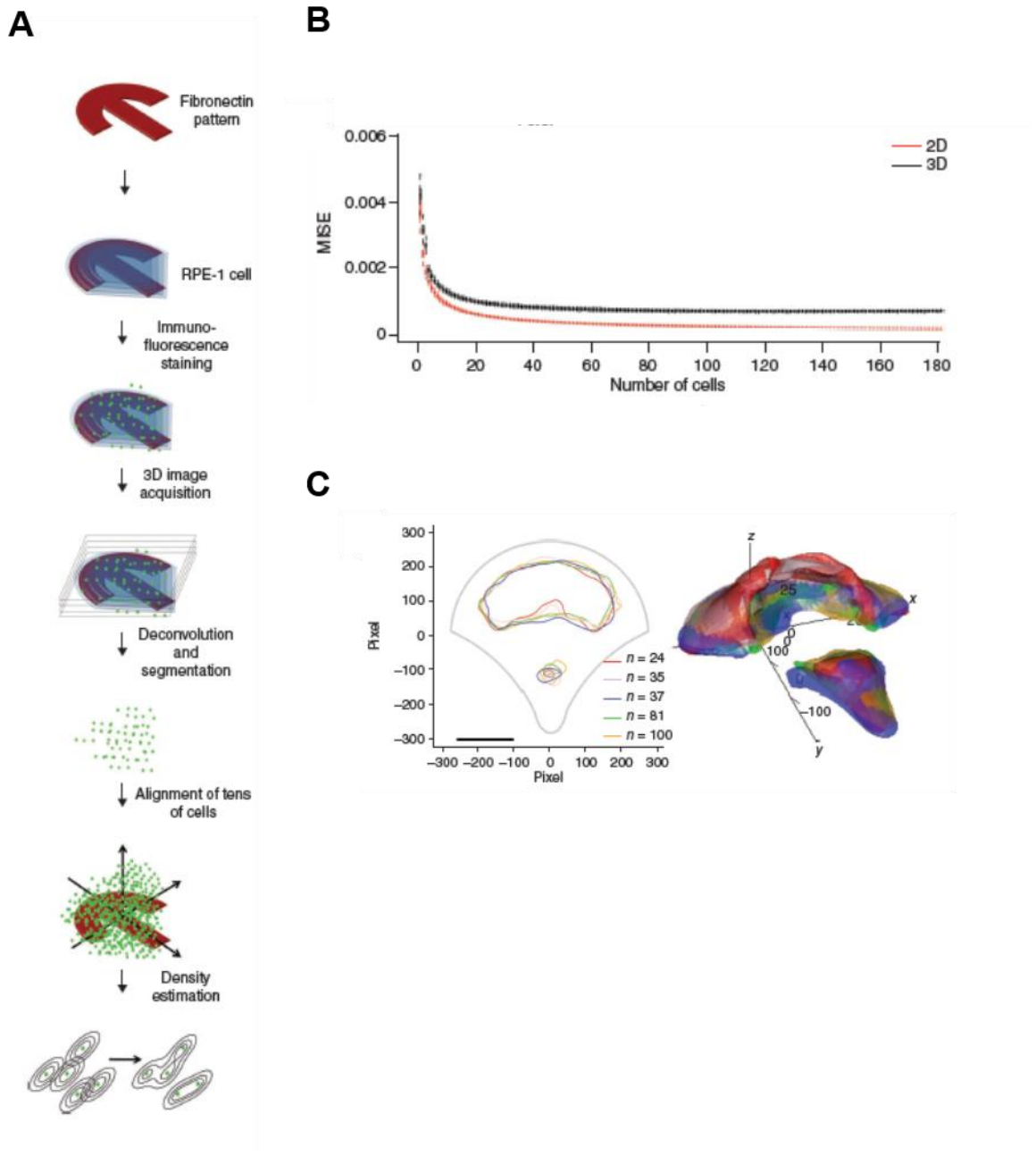

Figure 14: Density estimation of intracellular compartments. A. Outline of experimental procedure. B. Estimated statistical error for 2D and 3D. Stabilization of variability from 20 cells. **C.** Overlap of the 50% contour of the 2D and 3D estimation for five independent experiments; color-code for each independent experiment. Adapted from Schauer et al. 2010

Importantly, using this approach, it has been found that intracellular compartments, for instance lysosomes and Golgi apparatus, are well organized and that their positioning is stable and reproducible (Schauer et al., 2010a). Moreover, the kernel density estimation allows statistical unbiased comparison and quantification of multivariate data (Duong et al., 2012).

This approach provides the unique possibility to reveal how different compartments are organized in the cellular space. For instance, it has been shown that cell adhesion defines the topology of endocytosis in retinal pigment cells (RPE1) (Grossier et al., 2014a).

Kernel estimation requires cells to have a spatial normalized shape. Furthermore, it is ideal to study structures whose coordinates can be resolved in independent data points. Thus, the application to continuous structures, like the cytoskeleton, is not optimal (Duong et al., 2012).

OBJECTIVES

Objectives

Cancer is a multifactorial disease responsible for around 16% of deaths worldwide. The alteration of cell morphology is a hallmark of cancer cells. Indeed, cancer cells undergo changes in cell polarity and cell-cell interactions, which favor cell invasion and metastasis. Nonetheless, very little is still known on changes in intracellular compartments during cancer progression. This is because systematic studies on the organization of intracellular organelles are challenging due to strong morphological cell-to-cell variations in classical cell culture.

The global goal of my PhD thesis was to study changes in subcellular organization that occure during cancer progression. We used the model of bladder cancer, the 9th most common cancer worldwide, because bladder carcinomas show great diversity, giving rise to many morphologically distinct phenotypes. We took advantage of the micropatterning method combined with the technique of spatial density maps of intracellular compartments to compare intracellular organization between healthy cell and bladder cancer derived cell lines.

The first aim of this project was to identify specific alterations in intracellular architecture in bladder cancer cell lines representing different grades and stages of desease progression. The second aim was to characterize the impact of intracellular changes that we found in transformed cells on invasion that is caracteristic for cancer. Finally, we started a characterization of the molecular mechanisms leading to intracellular changes.

RESULTS AND DISCUSSION

1. Cell adhesion on micropatterned substrates

Several cell lines derived from different bladder cancers are available and are representative of the diversity of these tumors (Earl et al., 2015). In this project, we compared intracellular organization of bladder cancer cell lines representing different grades and stages of bladder cancer progression and normal human urothelial (NHU) cells. NHU are primary noncancerous bladder cells obtained from ureter specimens used as control for *in vitro* experiments (Southgate et al., 1994). Bladder cancer cell lines have been classified by: i) grades, concerning their similarity to normal cells, and ii) stages, depending on the degree of invasion of the primary tumor (Knowles, 2008). The non-muscle-invasive bladder cancer cell lines MGHU3 and RT112 are classified as stage Ta (papillary tumors) and grade 1 and 2, respectively, while muscle-invasive bladder cancers are represented by grade 3 cell lines, KU19-19 stage T3 (invasion of adipose tissue) and JMSU1 stage T4 (invasion of nearby organs). These cells present major morphological differences (Figure 15A), which make it difficult to systematically characterize intracellular changes. The micropatterning method enables standardization of cell shape and intracellular organization (Théry et al., 2006a). In addition, the density map estimation allows quantification of organelle distribution (Schauer et al., 2010a) (figure 15B).

In order to make cells properly spread on micropatterned surfaces, the coverslides need to be coated with an adhesive substrate, such as the extracellular glycoprotein fibronectin. We tested the adhesion of cancer cells on crossbow-shaped micropatterns coated either exclusively with fibronectin or with a mix of fibronectin and collagen I or fibranectin and concanavalin A. Collagen I is an abundant protein in human organism; it is synthesized intracellularly and participates in cell-matrix adhesion after secretion (Di Lullo et al., 2002). Concanavalin A is a lectin that binds sugars that are present on glycoproteins and glycolipids. We found that a mixture of 50 µg/ml of fibronectin and 100 µg/ml of concanavalin A allowed all bladder cancer cells to attach and spread on crossbow-shaped micropatterns as judged by staining of the actin cytoskeleton with phalloidin (Figure 15B). All following experiments have been performed using the established mixture of adhesion molecules.

All cells of one cell line presented a similar shape and comparable intracellular organization when well-spread on micropatterns, which was not obvious in classical cell culture (Figure 15C, example of JMSU1 cell line fluorescently stained for lysosomes with Lamp1 antibody). In order to confirm that the cell volumes of all tested baldder cancer cell lines were comparable to NHU cells, we measured the diameter of cells in suspension using automated analysis from standard trypan blue technique (Countess automated cell counter - Invitrogen).

There were no significant differences between NHU control cells and bladder cancer cells lines, indicating that cell size was comparable (Figure 15D) between cell types.

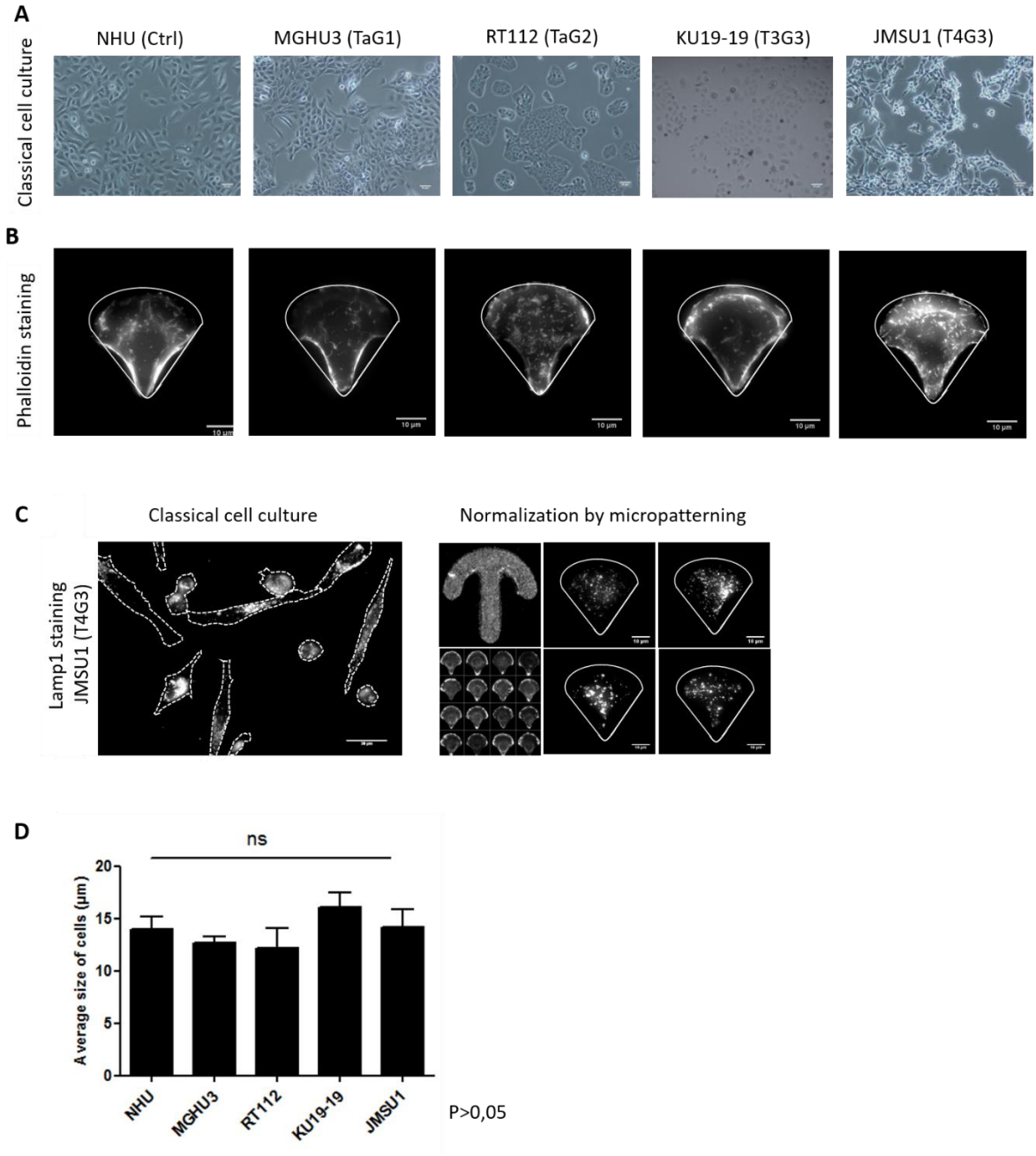

Figure 15: Standardization of bladder cells by micropatterning. A. Morphological differences between NHU control cells and bladder cancer cells in classical cell culture. Scale bar 50 µm. **B.** Cells well spread on micropatterns. Actin stained by Phalloidin. **C.** JMSU1 (T4) cells stained for lysosomes (Lamp1) on classical culture (left) and normalized using crossbow shape micropattern (right). Cells on micropatterns have similar shape and Lamp1 distribution. Scale bar: left 30 µm, right 10 µm. **D.** Average diameter of analyzed cells in µm. No significant differences between NHU control cells and bladder cancer cells. ns, p>0.5 in a Student's t-test.

Discussion:

In order to quantitatively compare different cell lines, it is crucial that cells are adherent and well spread on micropatterns. Different substrates were tested to optimize adhesion. Some cell lines, for instance RT112 (TaG2), were hardly adherent. The best results were found with a mixture of fibronectin and concanavalin A. This is probably due to the fact that concanavalin A binds sugars of the glycolipids and glycoproteins present on the cell membrane, which should increase the adhesion (Eagles et al., 1975).

Micropatterning provides geometrical constriction, that is typical for cells in tissues (Théry, 2010). It has been reported that normalized cells have normal cell cycle (Théry et al., 2006a). All analyzed cell types were successfully cultured and well spread on crossbow shape micropatterns, as juged by actin staining. Moreover, all analyzed cells revealed a comparable shape and cell size.

2. Changes in organelle organization during bladder cancer progression

To systematically characterize how intracellular organization changes in cancer progression, we have analyzed the positioning of major cellular compartments, such as lysosomes, mitochondria, Golgi apparatus, autophagosomes and peroxisomes, in NHU cells and bladder cancer cell lines derived from patients with different grades and stages of cancer progression. These organelles have been shown to be altered in cancer, however very little is known about alterations in their positioning during cancer.

After full adhesion on micropatterns, cells were fixed and fluorescently marked for intracellular compartments. We visualized the lysosomes (anti-Lamp1 antibody), the mitochondria (Mitotracker dye), peroxisomes (anti-ABCD3 antibody), the nucleus (DAPI) and the Golgi apparatus (anti-GM130 antibody). Micropatterns were fluorescently stained using fibrinogen to align all analyzed cells according to the micropattern. Then, the quantification of average cellular organization of the above compartments was performed using density maps. The analysis was based on more than 50 cells from three independent experiments. An 'average' density map was calculated for each compartment and each cell type using the 50% probability contours for visualization. 50% contour defines the smallest area where 50% of an organelle of interest is located. Additionally, a fluorescent image of a representative cell has been selected to exemplify the cellular compartment analyzed. Average numbers of identified structures per cells were calculated from the segmentation data and bilateral Student t-tests were performed to access the significance of difference. For the following analysis we considered: ns (non significant, $P > 0.05$); * ($P<0.05$); ** ($P<0.01$); *** ($P<0.001$).

2.1. Mitochondria

The function and morphology of mitochondria have been reported to be altered in cancer cells (Cavalli et al., 1997; Zong et al., 2016). Thus, we studied the mitochondrial distribution in bladder cells. These organelles were fluorescently stained using Mitotracker, a cell-permeant dye that contains a mildly thiol-reactive chloromethyl group that labels the mitochondria fluorescently (Figure 16A). Density maps of mitochondria showed a change in distribution towards the cell periphery as compared to NHU cells (Figure 16B compare

orange density maps to control in white). The most striking difference was observed in JMSU1 (T4G3) cells.

Moreover, increased number of mitochondria was observed in kidney cancer (Hasumi et al., 2012). Thus, we investigated if the number of mitochondria per cell was altered in bladder cancer cells. We indeed observed a significant increase in the number of the mitochondria in all analyzed cancer cells lines compared to control cells (Figure 16C).

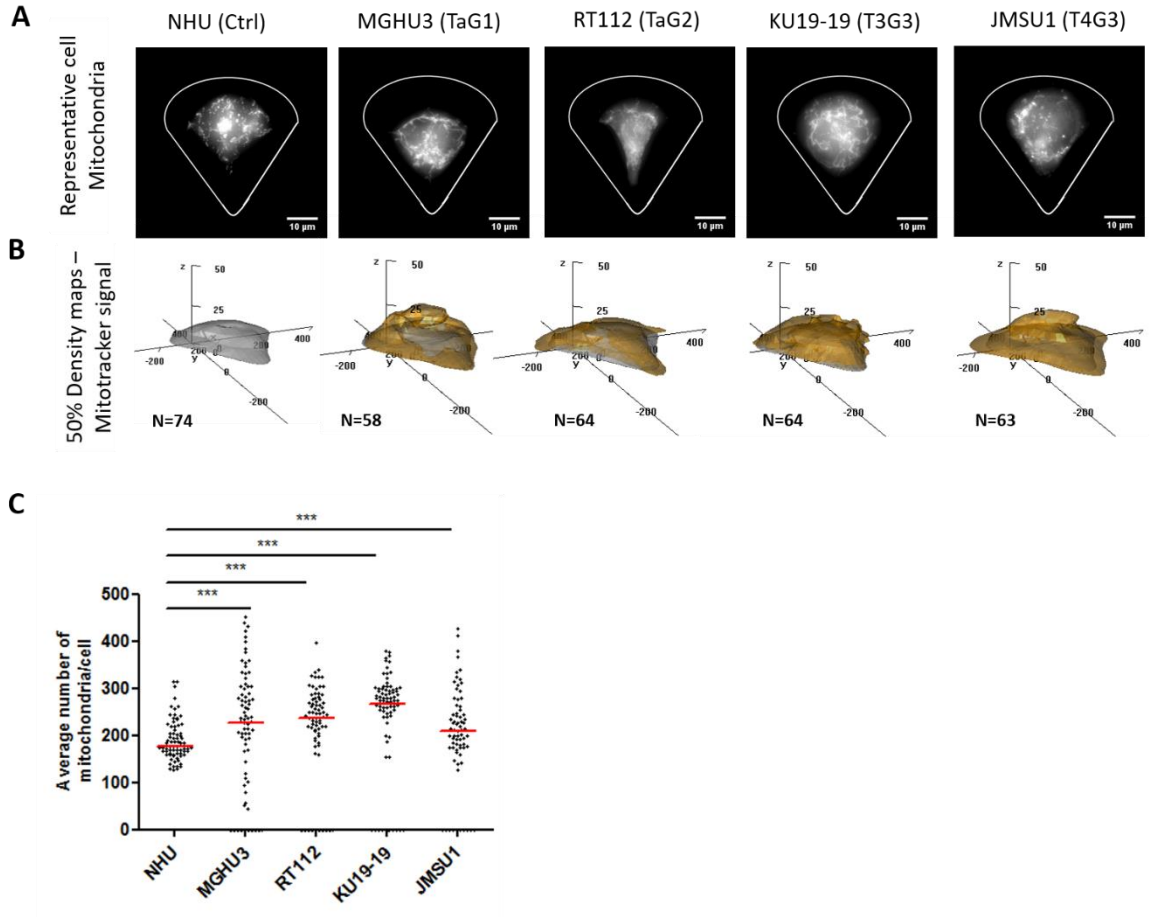

Figure 16: Alterations of mitochondria in bladder cells. A. Representative normalized single cell image of fluorescently stained mitochondria using Mitotracker dye for each analyzed bladder cell line. Scale bar 10µm. **B.** 50% contour of the 3D density maps quantifying mitochondria distribution (in orange), as compared to NHU control cells (in white). Mitochondria distribution is more peripheral in cells representing stage T4 of bladder cancer. 50% contour represents the smallest area where 50% of the labeled structures are found. N is the number of cells. **C.** Average number of mitochondria obtained from segmentation data. Significant increase of mitochondria per cell in all bladder cancer cells lines. Red lines represent median. ***, $p<0.001$ in a Student's t-test.

2.2. Peroxisomes

The expression of the peroxisome proliferator activated receptor γ (PPARγ) was shown to be increased in luminal muscle invasive bladder cancers (Choi et al., 2014). Additionally, it has been shown that increased number of peroxisomes could initiate or promote several cancers (Keller et al., 2000). Thus, we investigated the distribution and the number of peroxisomes in bladder cells (Figure 17). Peroxisomes were stained with an antibody recognizing ABCD3, an ATP-binding cassette sub-family D protein (Figure 17A). The average number of peroxisomes per cell was significantly reduced in MGHU3 (TaG1). Conversely, a significant increase was observed in RT112 (TaG2) and KU19-19 (T3G3) cells. Surprisingly, no significant changes were observed in JMSU (T4G3) cells (Figure 17C). Density maps of ABCD3 showed very different profiles for the four cell lines studied. In cells representing grades 1 and 2 (MGHU3 and RT112, respectively), no alterations in distribution, compared to the control, were observed (Figure 17B, compare red density maps with NHU in white). However, in grade 3 cells (KU19-19 and JMSU1), the peroxisomes were dispersed at the cell periphery.

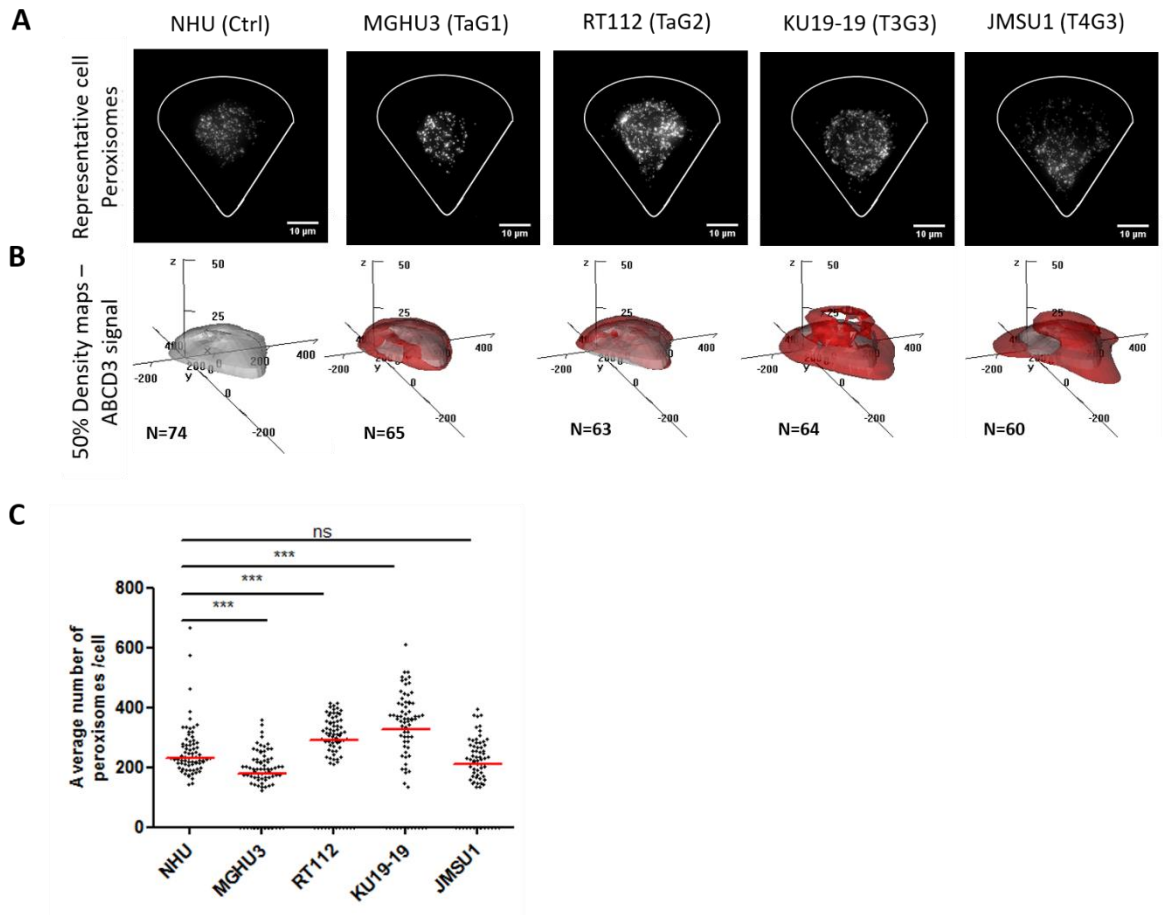

Figure 17: Changes in peroxisomes positioning in bladder cells. A. Representative cell fluorescently stained for peroxisomes using anti-ABCD3 antibody. Scale bar 10µm. **B.** 50% contour 3D density maps quantifying peroxisomes distribution (in red) in comparison with NHU (in white). Peroxisome distribution is more peripheral in cells representing grade 3 of bladder cancer. N is the number of cells **C.** Average number of peroxisomes per cell. MGHU3 (TaG1) presented less peroxisomes than control cells. An increase is observed in RT112 (TaG2) and KU19-19 (T3) cells. However, no significant changes were observed in JMSU1 (T4G3) cells. Red lines represent median. ns, $p>0.5$ and ***, $p<0.001$in a Student's t-test.

Discussion:

Our results reveal a significant increase in the number of mitochondria in all analyzed bladder cancer cells. Notably, the accumulation of functional mitochondria was reported to be increased in kidney cancer (Cavalli et al., 1997). Thus, our data suggest that increased mitochondria could also be a phenotype of bladder cancer. We additionally observed that JMSU1 (T4G3) cells, representing the most invasive stage of bladder cancer, display a peripheral distribution of mitochondria, as compared to NHU cells. It would be interesting to investigate whether these mitochondria are functional and if their activity is upregulated in bladder cancer cells.

The number of peroxisomes was significantly decreased in MGHU3 (TaG1) cells and no significant changes were observed in JMSU1 (T4G3) cells. Interestingly, MGHU3 (TaG1) cell were classified as basal-like tumors, while JMSU1 (T4G3) cells were considered as non-basal like cancers (Rebouissou et al., 2014). Because it was shown that the expression and activity of PPARγ are increased in luminal muscle invasive bladder cancers (Choi et al., 2014) and PPARγ induces the increase in the number of peroxisomes, our results sugest that the numbers of peroxisomes could indeed correlate with basal/luminal phenotypes in bladder cancer cell lines. The distribution of peroxisomes was similar in NHU cells and grades 1 and 2 cell lines. Remarkably, the positioning of peroxisomes is peripheral in cells representing grade 3. Interestingly, it was shown that peroxisome movement is mediated by binding to early endosomes (Salogiannis et al., 2016). Thus, it would be interesting to study if the distribution of early endosomes correlates with that of peroxisomes and is altered in bladder cancer cells.

Together, these results show that intracellular compartments are differently organized in bladder cells as compared to normal bladder cells.

3. Lysosomes

Increased protease secretion from lysosoms has been implicated in many cancers. In prostate cancer, peripheral lysosomes have been found to favor extracellular degradation and acidification of the extracellular milieu (Dykes et al., 2016; Steffan et al., 2009, 2010). To study the lysosome/late endosomal compartment, we analyzed Lamp1-positive structures (that we refer as lysosomes) (Figure 18A) using density-based analysis. In NHU control cells, the lysosomes (density maps in turquoise) were found at the cell center. However, lysosomes became more peripheral in cells representing grade 2 and 3 (Figure 18B compare turquoise density maps to control density map in white). This analysis was based on more than 60 cells per cell type. A multivariate two-sample statistical test, developed in our lab, allows a nonparametric comparison of density maps and thus organelle distribution (Duong et al., 2012). This test indicated that lysosome distribution was significantly different between bladder cancer cells and NHU cells (Table 01).

Although no differences in the number or volume of lysosomes were previously described in cancer cells, alterations in these parameters could impact lysosome distribution in cells. Thus, to better characterize lysosomes, their average number per cell and the average volume of this organelle was calculated using the data from the segmentation. A significant decrease of average number of lysosomes per cell was observed in MGHU3 (TaG1) and JMSU1 (T4G3) cells (Figure 18C). All analyzed cells showed a significant increase in the average volume of lysosomes (Figure 18D). These results indicated that lysosome morphology and number are altered in bladder cancer cells. However, changes in number of lysosomes do not correlate with grades of bladder cancer.

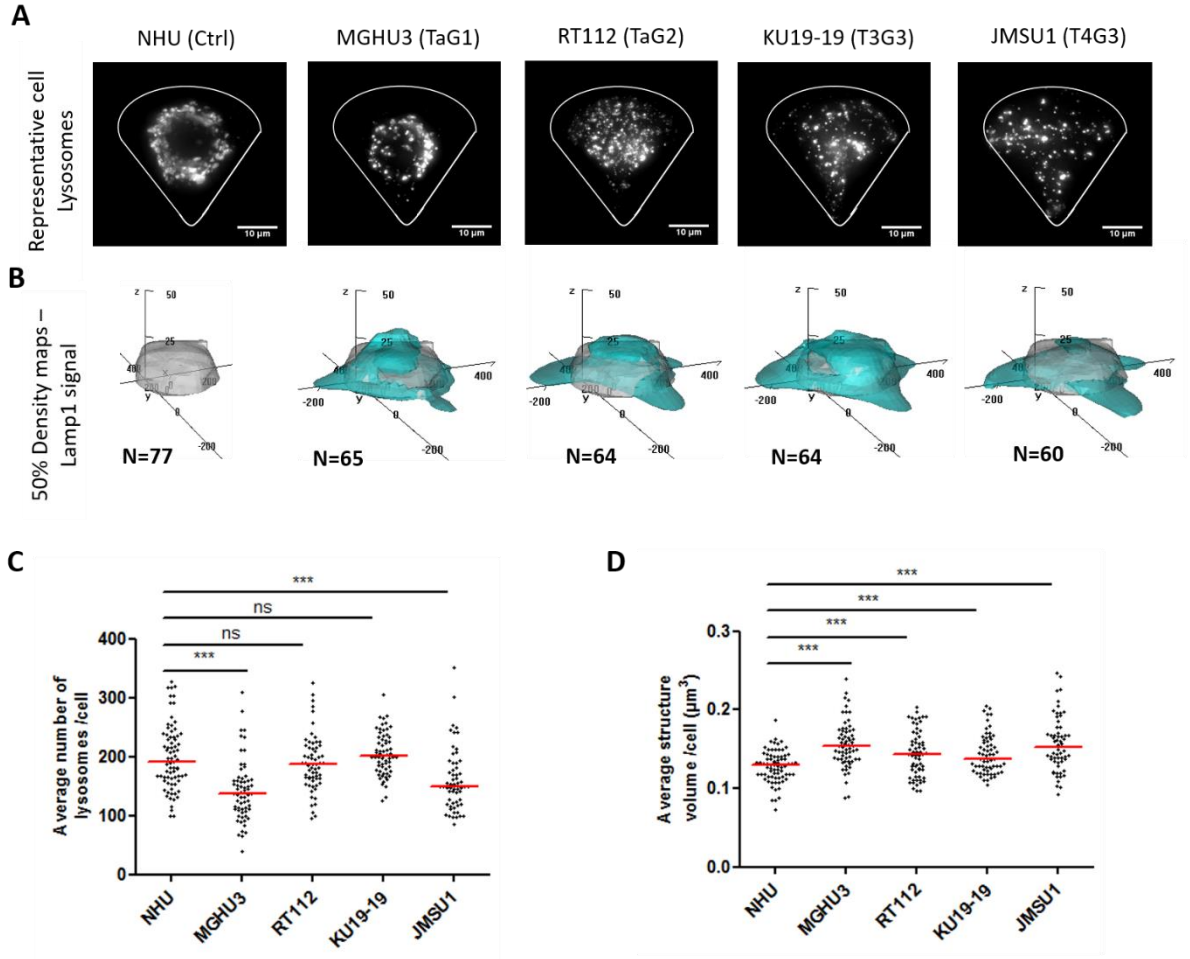

Figure 18: Alterations in lysosome distribution. A. Representative normalized single cell fluorescently stained for lysosomes using anti-Lamp1 antibody for of each analyzed bladder cell type **B.** 50% contour of the 3D density maps quantifying lysosome distribution (in turquoise), compared to NHU control cells (in white). Lysosome distribution is gradually more peripheral in bladder cancer cells. Scale bar 10µm. N is the number of cells. **C.** Average number of lysosomes per cell. Significant decrease in number of lysosomes in MGHU3 (TaG1) and JMSU1 (T4G3) cells. **D.** Average volume of lysosomes. Significant increase of volume in all analyzed cells compared with NHU cells. Red lines represent median. ns, $p>0.5$ and ***, $p<0.001$ in a Student's t-test.

In order to investigate if the alterations in lysosome distribution were due to the cell normalization by micropatterning, the distribution of lysosomes was quantified in unconstrained bladder cancer cell lines. The cells were stained for lysosomes (Lamp1), nucleus (DAPI) and actin cytoskeleton (Phalloidin) (Figure 19A). A cell mask was determined from the actin staining that we considered as the cell mask for cell membrane. The distance from each lysosome to the nearest cell membrane and nuclear edge was calculated. We

established 3 different regions in the cells: a perinuclear, an intermediate and a peripheral one (Figure 19B). About 60% of the lysosomes in MGHU3 (TaG1) cells accumulated in the perinuclear region, while only 10% were distributed at the cell periphery. The percentage of peripheral lysosomes gradually increases in cells representing grade 2 and 3, JMSU1 (T4G3) being the most peripheral (25% of lysosomes). This result, based on more than 60 cells, confirmed the peripheral distribution of lysosomes in cells representing later grades and stages of bladder cancer progression.

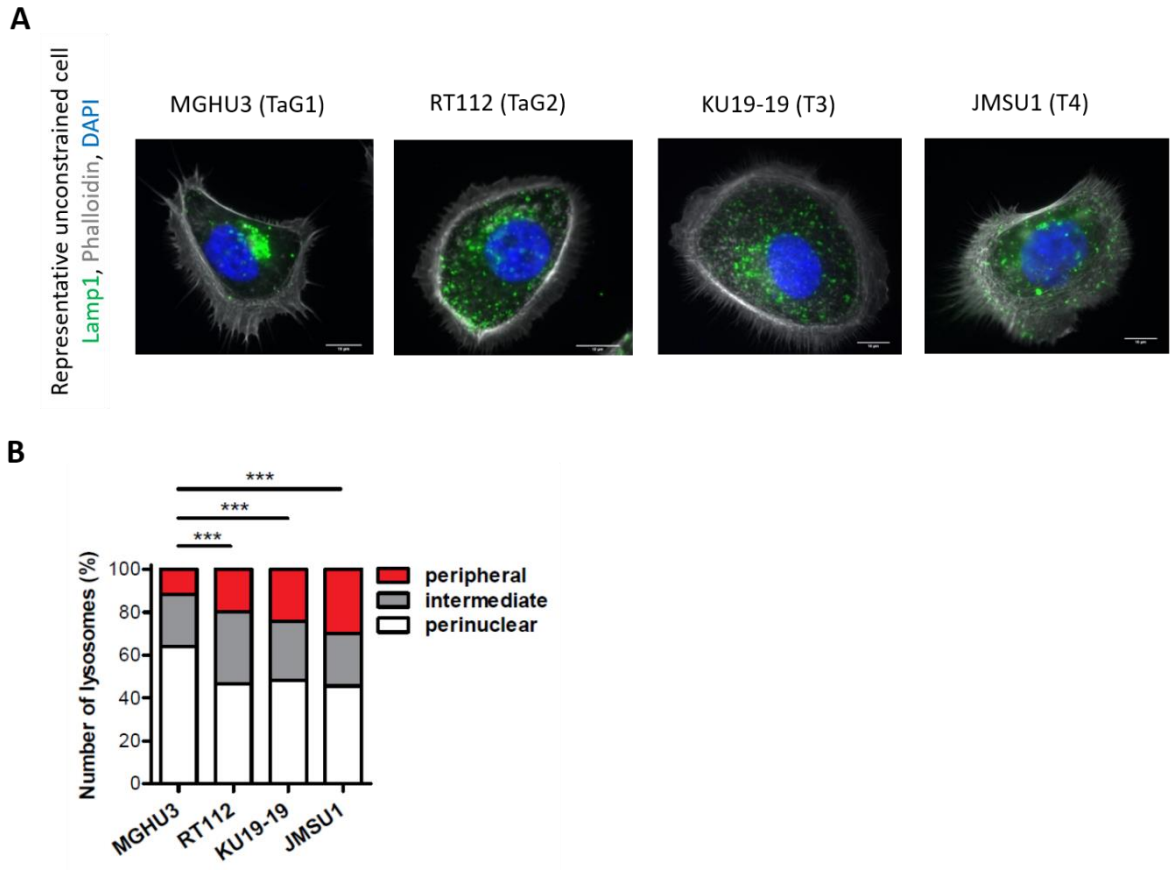

Figure 19: Lysosomes distribution in unconstrained cells. A. Representative unconstrained single cell image fluorescently stained for lysosomes (Lamp1), nucleus (DAPI) and actin cytoskeleton (Phalloidin) for each bladder cancer cell line. Scale bar 10µm. B. Distribution of lysosomes in unconstrained cells was divided in 3 regions: perinuclear (white), intermediate (gray) and peripheral (red). Lysosome peripheral dispersion is gradually increased depending on the bladder cancer cell grade. Analysis based in > 60 cells. ***, $p<0.001$ in Chi-squared test.

Because lysosome positioning changes have been previously implicated in cancer, we focused on this organelle. To further investigate the alterations in lysosome distribution, two additional grade 3 bladder cancer cell lines were tested, T24 and TCCSup (Figure 20). The distribution of lysosomes in the additional cell lines was more peripheral than NHU control cells (Figure 20B), as judged by Lamp1 staining in more than 45 cells per cell type (Figure 20A). Our results suggest that changes in lysosome positioning could be an important phenotype in bladder cancer.

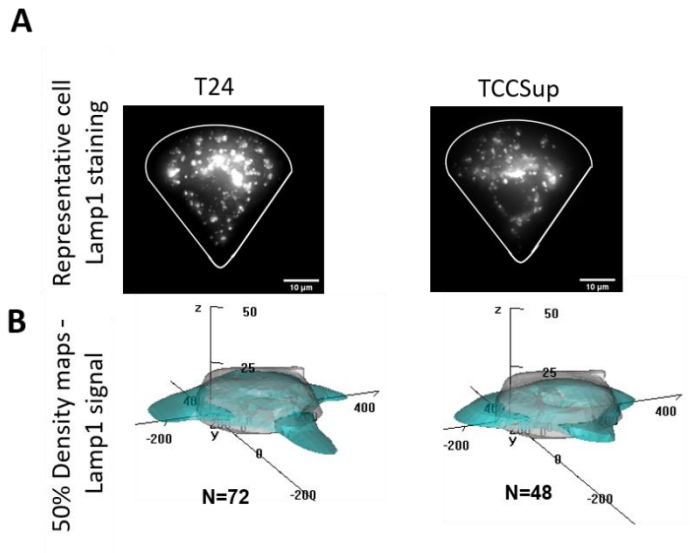

Figure 20: Alterations in lysosome distribution in grade 3 bladder cancer cells. A. Representative normalized single cell stained for Lamp1 **B.** 50% contour of the 3D density maps quantifying lysosome distribution (in turquoise), compared with NHU control cells (in white). Lysosome distribution is more peripheral in grade 3 bladder cancer cells. Scale bar 10µm. N is the number of cells.

Cell line	p-value
MGHU3 (TaG1)	3,51E-32
RT112 (TaG2)	3,51E-60
KU19-19 (T3G3)	1,16E-241
JMSU1 (T4G3)	4,34E-48
T24 (G3)	1,09E-114
TCCSup (G3)	1,30E-99

Table 01: Statistical differences between Lamp1 density maps. P-values correspond to differences between lysosome density maps of analyzed bladder cancer cells and NHU control cells based on nonparametric comparison of density maps. Larger differences are represented by smaller p-values.

3.1. Lysosomal functions

3.1.1. Lysosomal protease activity

The main function of lysosomes is the degradation of molecules. These organelles are enriched in acidic hydrolases that are responsible for the degradation of several substrates, such as proteins and sugars (Braulke and Bonifacino, 2009). Cathepsin B is an important protease present in lysosomes that is often overexpressed in cancers (Fennelly and Amaravadi, 2017). We performed an assay to measure the cathepsin B activity. The activity was detected via a fluorogenic cathepsin B activity assay (Calbiochem), in which relative fluorescence units are emitted when cathepsin B cleaves the carboxyl side of arginylarginine. Cathepsin B activity was increased in KU19-19 cells (T3G3), while the other cell lines had comparable cathepsin B activities to NHU (Figure 21). Thus, cathepsin B activity did not correlate with peripheral lysosome positioning in bladder cancer cells. However, more experiments are required to confirm this finding.

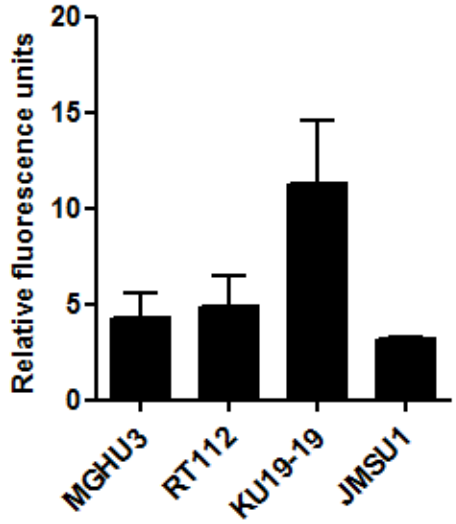

Figure 21: Cathepsin B activity. Cathepsin B activity is increased in KU19-19 (T3G3) cells as compared to the other cancer cell lines. Error bars from triplicates of 1 experiment.

Matrix metalloproteinases (MMPs) have been recognized as important proteases involved in invasive tumor growth (Hotary et al., 2003). MT1-MMP (MMP14) is manly located at lysosomes (Steffen et al., 2008). Therefore, we tested if proteolysis was induced by lysosome positioning. We tested the activity of MMPs using the fluorimetric SensoLyte® 520 generic, in which a FRET peptide emits fluorescence signal when cleaved by MMPs. This

generic test target certain MMPs depending on the incubation time (Figure 22A), we choose the 3 hour time point because it targets both collagenases MMP1 and MT1-MMP (MMP14). We found that the activity of collagenases MMPs were gradually increased in bladder cancer cells (Figure 22B).

A

Table 1: Protocols for pro-MMP activation.

MMPs	Activated by treating with
MMP-1 (collagenase)	1 mM APMA (diluted Component C) at 37°C for 3 h.
MMP-2 (gelatinase)	1 mM APMA (diluted Component C) at 37°C for 1 h.
MMP-3 (stromelysin)	1 mM APMA (diluted Component C) at 37°C for 3-6 h.
MMP-7 (matrilysin, PUMP-1)	1 mM APMA (diluted Component C) at 37°C for 1 h.
MMP-8 (neutrophil collagenase)	1 mM APMA (diluted Component C) at 37°C for 1 h.
MMP-9 (92 kDa gelatinase)	1 mM APMA (diluted Component C) at 37°C for 2 h.
MMP-10 (stromelysin 2)	1 mM APMA (diluted Component C) at 37°C for 2 h.
MMP-12 (macrophage elastase)	1 mM APMA (diluted Component C) at 37°C for 2 h.
MMP-13 (collagenase-3)	1 mM APMA (diluted Component C) at 37°C for 40 min.
MMP-14	1 mM APMA (diluted Component C) at 37°C for 2-3 h.

Adapted from manufacturer's protocol

B

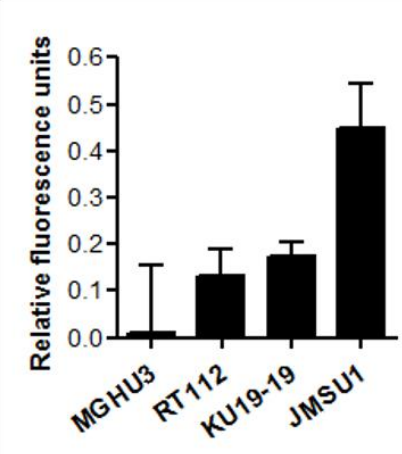

Figure 22: Activity of matrix metalloproteinases in bladder cancer cells. A. Table from the manufacturer's protocol indicating the time of incubation to target specific MMPs. Red rectangles indicate the targeted MMPs during the 3 hour incubation experiment. **B.** MMP activity is gradually increased during bladder cancer progression. Error bars from triplicates of 1 experiment

3.1.2. Signaling attenuation by lysosomal degradation

In addition to their classical role as final degradative compartments in eukaryotic cells, lysosomes are responsible for the intracellular attenuation of signaling (Taub et al., 2007). The epidermal growth factor receptor (EGFR) signaling pathway is often altered in different cancer types (Baumdick et al., 2015), and about 40 to 60% of bladder cancers present an overexpression of EGFR (Ahmad et al., 2012). We analyzed whether changes in lysosome positioning alter the degradation of EGFR in bladder cancer cells. After EGF-induced uptake, EGFR is sorted to lysosomes where it is finally degraded. To monitor the degradation of EGFR, we stimulated bladder cancer cells with 100 nM of EGF for 30 minutes or 1 hour. Cells without EGF stimulation were used as a control. Protein extraction from cell lysate was realized for Western Blot analysis and the levels of EGFR were visualized (Figure 23). The intensity of EGFR chemiluminescent signal was normalized by tubulin expression. The degradation of EGFR after EGF stimulation was observed in all cell lines. The biggest degradation activity was observed in JMSU1 (T4G3) cells after 1 hour. In MGHU3 (TaG1), RT112 (TaG2) and KU19-19 (T3G3) the EGFR signal decreased between 20- 45% after stimulation, whereas in JMSU1 (T4G3) cells we observed an 80% decrease in EGFR signal after 1 hour. Nonetheless, we could not detect a correlation between lysosome positioning and the EGFR degradation capacity, because KU19-19 (T3G3) and JMSU1 (T4G3), both showing peripheral lysosomes, revealed very different degradation of EGFR. These results suggest that lysosomes positioning does not correlate with the degradation capacity of bladder cancer cells.

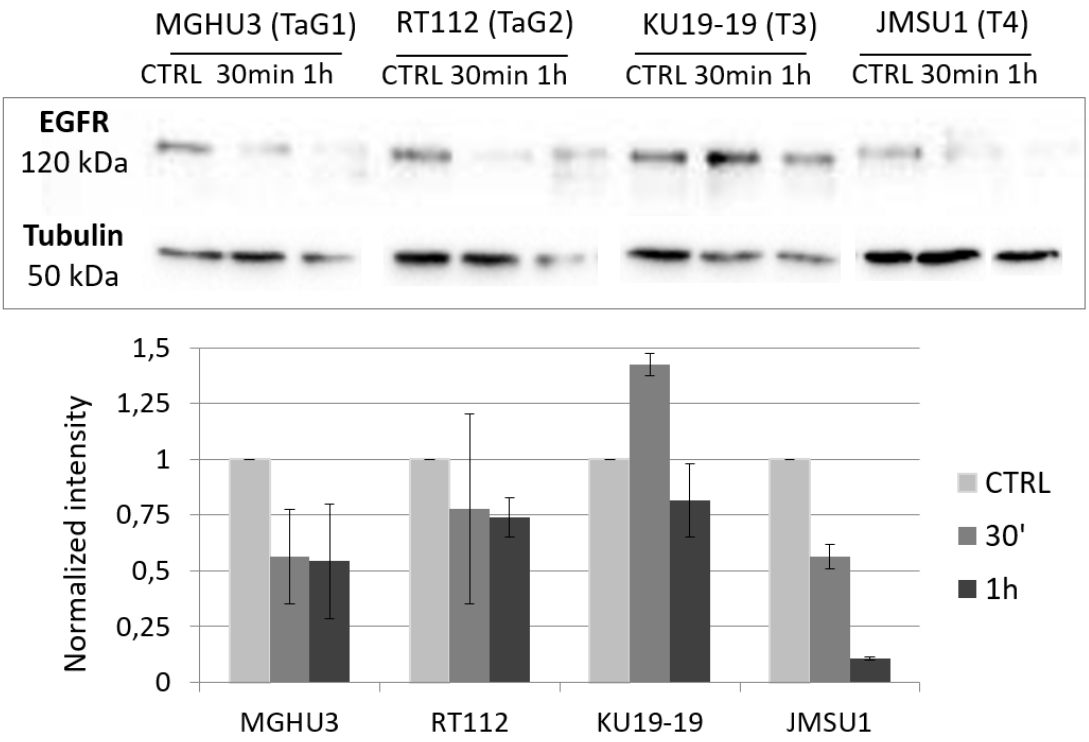

Figure 23: EGFR signaling attenuation. Degradation of epithelial growth factor receptor (EGFR). Western Blot of cell lysates from non-stimulated bladder cancer cells (CTRL), or cells stimulated with 100 nM of EGF for 30 minutes or 1 hour. The intensity of chemiluminescent EGFR signal was normalized by tubulin expression. EGFR intensity is strikingly decreased in JMSU1 (T4G3) after 1 hour. Error bars represent standard deviation of 2 independent experiments.

Discussion:

Our results showed that lysosomes are gradually distributed to the cell periphery in bladder cancer cells. We found similar results in micropattern-normalized and unconstrained cells. Furthermore, the changes in lysosome distribution in these cells were accompanied by changes in lysosome volume. The volume of this organelle was increased in bladder cancer cells. However, the number of lysosomes per cell was not systematically altered. A significant decrease in average number of structures was noticed in cells MGHU3 (TaG1) and JMSU1 (T4G3) cells. Together, our results suggest that lysosome alterations could be an important characteristic of bladder cancer. Interestingly, induced peripheral lysosome positioning as a result of the acidification of the extracellular matrix was observed during cancer progression (Glunde et al., 2003; Steffan et al., 2010). However, our work indicates an intrinsic change in the distribution of lysosomes in cells representing higher grades of bladder cancer.

We performed several experiments to investigate if lysosome distribution has an impact in lysosome functions, such as proteolysis and signaling attenuation. Our preliminary results indicated that peripheral lysosome positioning correlates with increased activity of MMPs. However, more experiments are needed to confirm these preliminary results. Cancer is a very heterogeneous disease, where cells acquire selective advantages to spread around the body (Hanahan and Weinberg, 2000). Thus, it is possible that different cell lines employ different mechanisms to invade and progress.

Cathepsin B overexpression is a common phenotype of several cancers (Fennelly and Amaravadi, 2017). Our preliminary results suggest that intracellular cathepsin B activity does not correlate with peripheral lysosome positioning. Interestingly, it was reported, in prostate cancer, that peripheral lysosomes secreted more cathepsin B, which favors invasion (Steffan et al., 2014). Therefore, it will be interesting to study whether changes in lysosome positioning, for instance induced by gene silencing, alter lysosomal exocytosis of other proteases.

EGFR is overexpressed in some bladder cancer cells from the basal-like subgroup (Rebouissou et al., 2014). EGF stimulation was sufficient to induce EGFR degradation in all analyzed cell lines. However, the attenuation of EGFR signaling is not dependent on grades of bladder cancer, since both cells from grade 3 presented very different phenotypes. While

JMSU1 (T4) cells degrade EGFR after 1 hour, only a small decrease in EGFR signal was observed in KU19-19 (T3) cells.

To further explore the implication of lysosome positioning in bladder cells, it would be interesting to deeper investigate its main function, the degradation capacity. For instance, it was shown that DQ-BSA (bovine serum albumin) is degraded by lysosomes (Amaya et al., 2016). This self-quenched fluorogenic substrate emits fluorescence when cleaved in the lysosomes. Additionally, the intraluminal, cytosolic and extracellular pH should be investigated because of the link between acidic pH and lysosomes. Acidic pH is essential for lysosomes proper function (De Duve et al., 1955), and it was shown that both cytoplasmic (Heuser, 1989) and extracellular (Steffan et al., 2009) pH play a role in lysosome positioning. Interestingly, it has been reported that lysosomes distributed at the cell periphery reveal a decrease in acidity of lysosomes (Johnson et al., 2016). Furthermore, the secretion of cathepsin B was correlated with peripheral lysosomes in prostate cancer. Therefore, it would be important to repeat our cathepsin B assay in the extracellular supernatant to investigate whether protease secretion correlates with lysosome positioning in the analyzed cells. Moreover, the secretion capacity of lysosomes can be tested with pH-sensitive cells expressing pHluorin-tagged lysosomal proteins (Miesenböck et al., 1998).

Autophagy is a recycling process in cells that mediates lysosomal degradation of intracellular compartments (Klionsky et al., 2012). The exact role of autophagy in cancer is still unclear. On the one hand, autophagy was shown to support cancer cell survival in hostile environment, such as tumor milieu (Mathew et al., 2009). On the other hand, autophagy was proposed as a tumor suppressor mechanism that prevents DNA damage and oxidative stress (White, 2015). Because autophagosomes are mainly found at the cell center (Korolchuk et al., 2011) and lysosomes need to fuse with autophagosomes for their maturation (Nakamura and Yoshimori, 2017), the peripheral peripheral positioning of lysosomes in high-grade bladder cancer cells could lead to an impairment in autophagy in these cells. Our preliminary data comparing 50% contour density maps of lysosomes (Lamp1 staining) and autophagosome (LC3 staining) suggested an alteration in relative positioning of these organelles in bladder cancer cells in comparison with NHU cells. Interestinlgy, it was reported that PI3K (phosphatidylinositol 3-kinase)/Akt (protein kinase B)/mTOR signaling, a major survival pathway, is abnormally activated in around 40% of bladder cancer, and this contributes to a poor prognosis (Knollman et al., 2015; Moon et al., 2014). Therefore, it would be interesting to test if mTOR inhibition, for instance by Rapamycin treatment or cell starvation, has an impact in autophagy of bladder cancer cell lines.

Our results suggest that lysosome positioning is potentially important in bladder cancer progression. Muscle-invasive bladder cancer cells have dispersed lysosome distribution compared with NHU control cells. Remarkably, the lysosomal membrane protein, Lamp1, was shown to be a potential clinical biomarker in bladder cancer (Duriez et al., 2017). Lamp1 expression was strikingly increased in urine samples from patients affected by bladder cancer as compared to healthy patients. A significant decrease in Lamp1 abundance was also observed in recurrent bladder cancers. Interestingly, bladder cancers from Ta pathway, are recurrent in about 50% of cases (Knowles, 2008).

4. Invasion

Invasion is an important hallmark of cancer, in which cells penetrate into tissues barriers (Hanahan and Weinberg, 2000). Moreover, the stages of bladder cancer are defined by the invasion of tissue layers (Ho et al., 2012). We investigated whether alterations in lysosome distribution lead to changes in invasion, using an invasion assays based on collagen I matrix invasion from cell aggregates called spheroids.

The cells were plated on agarose, a polysaccharide, which forms a concave surface after polymerization. Since the cells do not adhere to agarose, they clustered at the concave surface and formed cell spheroids after deposition. After 3 days, the spheroids were plated into a 2 mg/ml Collagen I matrix, from rat tail. The spheroids were monitored and imaged at different time points to analyze the invasion behavior.

First, we performed the invasion assay with the different bladder cancer cell lines analyzed (Figure 24A). Invasion was characterized by the escape of cells from spheroids. We found, as expected, that invasion was gradually faster depending on grades of cancer. Cells representing grade 1 (MGHU3) invaded on average after 4,5 days, grade 2 cells, RT112, invaded on average after 3 days, while grade 3 cell lines KU19-19 (T3G3) and JMSU1 (T4G3) invaded on average after 1 day (Figure 24C). Moreover, we quantified the percentage of invasive spheroids within 6 days (Figure 24B). The choice of this time point was due to the invasion of MGHU3 (TaG1) cells. About 26% of MGHU3 (TaG1) spheroids initiated invasion, while 80% of RT112 (TaG2) and 100% of KU19-19 (T3G3) and JMSU1 (T4G3) invaded within 6 days. Our data demonstrated that the beginning of invasion and the percentage of invasive spheroids correlated with bladder cancer grade.

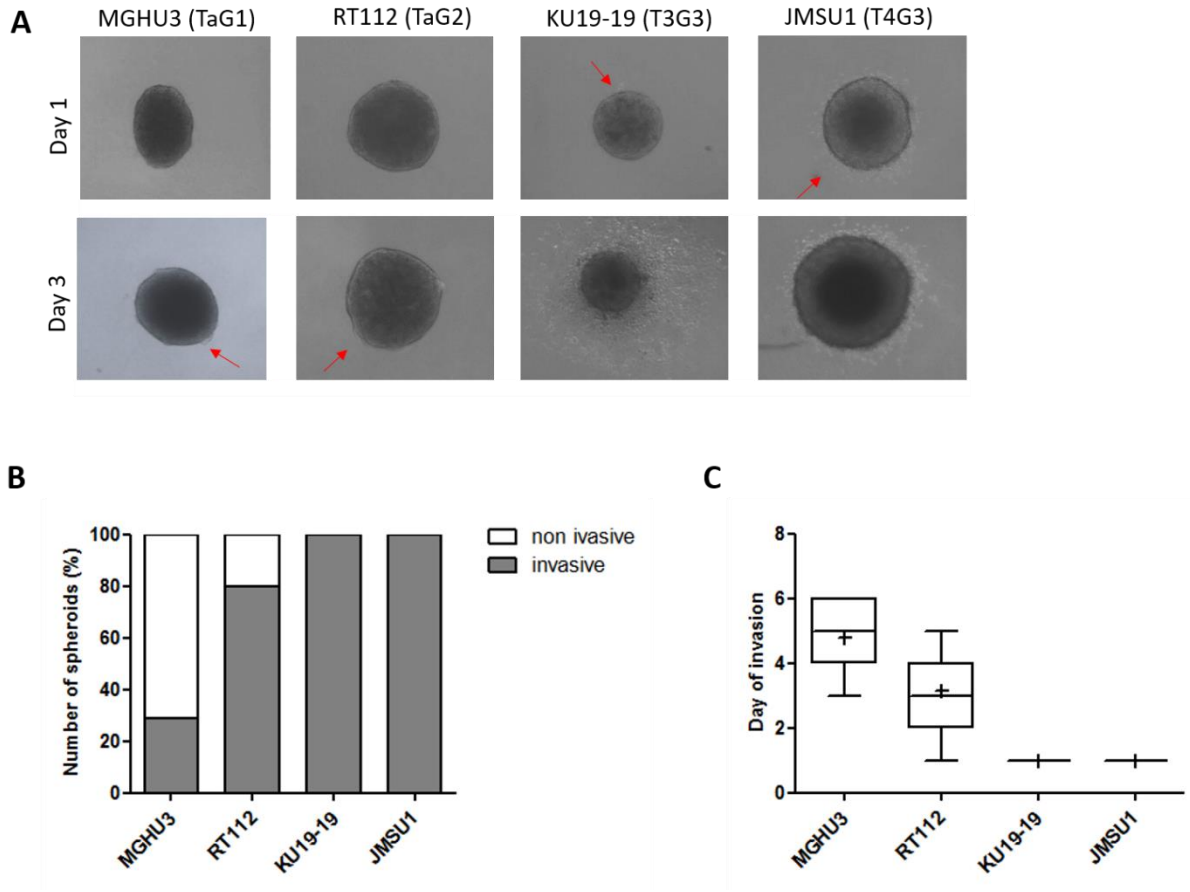

Figure 24: Invasion assay. A. Spheroids from bladder cancer cells at two time points, day 1 and 3. Cells representing higher grades start the invasion earlier (red arrows) than cells representing lower grade of bladder cancer. **B.** The percentage of invasive spheroids after 6 days gradually increases depending on grade of bladder cancer **D.** Median day of invasion. Gradual acceleration depending on grade of bladder cancer. Error bars from > 4 experiments.

4.1. Anterograde repositioning of lysosomes

It has been suggested that peripheral lysosome positioning participates in the increase of invasion (Dykes et al., 2016; Raiborg et al., 2015; Steffan et al., 2009). Thus, we investigated whether changes in lysosome positioning impacted cell invasion of bladder cancer cell lines. To change lysosomal distribution cells were silenced by siRNA for genes implicated in lysosome distribution, Rab7, Rab27 and RNF26. The 50% contours of 3D density maps were used to quantify the changes in positioning. The invasion was quantified based on images at different time points. The beginning of invasion refers to the visualization of the first cell that extrapolate from the cell spheroid. In addition, the percentage of invasive and non-invasive spheroids was compared between the silenced cells and the control.

4.1.1. Impact of Rab7 depletion on invasion

Rab7 and its effector Rab7-interacting lysosomal protein (RILP) have been shown to promote a central positioning of lysosomal compartments through recruitment of the dynein-dynactin complex (Jordens et al., 2001). The silencing of this protein has been implicated in peripheral lysosome dispersion, which leads to increase of invasion both *in vivo* and *in vitro* (Steffan et al., 2014). Therefore, we investigated the role of Rab7 depletion in invasion using bladder cancer cell lines with less peripheral lysosome distributions, MGHU3 (TaG1) and RT112 (TaG2).

The cells were transfected with siRNA targeting Rab7 (siRab7), or Luciferase (siLuc) as a control (Figure 25). To not perturb the formation of cell aggregates, the siRNA treatment was performed by adding the compound into the collagen mixture. In parallel, cells from the same passage were seeded on plates and transfected with siRNA. 3 days after the siRNA transfection, cells were plated on micropatterned surfaces and stained for Lamp1 to investigate changes in lysosome positioning, and cell lysates were used to quantify depletion either by Western Blot or qPCR. Rab7 protein level was substantially decreased in both cell lines to 15% in MGHU3 (TaG1) and 25% in RT112 (TaG2) of the control (siLuc) (Figure 25G-H).

The silencing of Rab7 led to a peripheral distribution of lysosomes in both cells lines (Figure 25A-B). Furthermore, we observed that Rab7 depletion increased invasion during the 6 days of monitoring. Only 26% of MGHU3 cells (TaG1) were invasive in siLuc control, while 60% of spheroids invaded in depleted cells (Figure 25C). The diagram of the fraction of non-invasive spheroids at different time points allowed to visualize the decrease of non-invasive spheroids each day (days 1-6). In MGHU3 (TaG1) cells, a significant decrease of non-invasive spheroids in comparison to control indicated an acceleration of invasion in these cells (Figure 25E compare depleted cells in red to control in black). 80% of control RT112 (TaG2) cells invaded after 6 days, a moderate increase to 85% was observed after Rab7 silencing (Figure 25D). Nonetheless, the diagram of the fraction of non-invading spheroids was significantly different between siRab7 and siLuc. This indicated a significant acceleration of invasion after Rab7 depletion in the early phase of the experiments, after 2 days (Figure 25F). Overall, Rab7 silencing positively impacted invasion behavior in both analyzed cell lines.

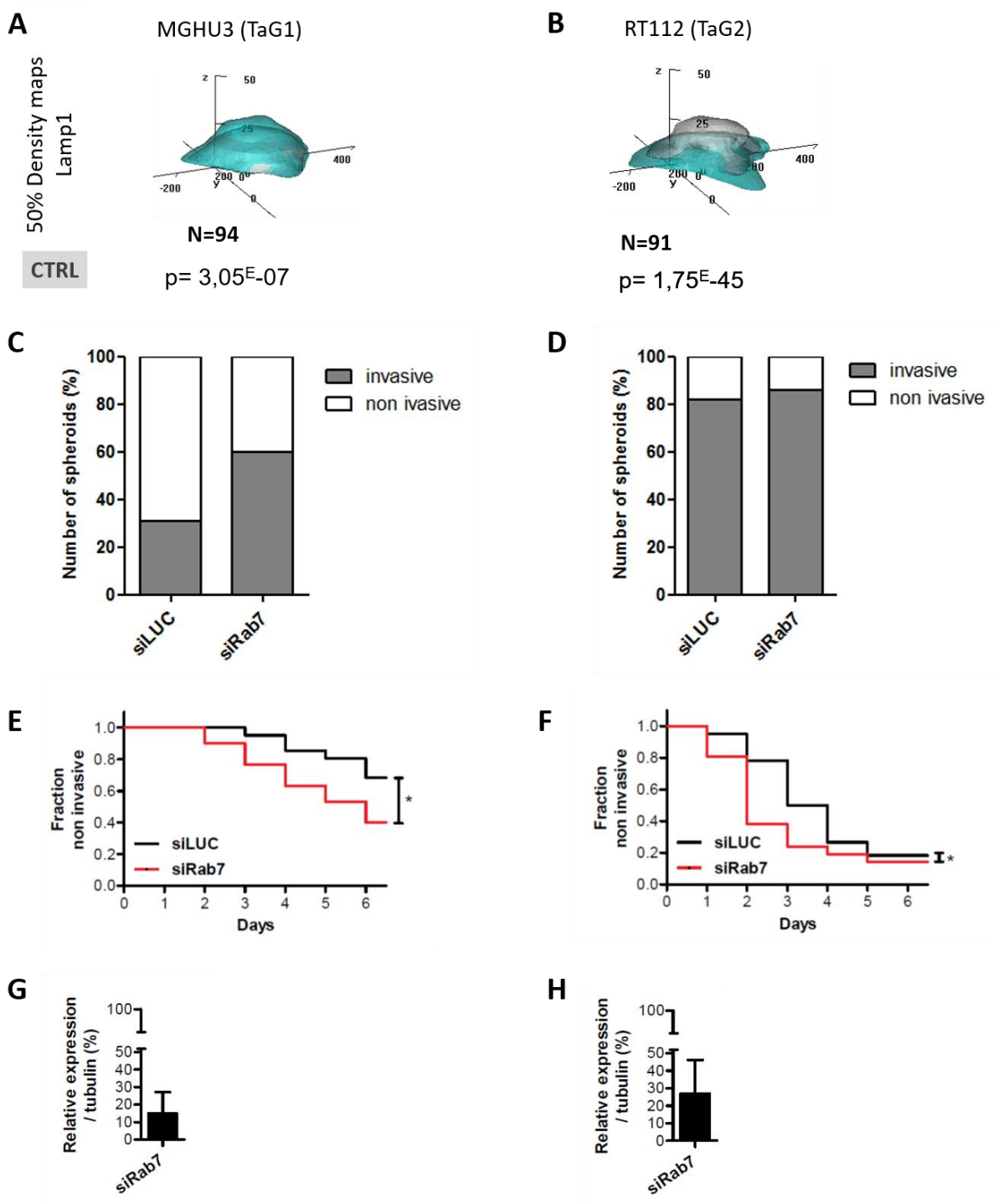

Figure 25: Impact of Rab7 depletion in bladder cancer invasion. (MGHU3 (TaGa1): **A, C, E, G;** RT112 (TaG2): **B, D, F, H**). **A-B.** 50% contour of the 3D density maps quantifying lysosome distribution in Rab7 depleted cells (in turquoise), compared to control cells treated with siLUC (in white). Lysosome distribution is more peripheral after Rab7 depletion. p corresponds to p-value in nonparametric comparison of density maps between depleted cell compared to control. **C-D.** Analysis of invasion from spheroids. A significant increase in the fraction of invasive spheroids is observed in Rab7 depleted MGHU3 (TaG1) cells (**C.**) **E-F.** Fraction of non-invasive spheroids at different time points. Significant differences between the diagrams of siRab7 and siLuc are observed. *, $p<0.05$ Mantel-Cox test. **G-H.** Quantification of Rab7 depletion from cell lysate in Western Blot analysis. Error bars from > 6 experiment.

Because it was shown that Rab7 is implicated in MT1-MMP trafficking (Williams and Coppolino, 2011), we tested if lysosomes dispersion by knockdown of Rab7 impacts secretion of collagenases in MGHU3 (TaG1) and RT112 (TaG2) cells. MMP activity was increased when Rab7 was depleted in both cells lines (Figure 26), which suggested that bladder cancer cell line invasion could be facilitated by collagenase proteolysis. However, more experiments are required to confirm these results.

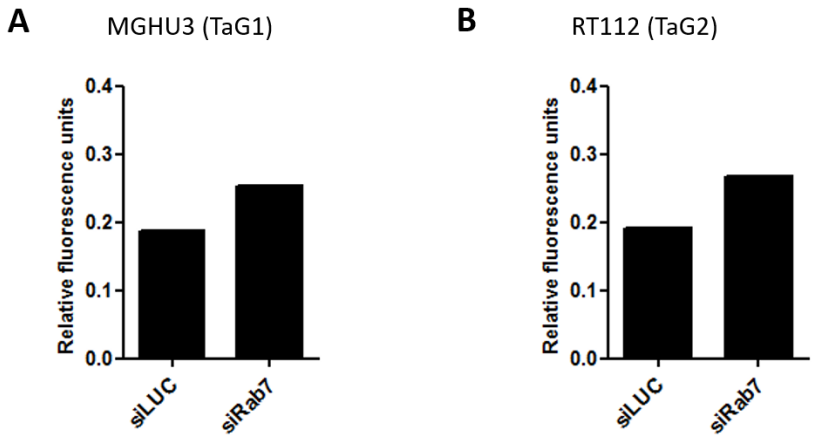

Figure 26: The activity of matrix metalloproteinases in bladder cancer cells tends to increase after Rab7 depletion. A. MGHU3. **B.** RT112.

4.1.2. Impact of Rab27 depletion on invasion

Rab27 is localized in multivesicular bodies/late endosomes that are lysosome-related compartments positive for Lamp1 (Ostrowski et al., 2010). Interestingly, negative expression of Rab27 was shown to increase invasion of colorectal cancers (Dong et al., 2015). We tested whether Rab27 silencing had an impact on bladder cancer invasion. Depletion of Rab27 dispersed the lysosomes to the cell periphery in both MGHU3 (TaG1) and RT112 (TaG2) cell lines (Figure 27A-B), and had a strong impact on invasion of MGHU3 (TaG1) cells. In Rab27 depleted cells, 80% of spheroids were invasive within 6 days, compared to 25% in control (Figure 27C). The diagram of the fraction of non-invading cells visualized a highly significant acceleration of invasion, with most spheroids invading after 4 days (Figure 27E). Although Rab27 silencing in RT112 (TaG2) led to a peripheral distribution of lysosomes, no significant impact on the fraction of invasive spheroids was observed (Figure 27D-F). Due to technical problems the depletion of this protein could not be quantified in these experiments. Thus, it is possible that Rab27 depletion was not sufficient to impact invasion in RT112 cells. This quantification will be performed in the near future.

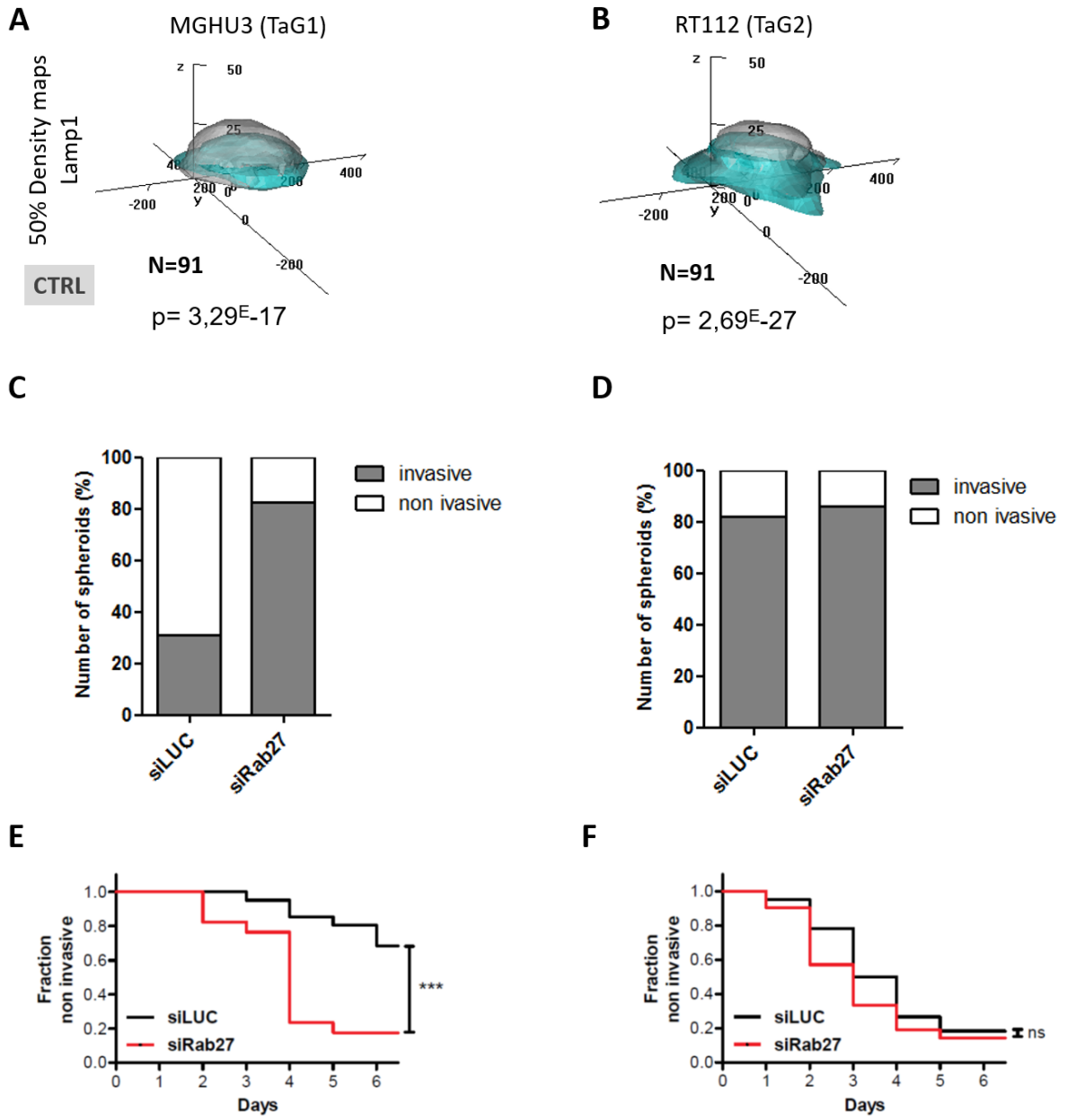

Figure 27: Impact of Rab27 depletion on bladder cancer invasion. (MGHU3 (TaGa1): **A, C, E;** RT112 (TaG2): **B, D, F**). **A-B.** 50% contour of the 3D density maps quantifying lysosome distribution of Rab27 depleted cells (in turquoise), compared with control cells (in white). Lysosome distribution is more peripheral after Rab27 depletion. p corresponds to p-value in nonparametric comparison of density maps between depleted cell compared to control. **C-D.** Number of invasive spheroids. Invasion is significantly increased in depleted MGHU3 (TaG1) cells (**C.**), but not in RT112 (TaG2) (**D.**). **E-F.** Fraction of non-invasive spheroids. Acceleration of invasion in MGHU3 (TaG1) silenced for Rab27 (in red) as compared to control (in black) (**E.**) No significant change in RT112 (TaG2) (**F.**) ns, p>0.5, ***, p<0.001in Matel-Cox test.

4.1.3. Impact of RNF26 depletion on invasion

The ER protein RNF26 was shown to recruit and retain lysosomes to the perinuclear region (Jongsma et al., 2016). Since the depletion of this protein was described as leading to peripheral lysosome distribution, we tested its impact in bladder cancer cells. We observed a redistribution of lysosomes towards the cell periphery after transfection with siRNF26 in MGHU3 (TaG1) and RT112 (TaG2) cells (Figure 28A-B). In MGHU3 (TaG1) cells, the number of invasive spheroids increased by 40% after RNF26 depletion (Figure 28C). Moreover, in depleted cells, we observed an acceleration of invasion (Figure 28E). In RT112 (TaG2) cells, 100% of spheroids invaded after silencing of RNF26 (Figure 28D). All spheroids invaded within 5 days as observed by the diagram representing the fraction of non-invading spheroids throughout time (Figure 28F), however, there was no significant difference in invasion behaviour between siRNF26 and siLuc. The mRNA level was decreased to 40 and 35% compared to control in MGHU3 (TaG1) and RT112 (TaG2), respectively (Figure 28G-H).

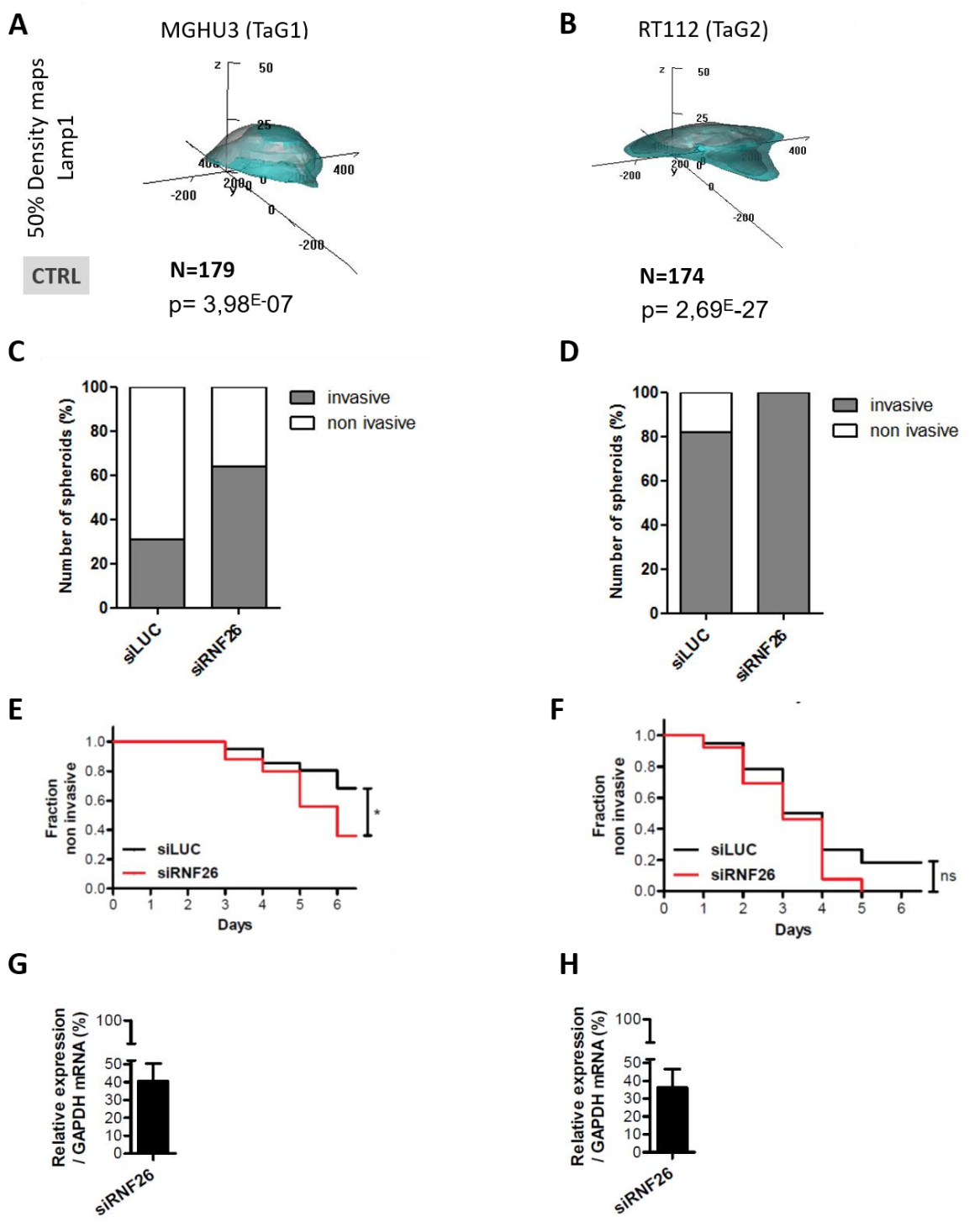

Figure 28: Impact of RNF26 depletion on bladder cancer invasion. (MGHU3 (TaGa1): **A, C, E, G;** RT112 (TaG2): **B, D, F, H**). **A.** 50% contour of the 3D density maps quantifying lysosome distribution of RNF26 depleted cells (in turquoise), as compared to control cells (in white) in MGHU3 (TaG1). Lysosome distribution is more peripheral after RNF26 depletion. p corresponds to p-value in nonparametric comparison of density maps between depleted cell compared to control. **C-D.** Number of invasive spheroids. Invasion is significantly increased in both cell lines after RNF26 silencing. **E-F.** Fraction of non-invasive spheroids. Acceleration of invasion in MGHU3 (TaG1) silenced for RNF26 (in red) as compared to control (in black) (**E.**). All depleted RT112 (TaG2) spheroids invaded after 5 days (**F.**). ns, p>0.5 and *, p<0.5 in Mantel-Cox test. **G-H.** Quantification of RNF26 depletion from qPCR. Error bars from > 4 experiments.

4.2. Retrograde repositioning of lysosomes

Our results show that dispersion of lysosomes to the cell periphery is positively correlated with invasion in bladder cancer cells. Moreover, it has been reported that cluster of lysosomes at the cell center negatively impacts invasion of cancer cells (Dykes et al., 2016). Thus, we aimed to change lysosomes to the cell center to investigate its impact in 3D cell invasion. Since 60% of lysosomes were concentrated at the perinuclear region in MGHU3 (TaG1) cells, this cell line was not used in these experiments. 100% of spheroids of grade 3 of bladder cancer cell lines (KU19-19 and JMSU1) invaded after 1 day, which demonstrated that these cells were highly invasive. Retrograde repositioning of grade 3 bladder cancer cells (KU19-19 and JMSU1) was targeted either by U18666A drug or by Arl8b and KIF5B depletion. Retrograde positioning of lysosomes was not suffient to impair invasion in KU19-19 (T3G3) and JMSU1 (T4G3) (data not shown). Thus, we used RT112 (TaG2) cells that are moderately invasive compared to grade 3 cells and have 55% of lysosomes distributed around the intermediate and peripheral regions of the cell.

4.2.1. Impact of Arl8b depletion on invasion

Arl8b localizes to lysosomes and participates in the trafficking of lysosomes towards cells periphery (Guardia et al., 2016; Rosa-Ferreira and Munro, 2011). The silencing of Arl8b prevented the anterograde transport of lysosomes and decreased the invasion in prostate cancer cells (Dykes et al., 2016).

We transfected the cells by adding siRNAs targeting Arl8b, or Luciferase as a control, into the collagen mixture. Quantification of lysosome positioning (Lamp1 staining) or protein depletion (qPCR) were performed in cells from the same passage transfected in parallel. The depletion of Arl8b to 10% (Figure 29D) redistributed the lysosomes to the cell center (Figure 29A) in RT112 (TaG2) cells. In control, 80% of spheroids were invasive within 6 days, while depletion of Arl8b decreased the percentage of invasive spheroids to 60% (Figure 29B). The fraction of non-invasive spheroids throughout time was significantly increased after siArl8b treatment, which indicated a significant delay in invasion compared to control (Figure 29C).

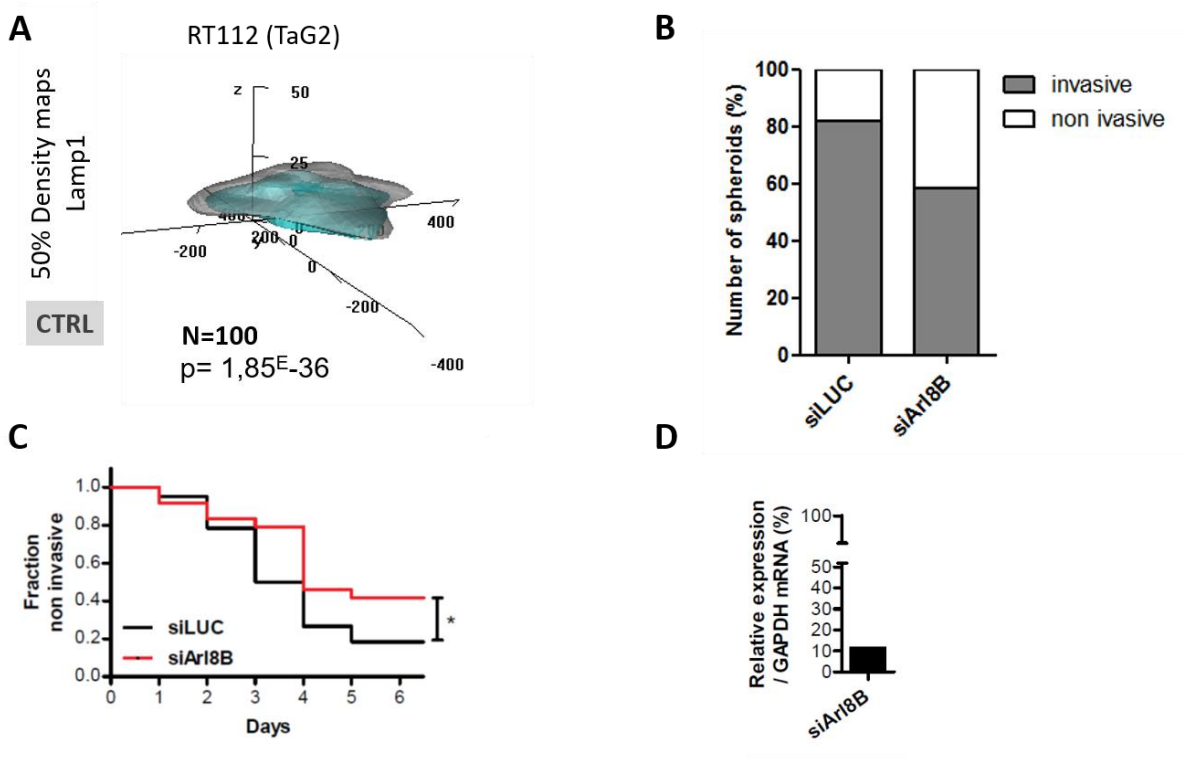

Figure 29: Impact of Arl8b depletion on bladder cancer invasion. RT112 (TaG2) **A.** 50% contour of the 3D density maps quantifying lysosome distribution of Arl8b depleted cells (in turquoise), as compared to control cells (in white). Lysosome distribution is more central after Arl8b depletion. p-value in nonparametric comparison of density maps between depleted cell compared to control. **B.** Number of invasive spheroids. Invasion is significantly decreased after Arl8b silencing **C.** Fraction of non-invasive spheroids. Delay in invasion in silenced RT112 (TaG2) (in red) as compared to control (in black). *, p<0.5 in Matel-Cox test. **D.** Quantification of Arl8b depletion by RT-PCR.

4.2.2. Impact of KIF5B depletion on invasion

KIF5B is a microtubule motor protein implicated in the trafficking of lysosomes to the cell periphery (Tanaka et al., 1998) and its depletion clusters the lysosomes at the cell center (Raiborg et al., 2015; Rosa-Ferreira and Munro, 2011). We investigated the impact of Kif5B silencing on invasion. We found a 30% decrease of invasive spheroids after siKIF5B transfection (Figure 30A). Furthermore, the fraction of non-invading spheroids was significantly different in siKif5B spheroids than in siLuc spheroids, indicating a delay in invasion in Kif5B silenced cells (Figure 30B). In the near future, the depletion levels and density map to quantify changes in lysosome positioning will be performed to confirm these results.

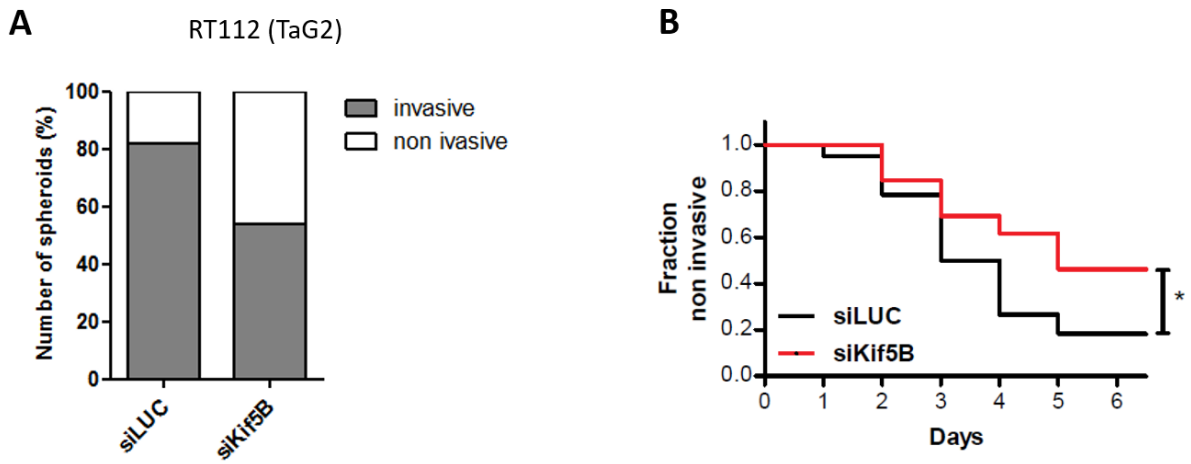

Figure 30: Impact of KIF5B depletion on bladder cancer invasion. RT112 (TaG2) **A.** Number of invasive spheroids. Invasion is significantly decreased after KIF5B silencing **B.** Fraction of non-invasive spheroids. Delay in invasion in silenced RT112 (TaG2) (in red) as compared to control (in black). *, $p<0.5$ in Matel-Cox test.

4.2.3. Chemically inducible changes in lysosome positioning

The “inducible cargo trafficking” assay consists in chemically connecting the domain FKBP (FK506), associated with an organelle-specific membrane protein, to the domain FRB (FKBP-rapamycin-binding) coupled with a motor protein or its adaptor effector (Kapitein et al., 2010). In the presence of the heterodimerizer Rapalog (Rapamycin homolog) the FKBP domain is recruited to FRB. Then, the FKBP-FRB complex is transported by the coupled

motor protein. We stably co-expressed Lamp1-mCherry-FKBP and BicD2-HA-FRB constructs in RT112 cells. BicD2 is a cargo adaptor of the motor protein dynein (Reck-Peterson, 2015). The addition of 1 µM of A/C heterodimerizer, a compound identical to Rapalog, clustered the lysosomes at the perinuclear region of transfected cells (Figure 31, example of KU19-19 cells). The stable RT112 expressing both constructs and the A/C heterodimerizer will be referred as RT112-BicD2 and Rapalog, respectively, in this report.

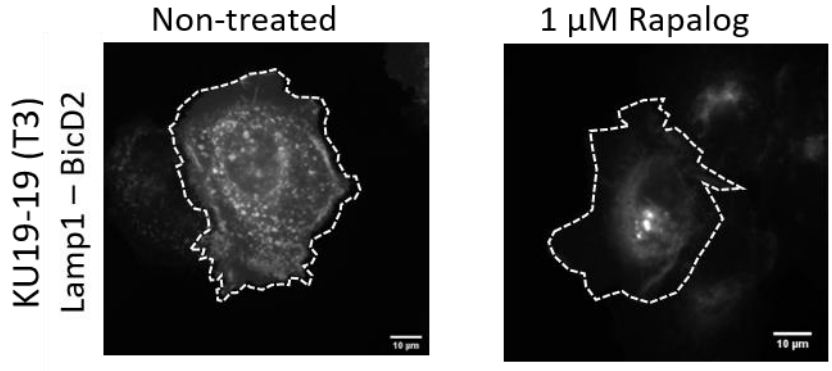

Figure 31: Impact of inducible trafficking of lysosomes by dynactin effector BicD2 in lysosome positioning. KU19-19 cells: (left) Lysosomes dispersed around the cytosol, (right) after heterodimerization by Rapalog, lysosomes clustered at the perinuclear region.

RT112-BicD2 and wild type (wt) RT112 were cultured with (+) or without (-) 1 µM Rapalog to form cell aggregates. After 3 days, the spheroids were plated into collagen I matrix to analyse the cell invasion. RT112-BicD2+ cells were compared to untreated RT112-BicD2-. In addition, to investigate whether Rapalog treatment impacts invasion wt RT112+ were compared to RT112- cells.

A 20% decrease of invasive spheroids (Figure 32C) and a delay in invasion (Figure 32D) was observed in wt RT112+ as compared to wt untreated cells. This indicates that Rapalog had an impact on invasion. The invasion was also moderately delayed in RT112-BicD2+ invasive spheroids as compared to untreated RT112-BicD2- (Figure 32B). Since both controls show a negative impact on cell invasion, this preliminary result does not allow us to conclude the role of chemically inducible changes in cell invasion. More experiments are necessary to further explore these observations.

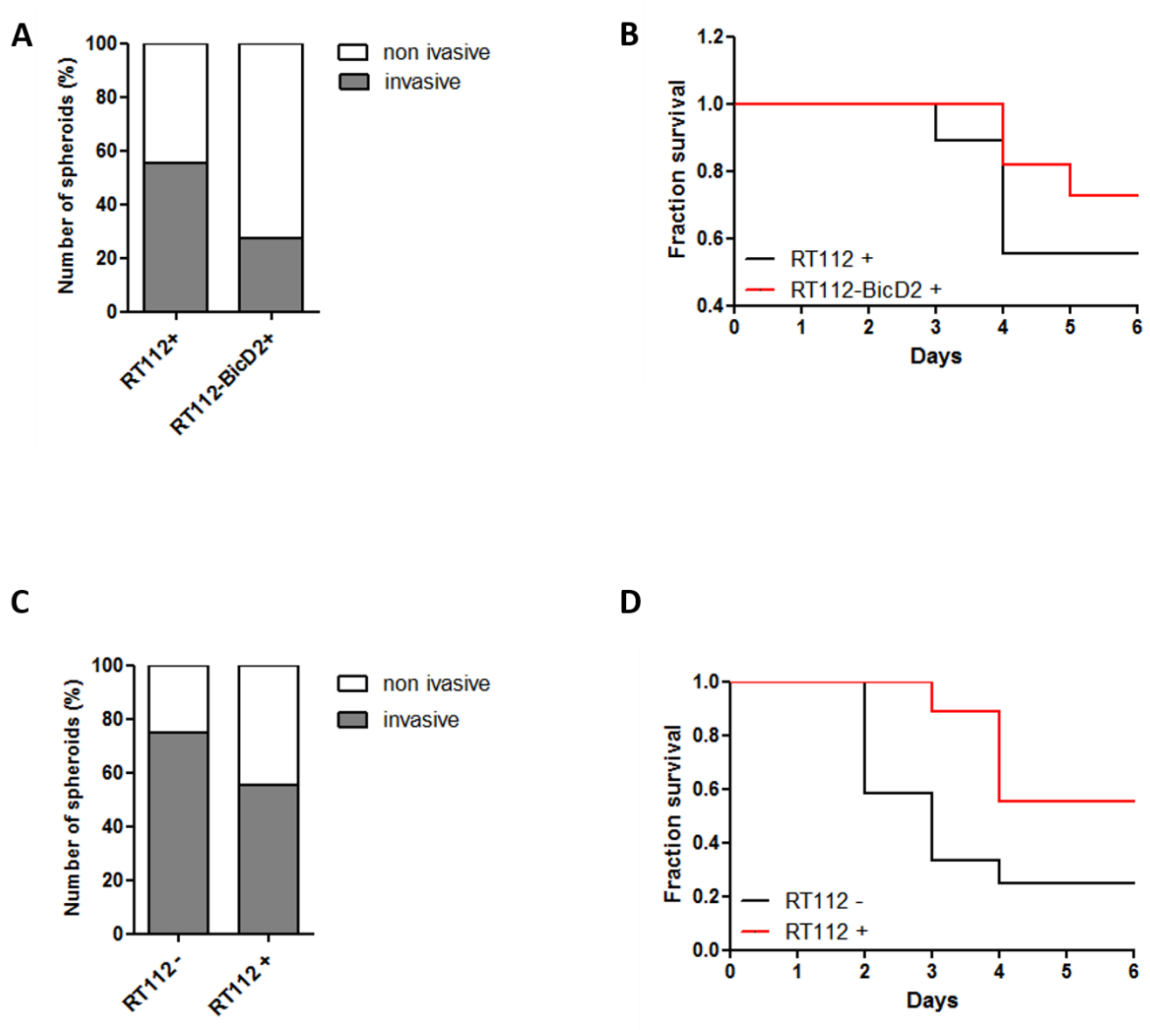

Figure 32: Impact of inducible trafficking of lysosomes by dynactin effector BicD2 in bladder cancer invasion. "+" indicate addition of 1 μM Rapalog, "-" indicate non-treated cells **A.** Number of invasive spheroids. Invasion is significantly decreased in RT112-BiD2+ cells compared to wild type (wt) RT112+ **B.** Fraction of non-invasive spheroids. Delay in invasion in RT112-BiD2+ cells (in red) as compared to wild type (wt) control (in black). **C.** Number of invasive spheroids. Invasion is moderately decreased in wild type RT112+ cells as compared to wild type control RT112- cells **D.** Fraction of non-invasive spheroids. Delay in invasion in wild type RT112+ compared to wild type control RT112- cells

4.2.4. Impact of drug-induced alterations in lysosome positioning

Lysosome positioning changes can be induced with the drug U-18666A, an inhibitor of cholesterol synthesis, that leads to the accumulation of non-esterified cholesterol in lysosomes at the cell center (Rocha et al., 2009). To test the drug efficacy, we treated cells with 3uM of U-18666A and performed a filipin staining in fixed cells; non-treated cells were used as control. The filipin stains fluorescently non-esterified cholesterol in lysosomes. Cells treated with U-18666A showed an important increase in filipin staining, in comparison with non-treated control cells (Figure 33A, example of KU19-19 cells). 50% contour density maps of lysosomes in micropatterned KU19-19 cells, demonstrated that U-18666A changed the lysosomal positioning in these cells, since the lysosome distribution of treated cells (in turquoise) is more central than in non-treated cells (in white) (Figure 33B).

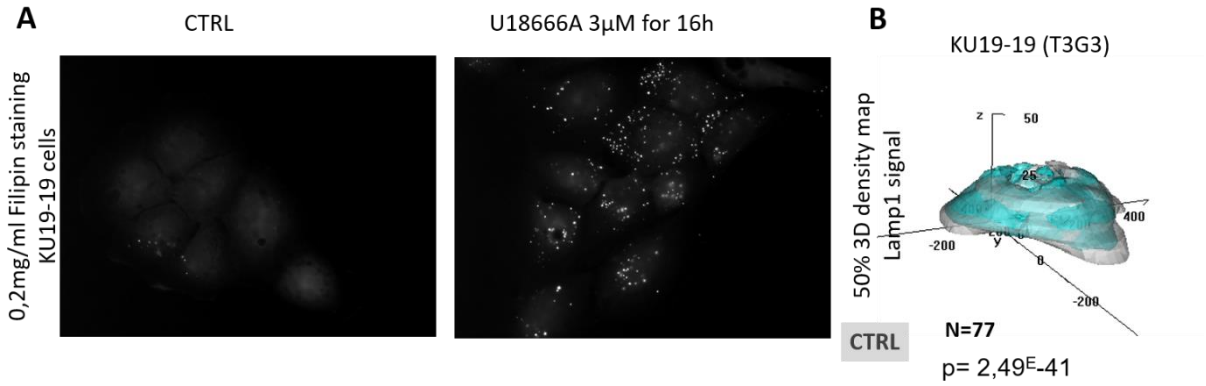

Figure 33: Impact of U-18666A in lysosome positioning. A. 0,2 mg/ml Filipin staining. An increase in the fluorescent signal is observed in KU19-19 (T3) cells treated with 3 µM of U18666A for 20 hours, as compared to non-treated control cells. **B.** 50% 3D density map of Lamp1 staining showing a slight change in lysosomal positioning after treatment (in turquoise), as compared to control non-treated cells (in white). p-value in nonparametric comparison of density maps between depleted cell compared to control.

We treated KU19-19 (T3) and JMSU1 (T4) spheroids with U-18666A drug, non-treated cells were used as control. We observed no difference in cell invasion in treated cell as compared to control (Figure 34). Since these cells are highly invasive with 100% of spheroids invading after 1 day, it is possible that the effect of this drug is not sufficient to impair the invasion

behavior. It would be interesting to test if changes of MCS dynamics affect invasion using grade 2 RT112 cells.

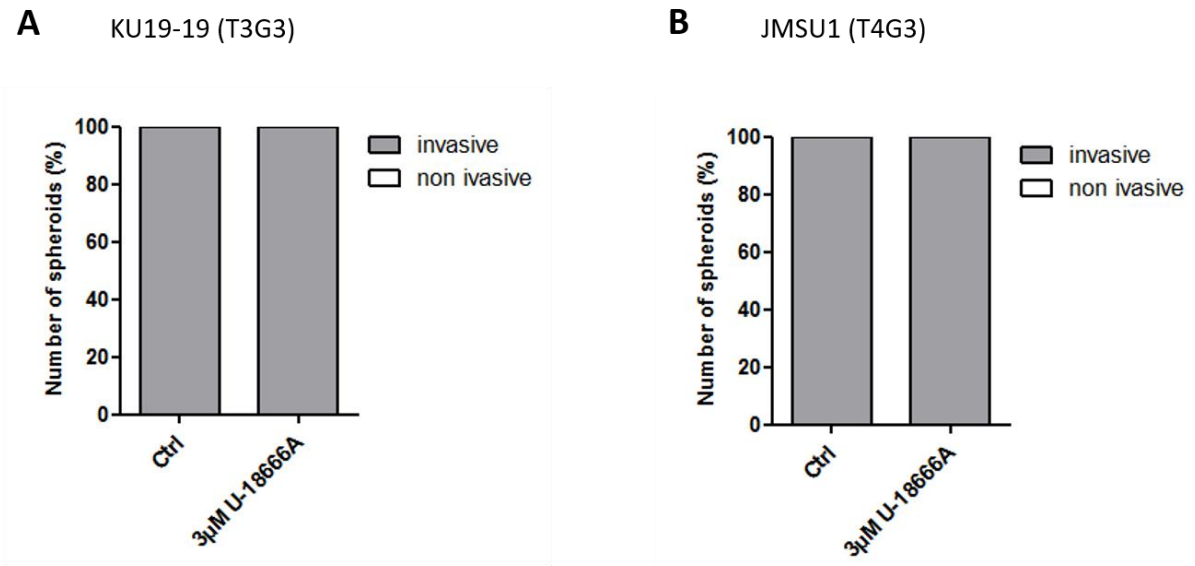

Figure 34: U-18666A does not impact invasion in grade 3 bladder cancer cells.

Discussion:

Lysosomes have been implicated in cell migration and invasion. For instance, lysosomes participate in the fast recycling of integrins to the plasma membrane to support cell migration (Dozynkiewicz et al., 2012; Pu et al., 2015; Schiefermeier et al., 2014). Moreover, lysosomes are implicated in pericellular proteolysis to favor cell invasion (Macpherson et al., 2014; Marchesin et al., 2015; Poincloux et al., 2009; Steffan et al., 2014; Steffen et al., 2008).

Lysosome dispersion to the cell periphery induced by depletion of Rab7, Rab27 and RNF26 significantly increased invasion in grade 1 and 2 cells into collagen matrix. Interestingly, the role of Rab7 seems to be dependent on the cancer type. On the one hand, Rab7 was proposed as a tumor suppressor *in vivo* (Steffan et al., 2014) and its depletion was associated with peripheral lysosome positioning and increased invasion behavior of prostate cancer cells. Rab7 silencing has been shown to decrease cell proliferation, but increase cell motility and invasion of moderately metastatic melanoma cells (Alonso-Curbelo et al., 2014). On the other hand, the expression of dominant negative Rab7 reduced the recycling of MT1-MMP to the plasma membrane, which reduced migration and invasion of fibrosarcoma cells (Williams and Coppolino, 2011). In addition, Rab7 depletion impaired degradation of gelatin substrate by breast cancer cells (Kajiho et al., 2016), although this effect seems to depend on siRNA type: a 5-fold increase in gelatin degradation was observed in one individual siRNA as compared to siRNA pool.

Rab27 silencing correlates with increased invasion of grade 1 MGHU3 cells, but not with grade 2 RT112. The impact of Rab27 on cancer is not clear. It was reported that Rab27 overexpression increases invasion in breast cancer (Hendrix and De Wever, 2013). Rab27 inhibition impairs tumor growth and metastasis, in xerographic metastatic breast cancer in mice (Bobrie et al., 2012). Additionally, Rab27 depletion has been shown to decrease invadopodia formation and associated matrix degradation (Hoshino et al., 2013). However, negative expression of Rab27 correlates with increased invasion in colorectal cancers (Dong et al., 2015). Notably, genes encoding Rab27 and its effector proteins were shown to be repressed in bladder cancers from both Ta and Cis pathway (Ho et al., 2012b). Interestingly, an impairment of grade 3 bladder cancer invasion upon Rab27 knock-down was reported (Ostenfeld et al., 2014). Depletion of Rab27 decreased exosome secretion, which negatively impacted invasion. Therefore, it is possible that the impact of Rab27 depletion in bladder cancer cells depends on grading.

Conversely, a central repositioning of lysosomes impaired 3D invasion of bladder cancer cells. Arl8b mediate peripheral lysosome distribution by recruiting KIF5B and the silencing of both proteins was implicated in lysosome clustering at the cell center (Rosa-Ferreira and Munro, 2011). Recently, Arl8b was reported to impact prostate cancer progression through secretion of proteases, degradation of extracellular matrix proteins and tumor growth and invasion both *in vitro* and *in vivo* (Dykes et al., 2016). Indeed, depletion of Arl8b led to a central positioning of lysosomes, and silencing of both Arl8b and KIF5B impaired cell 3D invasion in RT112 (TaG2) cells.

Furthermore, a striking cluster of lysosomes was induced by Rapalog hetero-dimerization of Lamp1-mCherry-FKBP and BicD2-HA-FRB domains. Our preliminary results suggest that the heterodimerizer Rapalog impairs cell invasion. Therefore, we cannot conclude on the results obtained with RT112-BicD2 cells after addition of Rapalog. Interestingly, mTOR signaling pathway was reported to be hyperactivated in bladder cancer, a signature of poor prognosis (Knollman et al., 2015; Moon et al., 2014). Therefore, it is possible that treatment with Rapalog, a Rapamycin homolog, induced mTOR inhibition that led to decrease of invasion. It would be important to test the activation of mTOR in cells treated with Rapalog. Moreover, it would be interesting to investigate the impact of autophagy on cell invasion. Notably, a link between mTOR signaling and invasion was reported. Rainero and collaborators have shown mTOR activation, upon low nutrient conditions, increased integrin trafficking, which contributes to invasion (Rainero et al., 2015).

Rocha and collaborators have shown that the drug U18666A redistributed the lysosomes to the cell center (Rocha et al., 2009). Therefore, we investigated if the central repositioning of lysosomes had an impact on invasion of grade 3 bladder cancer cell lines. Although lysosome positioning was altered, no impact on cell invasion was observed in these cell lines. Since these cells are highly invasive, it is possible that the drug treatment was not sufficient to impair invasion. Thus, it would be interesting to test the effect of lysosome anterograde distribution induced by U18666A drug on grade 2 cells.

How does lysosome positions impact cellular invasion?

Our results indicate that peripheral lysosome distribution correlates with increased invasion in bladder cancer cell lines. Peripheral lysosomes were reported to increase protease

secretion, acidify extracellular milieu and induce filopodia formation in cancers (Dykes et al., 2016; Glunde et al., 2003; Poincloux et al., 2009; Steffan et al., 2010, 2014). Matrix metalloproteinases (MMPs) have been recognized as important proteases involved in invasive tumor growth (Hotary et al., 2003). It was shown that Rab7 is implicated in MT1-MMP (MMP14) trafficking (Williams and Coppolino, 2011). MMP activity tends to increase when Rab7 is depleted in both MGHU3 (TaG1) and RT112 (TaG2) cell lines (Figure 26). Therefore, it would be important further explore if bladder cancer cell line invasion is facilitated by collagenase proteolysis, for instance by targeting specifc MMPs. Moreover, to address the question if increased MMP activity is specifically linked to Rab7 trafficking or whether is a result of lysosome dispersion to the cell periphery, more regulators of lysosome positioning need to be tested, such as Arl8b, Rab27, RNF26 and the inducible cargo trafficking.

Our results show that cell invasion correlates with bladder cancer grades. Remarkably, we showed that lysosome positioning could play a role on cell invasion of bladder cancer cells. The anterograde transport of lysosomes correlated with accelerated invasion of grade 1 and 2 bladder cancer cells. Conversely, the retrograde transport of lysosomes correlated with a delay of invasion of grade 2 cells, although no impact was observed in highly invasive grade 3 cells. Moreover, MMP proteolysis is a potential mechanism by which invasion could be accelerated in cells with peripheral lysosome positioning.

5. Polarity in bladder cells

Loss of polarity is an important phenotype of epithelial cancers (Wodarz and Näthke, 2007). The maintenance of polarity is regulated by intracellular trafficking, cell-cell contact and cytoskeleton (Muthuswamy and Xue, 2012). The nucleus and Golgi apparatus are often used to define the polarity axis of front-rear polarized cells (for instance migrating cells) and the Golgi apparatus has been implicated in cell polarity (Uetrecht and Bear, 2009). Thus, we investigated whether bladder cells have altered distribution and relative positioning of these organelles.

5.1. Nucleus

The nucleus is the biggest organelle in cells. Changes in shape and size of nuclei are a common phenotype of cancer cells (Denais et al., 2016; Raab et al., 2016; Zink et al., 2004a). Nuclei were visualized with DAPI, a dye that fluorescently stains the DNA (Figure 37A in blue).

Since an alteration in nuclear size is a cancer characteristic, we analyzed the volume of nuclei, based on segmentation data. Analysis was based on more than 140 cells and each nucleus was represented by one point coordinate (Figure 35B). Remarkably, the average volume of nuclei was gradually increased during bladder cancer progression (Figure 35B). Moreover, a gradual alteration in nuclear positioning was noticed in the analyzed bladder cells (Figure 35A). Statistical comparison of density maps revealed stronger differences in distribution in JMSU1 (T4G3) cells as compared to NHU, while MGHU3 (TaG1) have the most similar distribution to control cells (Table 02).

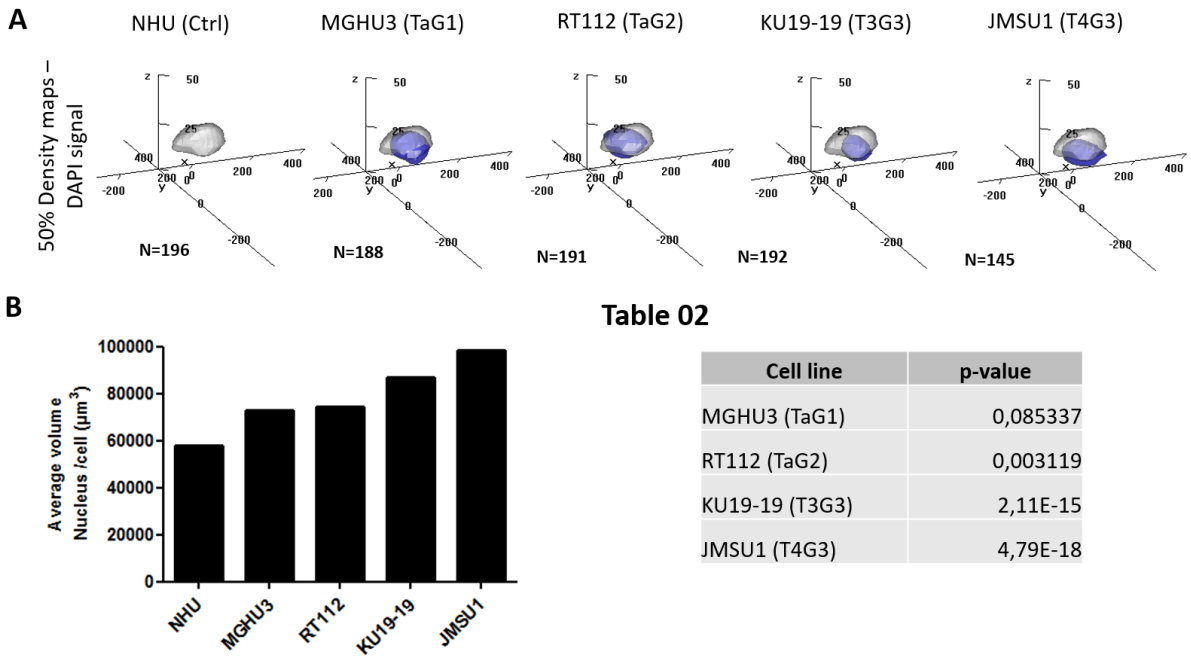

Table 02

Cell line	p-value
MGHU3 (TaG1)	0,085337
RT112 (TaG2)	0,003119
KU19-19 (T3G3)	2,11E-15
JMSU1 (T4G3)	4,79E-18

Figure 35: Change in nuclear compartment in bladder cells. A. 3D density maps 50% contour quantifying nuclei distribution (in blue) compared with NHU control cells (in white). B. Average volume of nuclei gradually increases in bladder cancer cells.

Table 02. Statistical differences between DAPI density maps. P-values correspond to differences between lysosome density maps of analyzed bladder cancer cells and NHU control cells based on nonparametric comparison of density maps. Larger differences are represented by smaller p-values.

5.2. Golgi apparatus

The Golgi apparatus was reported to be fragmented and dispersed in cancers cells (Chia et al., 2012; Petrosyan, 2015). The Golgi apparatus was labeled with an antibody recognizing the protein GM130 (Golgi matrix protein of 130 kDa) (Figure 37A in green). Since fragmentation of the Golgi apparatus is associated with cancer, we investigated whether bladder cancer cells have more Golgi apparatus structures, which could represent a fragmentation of this organelle. A significant increase in number of structures was observed in cells from grade 1, 2 and 3, except for JMSU1 (T4G3) cells (Figure 36B). Thus, alteration in number of these structures did not correlate with grades of bladder cancer. The distribution of Golgi apparatus is slightly modified in bladder cancer cells as compared to NHU (Figure 36A compare green density maps with control in white).

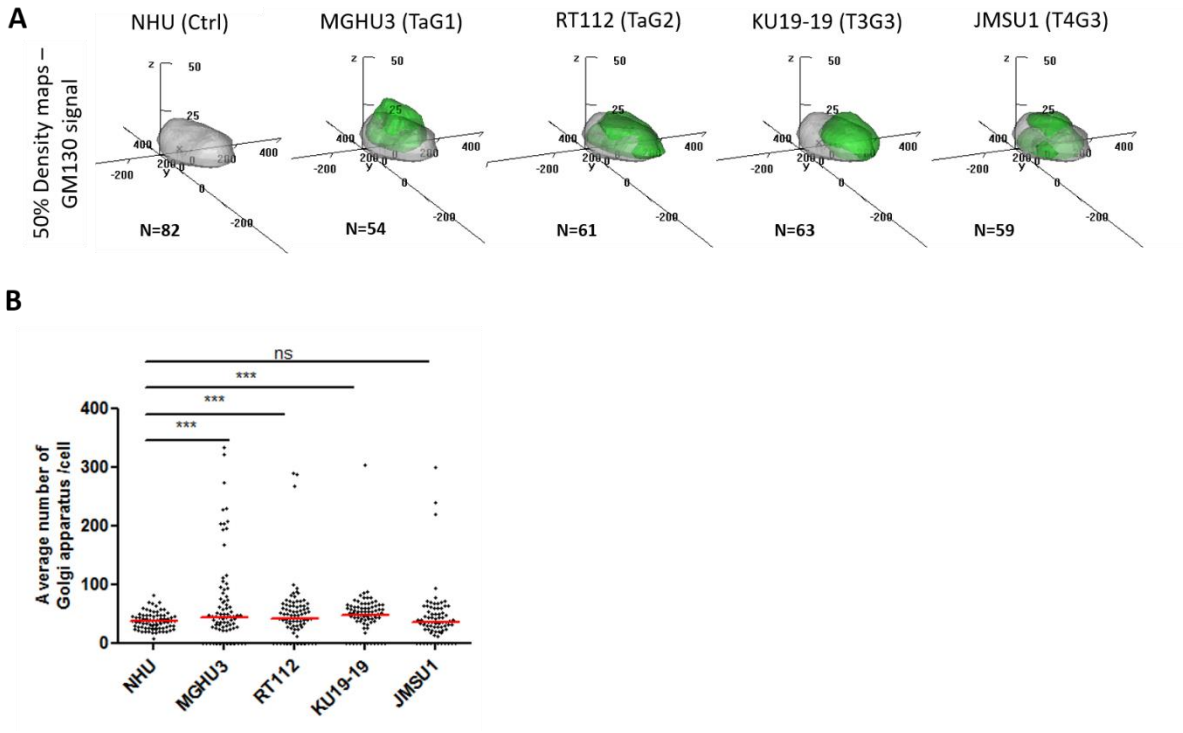

Figure 36: Changes of Golgi apparatus in bladder cells. A. 3D density maps 50% contour quantifying GM130 distribution (in green) compared with NHU control cells (in white). Slight differences in distribution between bladder cancer cells and control. **B.** Average number of Golgi apparatus structures in bladder cells. Significant increase in MGHU3 (TaG1), RT112 (TaG2) and KU19-19 (T3G3) cells. ns, $p>0.5$ and ***, $p<0.001$ in a Student's t-test.

5.3. Nucleus-Golgi apparatus polarization axis

It was demonstrated that the polarization axis from the center of the nucleus towards the center of the Golgi apparatus pointed towards the leading edge of normalized non-transformed human Tert-RPE1 cells on crossbow shaped micropatterns (Théry et al., 2006a). The larger region of adhesion represents the leading edge of crossbow-shaped micropatterns, while the smallest region represents the cell rear. We investigated if this polarization axis is altered in bladder cancer cells, compared to normal human urothelium cells. An analysis of the orientation of the axis between the center of the nucleus and the center of the Golgi apparatus was performed in 2D and in 3D 50% contour density maps.

The vector (Figure 37B in blue) represented the direction of the nucleus-Golgi polarization axis in 2D. In NHU and grade 1 cells (MGHU3) the axis was pointing towards the leading edge. While an inversion is observed in cells representing grades 2 and 3, where vectors are pointing towards the cell rear.

Next, the relative positioning between the 50% 3D density maps of both organelles was compared (Figure 37C). We observed a change in the relative positioning between GM130 (in green) and DAPI (in blue). The nucleus is over the Golgi apparatus in NHU cells, whereas this distribution is changed in bladder cancer cells.

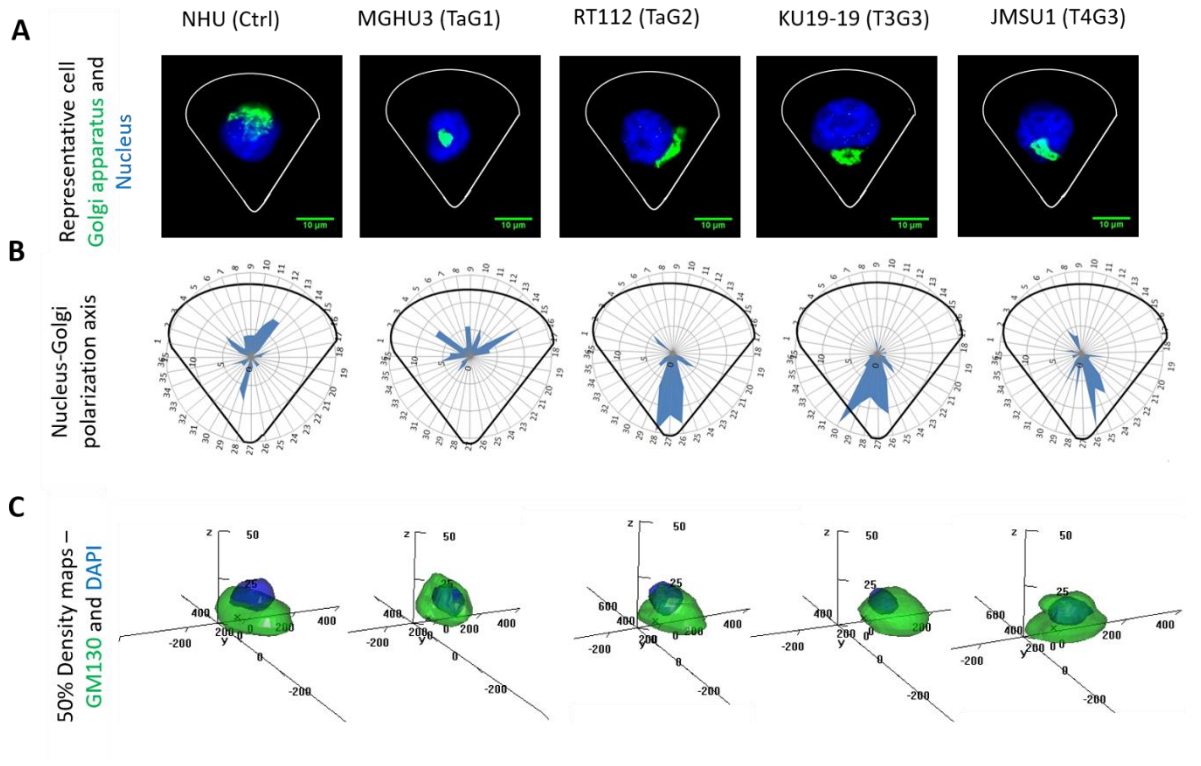

Figure 37: Nucleus-Golgi apparatus polarization axis. A. Representative single cell fluorescent image from GM130 (green) and DAPI (blue). **B.** 2D analysis if nucleus-Golgi polarization axis towards the leading edge in NHU and MGHU3 (TaG1) cells. Inversion of axis in cells representing grades 2 and 3. **C.** 50% contour of the 3D density maps quantifying Golgi apparatus (in green), compared to nucleus (in blue). Differences in relative positioning between the two organelles in bladder cancer cells as compared to NHU cells.

Discussion:

We observed slight differences in Golgi distribution in bladder cancer cells, whereas for the nucleus the positioning is gradually different from normal human urothelium cells. Interestingly, these organelles are tightly connected and are related to cell polarity (Gomes et al., 2005). Loss of cell polarity is a hallmark of malignant cells and correlates with migration, invasion and dissemination (Gomes et al., 2005; Uetrecht and Bear, 2009; Wodarz and Näthke, 2007). It was proposed that crossbow shaped micropatterns mimic a front-rear polarized, migrating cell (Théry et al., 2006a). In RPE1 cells the nucleus-Golgi polarity axis, in 2D, is pointing towards the leading edge. Therefore, we compared the relative positioning between these organelles in crossbow-shaped bladder cancer cells using density maps. Our 2D results suggest an inversion in the nucleus-Golgi apparatus polarization axis in bladder cancer cells from grade 2 and 3 compared to NHU and grade 1 cells. However, the 3D polarity in micropatterns is a complex process that involves several proteins, such as kinesins and proteins from nuclear envelope (Latgé B et al., unpublished work). We observed a change in the relative positioning between the two organelles in 3D. The nuclei are distributed on top of the Golgi apparatus in NHU cells. However this organization is lost in bladder cancer cells, where the density maps of the Golgi apparatus are distributed around the nuclei. Our results suggest alterations in cell polarity in bladder cancer cells.

Additionally, the volume of nuclei was gradually increased and corresponded to bladder cancer progression. Interestingly, changes in the nuclear shape and size is a hallmark of cancer that is explored for diagnosis (Zink et al., 2004a). Moreover, the number of structures corresponding to the Golgi apparatus is significantly increased in all bladder cancer cell lines, except for JMSU1 (T4G3), which indicate that this phenotype does not correlate with grades of bladder cancer. The increased number of structures could suggest a fragmentation of Golgi apparatus, however more analysis are required to conclude on this.

The nuclear size of bladder cancer cells increases gradually. Moreover, we observed alterations in Golgi-nucleus polarization axis in 2D and 3D. Our results suggest that nucleus volume and polarization are important phenotypes of bladder cancer progression.

CONCLUDING REMARKS

Concluding remarks

The changes in organelle distribution during cancer progression is poorly understood. We aimed to fill this gap and study how alterations in distribution of organelles affect bladder cancer progression by normalizing cells on micropatterned adhesive surfaces, combined with quantitative density estimation. We successfully normalized cells representing different stages and grades of bladder cancer, and primary normal human urothelium cells (control). Moreover, all analyzed cells have comparable size, which indicates that alterations observed in 50% contour density maps are indeed due to changes in distribution of organelles.

We performed quantitative comparison of the topology of several major compartments in bladder cells. We observed changes of nucleus-Golgi apparatus polarity axis in cells representing higher grades of bladder cancer. We found that the size of nuclei was gradually increased in bladder cancer cells. Interestinlgy, increased nuclear size is a common feature in cancer cells (Zink et al., 2004). In addition, changes in distribution and number of mitochondria and peroxisomes were observed. However, no direct correlation between alterations in these organelles and bladder cancer grading could be found.

Notably, we found that lysosomes were gradually distributed to the cell periphery in the analyzed bladder cancer cells. These results were confirmed with two additional cell lines that present a similar phenotype. We tested whether lysosome distribution was affected by micropatterns by quantifying lysosome distribution in unconstrained cells and found that lysosomes were also gradually peripheral in this condition. This suggests that lysosome positioning is potentially important in bladder cancer progression.

To further investigate the impact of lysosome positioning in bladder cancer cells, we investigated lysosome-related processes, such as cathepsin B activity (Kallunki et al., 2013) and EGFR signaling attenuation (Taub et al., 2007), in bladder cancer cell lines. No direct correlation between EGFR degradation or cathepsin B activity and peripheral lysosome positioning was found in bladder cancer cell lines.

To further explore the impact of lysosome positioning in bladder cancer cell lines, we aimed to investigate its impact in an important hallmark of cancer, invasion (Hanahan and Weinberg, 2000). We altered the lysosome positioning by targeting several regulators of

lysosome trafficking, Rab7 (Jordens et al., 2001), Rab27 (Neeft et al., 2005), Arl8b (Rosa-Ferreira and Munro, 2011), RNF26 (Jongsma et al., 2016) and KIF5B (Tanaka et al., 1998). Our results showed that distribution of lysosomes to the cell periphery correlates with invasion in grade 1 and 2 bladder cancer cells. Interestingly, it was reported that redistribution of lysosomes to the cell periphery increases cancer invasion (Glunde et al., 2003; Hotary et al., 2003; Steffan et al., 2010). Conversely, preventing anterograde transport of lysosomes by Arl8b depletion was reported to impair invasion of prostate cancer cells (Dykes et al., 2016). Next, we aimed to investigate if moving lysosomes to the cell center negatively correlate with cell invasion of moderately invasive bladder cancer cell line. Our data suggest a delay in cell invasion after retrograde redistribution of lysosomes in RT112 (TaG2) cells. These data suggest that lysosome positioning is potentially relevant in invasion and progression of moderately invasive bladder cancer cell lines.

A possible mechanism by which peripheral lysosomes correlates with invasion could be increased secretion of matrix metalloproteinases. Indeed, MT1-MMP is a collagenase mainly located at lysosomes (Steffen et al., 2008) that accumulates in membrane protusions (Poincloux et al., 2009). We found that MMPs collagenases were gradually increased in the analyzed bladder cancer cell lines. Moreover, preliminary results suggest that Rab7-mediated anterograde transport of lysosomes increases activity of these collagenases. Interestingly, Rab7 is implicated in MT1-MMP trafficking, and its depletion impaired the recycling of this protease to the cell surface, which negatively impacted invasion (Williams and Coppolino, 2011).

Altogether, our results highlight that lysosome distribution could represent a phenotypic signature distinguishing grades and stages of bladder cancer. Of note, cytology exams of urine are currently used to detect bladder cancer. In agreement with our findings, Lamp1 was recently reported as a potential clinical biomarker in bladder cancer (Duriez et al., 2017).

EXPERIMENTAL PROCEDURES

Experimental procedures

Cell culture

Bladder cancer cells lines MGHU3 (Lin et al., 1985), RT112 (Marshall et al., 1977), KU19-19 (Tachibana et al., 1997), JMSU1 (Morita et al., 1995), T24 (Bubeník et al., 1973) and TCCSup (Nayak et al., 1977) were grown in RPMI medium (Life Technologies, Carlsbad, CA, USA) supplemented with 10% Fetal Bovine Serum (FBS; Eurobio, Courtaboeuf, France). Primary normal human urothelium (NHU) (Southgate et al., 1994) cells were grown in KSFMC medium (Life Technologies). All cells were kindly provided by François Radvayi's laboratory (Institut Curie, France). RT112 stably expressing Lamp1-mCherry-FKBP and BicD2-HA-FRB (Figure 38) were obtained by transfection of a Lamp1-mCherry-FKBP and BicD2-HA-FRB gateaway plasmids and selection with 0.5 $mg.mL^{-1}$ Geneticin. The plasmids were a kind gift from Lukas Kapitein's laboratory (Utrecht University, The Netherlands). All cells were cultivated in a humidified atmosphere containing 5% CO_2.

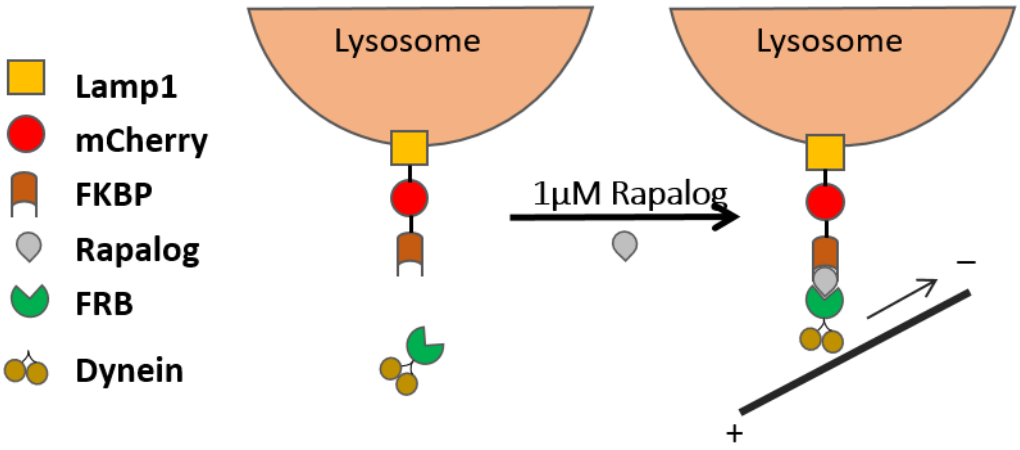

Figure 38: Inducible trafficking of lysosomes by the dynactin effector BicD2.

Cell transfection

$2x10^5$ cell were transfected in 6 well plates with 25 $pmol.mL^{-1}$ siRNA (Table 03) using Lipofectamine RNAiMAX Transfection Reagent (Life Technologies), in Opti-MEM medium (Life Technologies). Cells were incubated 72 hours prior to further manipulations. Efficiency of siRNA gene silencing was verified by performing RT-PCR on cell mRNA or Western Blot on cell lysates after 3 days of transfection. Controls were performed with a siRNA targeting Luciferase, a protein that is not expressed in human cells.

Gene	Sequence
Luciferase	5'-CGTACGCGGAATACTTCGA-3'
Rab7-5	5'-CACGTAGGCCTTCAACACAAT-3'
Rab7-6	5'-CTGCTGCGTTCTGGTATTTGA-3'
Rab27a	
RNF26-1	5'-GAGAGGAUGUCAUGCGGCU-3'
RNF26-2	5'-GCAGAUCAGAGGCAGAAGA-3'
Arl8b	5'- GAUAGAAGCUUCCCGAAAU-3'
KIF5B#2	5'-GCACATCTCAAGAGCAAGT-3'
KIF5B#3	5'-AACGTTGCAAGCAGTTAGAAA-3'

Table 03: siRNA sequences

Micropatterned coverslips preparation and cell seeding

This technique, described by Théry and collaborators in 2006 and adapted by Azioune and collaborators in 2009 (Azioune et al., 2009a; Théry et al., 2006b), allows production of micropatterned surfaces using photo-lithography (Figure 39). Clean glass coverslides were irradiated by Ultraviolet (UV) for 5 minutes. The radiated surface of the coverslips was incubated for 1 hour at room temperature (RT) with PLL-g-PEG (Poly-L-Lysine(20)-grafted[3.5]-Polyethyleneglycol(2), from SuSoS - Dübendorf, Switzerland) at a final concentration of 0.1 mg.mL in 10 mM HEPES (pH 7,3) solution (from Surface Solutions, Zürich). Then, coverslides were exposed to deep UV during 5 min using photomask. Crossbows (37 µm diameter, 7 µm thick) were therefore photo-printed. Prior to cell seeding, the micropatterned surfaces were incubated for 1h with a mixture of fibronectin (Sigma-

Aldrich, St. Louis, MO, USA) at a concentration of 50 µg.mL, concanavalin A (Sigma-Aldrich) at a concentration of 0,1 mg/ml and 10 µg/ml of fibrinogen–Cy5 from (Invitrogen) to stain the micropatterns . Cells were incubated in 20 mM of HEPES (Life Technologies) in serum free RPMI medium.

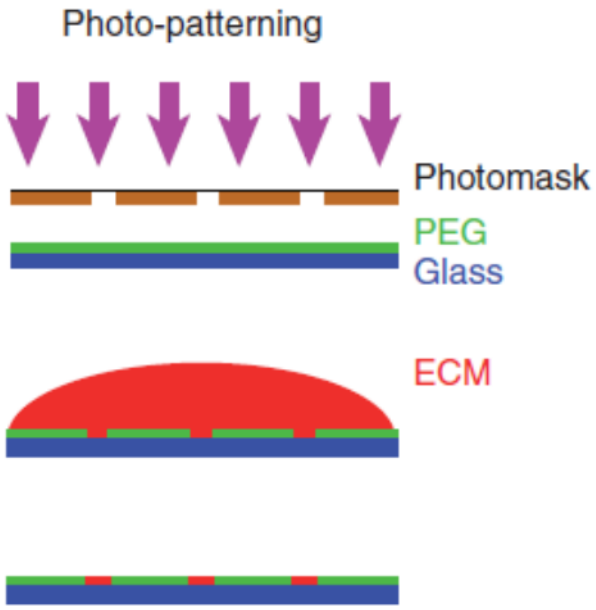

Figure 39: Photoprinting patterning UV light pass trough micropatterns on cell mask and degrade PLL-g-PEG on glass coverslide. Next, the coverslide is coated with extracellular substrate.

Drug treatment

To induce autophagy, 10 µM of Rapamycin (InvivoGen) was added to the cell medium 4 hours prior to fixation or cell lysate for Western Blot. To inhibit cholesterol synthesis and induce accumulation of non-esterified cholesterol in lysosomes, 3 µM of U-18666A (Calbiochem) was incubated for 20h (Rocha et al., 2009) prior to fixation.

Immunofluorescence, image acquisition and analysis

Cells were fixed with 4% Paraformaldehyde (PFA) for 15 minutes at room temperature (RT)

in the dark and then washed 3 times with PBS solution. To quench the PFA, ammonium chloride (NH_4CL) was added at a concentration of 50 mM for 10 minutes following 3 washes with PBS solution. Cells were permeabilized with PBS-2% Bovine Serum Albumine (BSA)-0,05% Saponin for 20 minutes in the dark at RT. Cells were then incubated with a primary antibody (Table 04) for 45 minutes, washed in PBS and incubated with Alexa Fluor 488- or Cy3- coupled secondary antibodies (Jackson ImmunoResearch) or FluoProbes 547H (557/572nm) coupled Phalloïdin (Interchim). Mitotracker (Invitrogen) was used to stain mitochondria at final concentration 100 nM for 15 minutes prior to fixation. Slices were mounted in Mowiol (Sigma-Aldrich). Nuclei were marked using 0.2 $\mu g.ml^{-1}$ 4',6-diamidino-2-phenylindole (DAPI; Sigma-Aldrich). Z images from fixed and immunolabelled cells were acquired with an inverted widefield Deltavision Core Microscope (Applied Precision) equipped with highly sensitive cooled interlined charge-coupled device (CCD) camera (CoolSnap Hq2,Photometrics). Z-dimension series were acquired every 0.5 µm using 40X (1,35 NA) oil objective.

Protein	Species	Company	Dilution
GM130	Mouse	BD Biosciences	1:1000
Lamp1	Mouse	BD Biosciences	1:300
LC3	Rabbit	MBL	1:200
ABCD3	Rabit	Sigma-Aldric	1:200
Tubulin	Human	F2C-hFc LabCollector	1:400
UKHC	Rabbit	Santa Cruz Biotechnology	1:1000
Rab7	Rabbit	Cell Signaling	1:1000
EGFR	Mouse	Calbiochem	1:500
PTP1B	Rabbit	Santa Cruz	1:500

Table 04: Primary antibodies

For each independent experiment, several tens of cells were imaged and aligned using the coordinates of the center and the angle of rotation of the micropattern (determined on ImageJ (Bethesda, MD, USA) as previously described (Grossier et al., 2014; Schauer et al.,

2010). Images were segmented with the multidimensional image analysis (MIA) interface in MetaMorph (Molecular Devices, Sunnyvale, CA, USA) based on wavelet decomposition to extract 3D spatial coordinates of intracellular structures. Unconstrained cells were imaged and segmented as previously described for normalized cells. Using ImageJ, a cell mask was determined based on actin staining. Then, the smallest distance from the center of each segmentation point towards the closest nuclear and membrane edges was calculated. Next, the calculated distance was used to classify the lysosomes according to their sub-cellular localization: perinuclear, intermediate or peripheral.

Kernel density estimation

The coordinates of the segmented structures were processed for density estimation programmed in the ks library in the R programming language (R Development Core Team, 2013) (Schauer et al., 2010). Briefly, Gaussian functions (kernels) with a mean 0 were centered at each segmentation point. Then, kernel functions were summed using a non-parametric, unbinned kernel density estimator. Kernel density estimation could then be visualized by probability contours and the extension libraries mvtnorm, rgl, and miscd.

Analysis of volume and number of intracellular compartments

The segmentation data provides information about the number and volume of structures. This data was calculated for each individual cell. Then, the average number and volume of organelles were calculated and compared.

2D polarity axis between the center of the Golgi apparatus and the center of the nucleus

From segmentation data of the Golgi apparatus and the nucleus, a histogram of angles in Excel was realized and the values were plotted on 360°. The formulas, using 0-2π interval, were: arctan (y/x) for x and y > 0; arctan (y/x) + 2 π for x > 0 and y < 0 and.arctan (y/x) + π if x < 0. The histogram represents the direction of the axis between the center of the nucleus towards the center of the Golgi apparatus.

Immunoblotting

After cell lysis, identical amounts of proteins were loaded in wells of 15% polyacrylamide gels (15-20 µL) and subject to electrophoresis. PageRuler (Thermo Scientific) molecular weight was used for calibration. Proteins were then transferred onto XXX membranes (marque) by semi-dry transfer. PBS + Tween20 (PBST) containing 5% milk (Régilait) was used to block the membranes and dilute the antibodies. PBST was used as wash solution. Primary antibodies (Table 04) were incubated overnight at 4°C, while HRP-conjugated secondary antibodies (Jackson ImmunoResearch) were incubated for 1 hour at RT. Femto or Pico kits (Thermo Scientific, Massachusetts, EUA) were used for the detection of the chemiluminescent signal in ChemiDoc (Biorad). Quantification analysis were performed using ImageJ. For EGFR attenuation of signaling assay, cells were stimulated with 100 nM EGF for 30 minutes or 1 hour prior to cell lysis.

Real-time PCR

Total RNA from cells in different conditions were isolated using xxx kit (Sigma- Aldrich) according to the manufacturer's instructions, and cDNA was synthetized using High capacity cDNA reverse transcription kit, 2500 U (Applied Biosystems, Ref. 4368814). Real-time PCR was performed using LightCycler 480 (Roche) detection system. Relative mRNA levels (Table 05) were calculated using $2^{(-\Delta\Delta Ct)}$ and normalized to GAPDH mRNA expression. All experiments were run in duplicate.

cDNA	Forward	Reverse
GAPDH	5'-TCCACTGGCGTCTTCACC-3'	5'-GGCAGAGATGATGACCCTTTT-3'
Arl8b	5'-AAGCATGTGGGAGCGGTAT-3'	5'-CGATCTGCAGCATCTATCATGT-3'
RNF26	5'-AGCCTGGTGGCTTATGTGAT-3'	5'-AGGTTCTGAGTGCCGATGAG-3'

Table 05: RT-PCR primer sequences

3D Spheroid preparation and invasion assay

Spheroid preparation was done as previously described (Thuault et al., 2016). Cells were trypsinized and 10^4 cells/ml were ressuspended in RPMI medium containing 10% FBS and 1% Penicillin-Streptomycin (Life Technologies). Then 100 µl of cell suspension was plated in 48-well plates coated with 1% agarose (Life Technologies) and incubated for 3 days (Figure 40). In each well, a spheroid was formed from 10^3 cells. Next, the spheroids were plated on Lab-Tek chambers (Sigma), in a mixture of collagen I from rat tail (Corning) at a final concentration of 2 $mg.ml^{-1}$, PBS, sodium hydroxide (NaOH) and serum-free medium. For siRNA experiments, the medium was replaced with the transfection mixture (Opti-MEM medium from Life Technologies, Lipofectamin RNAiMAX and siRNA). For inducible cargo trafficking assays, 1 µM of A/C heterodimerizer (Clontech, California-USA) was added in the collagen mixture and in the culture medium. The spheroids were monitored for 6 consecutive days by using an inverted Leica microscope (Wetzlar, Germany) equipped with camera device using a 4x objective.

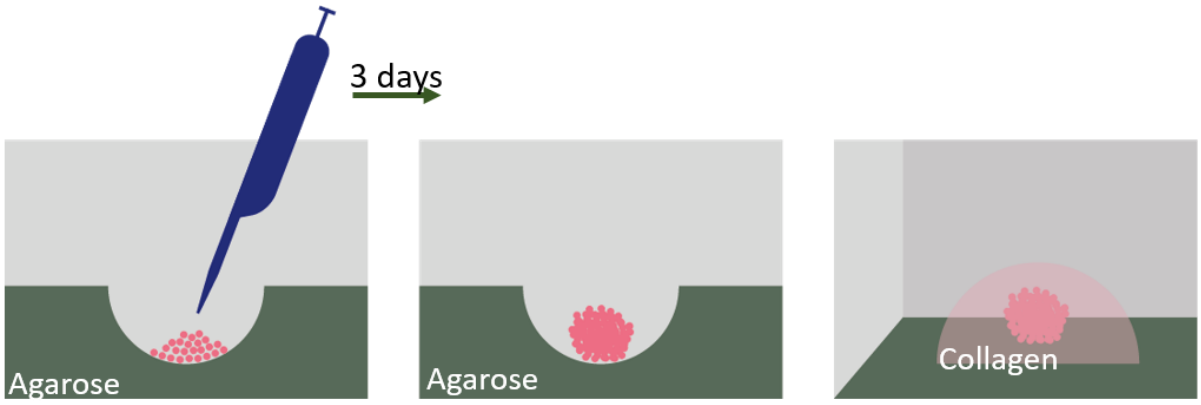

Figure 40: Spheroid formation.

Matrix metalloproteinases activity

MMPs activity was tested following the manufacturer's protocol of the fluorimetric SensoLyte® 520 generic MMP activity assay (AnaSpec). Briefly, cell supernatant was centrifuged to eliminate floating cells. Then, samples were incubated with APMA (4-

aminophenylmercuric acetate) for 3 hours at 37°C to target MMP1 and MMP14. Then, the MMP substrate containing 5-FAM/QXL™520 FRET peptide was incubated 1 hour at RT prior to measurement of fluorescence signal (450 nm excitation and 520 nm emission).

Cathepsin B activity

Cathepsin B activity was tested following the manufacturer's protocol (InnoZyme - Millipore). Briefly, cell pellets were washed with cold PBS and lysed during 30 minutes on ice. Cathepsin B substrate containing the carboxyl side of arginylarginine was incubated for 30 minutes at 37°C prior to measurement of fluorescence signal (360 nm excitation and 440 nm emission).

Statistical analysis

For each experiment, a large number of cells from 3 to 6 independent experiments were monitored. Bilateral Student t-tests were performed on averages to assess the significance of the difference. To compare the fraction of non-invasive spheroids Matel-Cox test was performed in Prism software. Additionally, to compare the global distribution of cell populations, χ^2 tests were performed (R function "chi-square()"). In this case, results from independent experiments were individually compared and combined for representation and statistical analysis. For the three analysis, consider: ns, $P > 0.05$; *, $P<0.05$; **, $P<0.01$; ***, $P<0.001$. Comparison between density maps was realized using multivariate two-sample nonparametric statistical test (R software) (Duong et al., 2012).

REFERENCES

References

Ahmad, I., Sansom, O.J., and Leung, H.Y. (2012). Exploring molecular genetics of bladder cancer: lessons learned from mouse models. Dis. Model. Mech. *5*, 323–332.

Alberts, B., Johnson, A., Lewis, J., Raff, M., Roberts, K., and Walter, P. (2002). Integrins.

Alonso-Curbelo, D., Riveiro-Falkenbach, E., Pérez-Guijarro, E., Cifdaloz, M., Karras, P., Osterloh, L., Megías, D., Cañón, E., Calvo, T.G., Olmeda, D., et al. (2014). RAB7 controls melanoma progression by exploiting a lineage-specific wiring of the endolysosomal pathway. Cancer Cell *26*, 61–76.

Amaya, C., Militello, R.D., Calligaris, S.D., and Colombo, M.I. (2016). Rab24 interacts with the Rab7/Rab interacting lysosomal protein complex to regulate endosomal degradation. Traffic Cph. Den. *17*, 1181–1196.

Amillet, J.-M., Ferbus, D., Real, F.X., Antony, C., Muleris, M., Gress, T.M., and Goubin, G. (2006). Characterization of human Rab20 overexpressed in exocrine pancreatic carcinoma. Hum. Pathol. *37*, 256–263.

Attieh, Y., and Vignjevic, D.M. (2016). The hallmarks of CAFs in cancer invasion. Eur. J. Cell Biol. *95*, 493–502.

Azioune, A., Storch, M., Bornens, M., Théry, M., and Piel, M. (2009a). Simple and rapid process for single cell micro-patterning. Lab. Chip *9*, 1640–1642.

Azioune, A., Storch, M., Bornens, M., Théry, M., and Piel, M. (2009b). Simple and rapid process for single cell micro-patterning. Lab. Chip *9*, 1640–1642.

Baba, A.I., and Câtoi, C. (2007). TUMOR CELL MORPHOLOGY (The Publishing House of the Romanian Academy).

Baumdick, M., Brüggemann, Y., Schmick, M., Xouri, G., Sabet, O., Davis, L., Chin, J.W., and Bastiaens, P.I. (2015). EGF-dependent re-routing of vesicular recycling switches spontaneous phosphorylation suppression to EGFR signaling. eLife *4*.

Bazellières, E., Conte, V., Elosegui-Artola, A., Serra-Picamal, X., Bintanel-Morcillo, M., Roca-Cusachs, P., Muñoz, J.J., Sales-Pardo, M., Guimerà, R., and Trepat, X. (2015). Control of cell-cell forces and collective cell dynamics by the intercellular adhesome. Nat. Cell Biol. *17*, 409–420.

Benhamou, S., Bonastre, J., Groussard, K., Radvanyi, F., Allory, Y., and Lebret, T. (2016). A prospective multicenter study on bladder cancer: the COBLAnCE cohort. BMC Cancer *16*, 837.

Bergfeld, S.A., and DeClerck, Y.A. (2010). Bone marrow-derived mesenchymal stem cells and the tumor microenvironment. Cancer Metastasis Rev. *29*, 249–261.

Bhowmick, N.A., Neilson, E.G., and Moses, H.L. (2004). Stromal fibroblasts in cancer initiation and progression. Nature *432*, 332–337.

Billerey, C., Chopin, D., Aubriot-Lorton, M.H., Ricol, D., Gil Diez de Medina, S., Van Rhijn, B., Bralet, M.P., Lefrere-Belda, M.A., Lahaye, J.B., Abbou, C.C., et al. (2001). Frequent FGFR3 mutations in papillary non-invasive bladder (pTa) tumors. Am. J. Pathol. *158*, 1955–1959.

Blasco, M.A. (2005). Telomeres and human disease: ageing, cancer and beyond. Nat. Rev. Genet. *6*, 611–622.

Bobrie, A., Krumeich, S., Reyal, F., Recchi, C., Moita, L.F., Seabra, M.C., Ostrowski, M., and Théry, C. (2012). Rab27a supports exosome-dependent and -independent mechanisms that modify the tumor microenvironment and can promote tumor progression. Cancer Res. *72*, 4920–4930.

Bonifacino, J.S., and Neefjes, J. (2017). Moving and positioning the endolysosomal system. Curr. Opin. Cell Biol. *47*, 1–8.

Braulke, T., and Bonifacino, J.S. (2009). Sorting of lysosomal proteins. Biochim. Biophys. Acta *1793*, 605–614.

Bravo-Cordero, J.J., Marrero-Diaz, R., Megías, D., Genís, L., García-Grande, A., García, M.A., Arroyo, A.G., and Montoya, M.C. (2007). MT1-MMP proinvasive activity is regulated by a novel Rab8-dependent exocytic pathway. EMBO J. *26*, 1499–1510.

Brooks, P.C., Silletti, S., von Schalscha, T.L., Friedlander, M., and Cheresh, D.A. (1998). Disruption of angiogenesis by PEX, a noncatalytic metalloproteinase fragment with integrin binding activity. Cell *92*, 391–400.

Bubeník, J., Baresová, M., Viklický, V., Jakoubková, J., Sainerová, H., and Donner, J. (1973). Established cell line of urinary bladder carcinoma (T24) containing tumour-specific antigen. Int. J. Cancer J. Int. Cancer *11*, 765–773.

Bucci, C., Thomsen, P., Nicoziani, P., McCarthy, J., and van Deurs, B. (2000). Rab7: a key to lysosome biogenesis. Mol. Biol. Cell *11*, 467–480.

Burger, M., Catto, J.W.F., Dalbagni, G., Grossman, H.B., Herr, H., Karakiewicz, P., Kassouf, W., Kiemeney, L.A., La Vecchia, C., Shariat, S., et al. (2013). Epidemiology and risk factors of urothelial bladder cancer. Eur. Urol. *63*, 234–241.

Calvo, E., and Rowinsky, E.K. (2004). Effect of epidermal growth factor receptor mutations on the response to epidermal growth factor receptor tyrosine kinase inhibitors: target-based populations for target-based drugs. Clin. Lung Cancer *6 Suppl 1*, S35-42.

Capell, B.C., and Collins, F.S. (2006). Human laminopathies: nuclei gone genetically awry. Nat. Rev. Genet. *7*, 940–952.

Cappellen, D., De Oliveira, C., Ricol, D., de Medina, S., Bourdin, J., Sastre-Garau, X., Chopin, D., Thiery, J.P., and Radvanyi, F. (1999). Frequent activating mutations of FGFR3 in human bladder and cervix carcinomas. Nat. Genet. *23*, 18–20.

Carter, S.B. (1967). Haptotactic islands: a method of confining single cells to study individual cell reactions and clone formation. Exp. Cell Res. *48*, 189–193.

Causeret, M., Taulet, N., Comunale, F., Favard, C., and Gauthier-Rouvière, C. (2005). N-cadherin association with lipid rafts regulates its dynamic assembly at cell-cell junctions in C2C12 myoblasts. Mol. Biol. Cell *16*, 2168–2180.

Cavalli, L.R., Varella-Garcia, M., and Liang, B.C. (1997). Diminished tumorigenic phenotype after depletion of mitochondrial DNA. Cell Growth Differ. Mol. Biol. J. Am. Assoc. Cancer Res. *8*, 1189–1198.

Cheng, N., Chytil, A., Shyr, Y., Joly, A., and Moses, H.L. (2008). Transforming growth factor-beta signaling-deficient fibroblasts enhance hepatocyte growth factor signaling in mammary carcinoma cells to promote scattering and invasion. Mol. Cancer Res. MCR *6*, 1521–1533.

Chia, J., Goh, G., Racine, V., Ng, S., Kumar, P., and Bard, F. (2012). RNAi screening reveals a large signaling network controlling the Golgi apparatus in human cells. Mol. Syst. Biol. *8*, 629.

Cho, R.W., and Clarke, M.F. (2008). Recent advances in cancer stem cells. Curr. Opin. Genet. Dev. *18*, 48–53.

Choi, W., Porten, S., Kim, S., Willis, D., Plimack, E.R., Hoffman-Censits, J., Roth, B., Cheng, T., Tran, M., Lee, I.-L., et al. (2014). Identification of distinct basal and luminal subtypes of muscle-invasive bladder cancer with different sensitivities to frontline chemotherapy. Cancer Cell *25*, 152–165.

Chow, K.-H., Factor, R.E., and Ullman, K.S. (2012). The nuclear envelope environment and its cancer connections. Nat. Rev. Cancer *12*, 196–209.

Clark, A.G., and Vignjevic, D.M. (2015). Modes of cancer cell invasion and the role of the microenvironment. Curr. Opin. Cell Biol. *36*, 13–22.

Conklin, M.W., Eickhoff, J.C., Riching, K.M., Pehlke, C.A., Eliceiri, K.W., Provenzano, P.P., Friedl, A., and Keely, P.J. (2011). Aligned collagen is a prognostic signature for survival in human breast carcinoma. Am. J. Pathol. *178*, 1221–1232.

Cukierman, E., Pankov, R., Stevens, D.R., and Yamada, K.M. (2001). Taking cell-matrix adhesions to the third dimension. Science *294*, 1708–1712.

Daniele, T., Hurbain, I., Vago, R., Casari, G., Raposo, G., Tacchetti, C., and Schiaffino, M.V. (2014). Mitochondria and melanosomes establish physical contacts modulated by Mfn2 and involved in organelle biogenesis. Curr. Biol. CB *24*, 393–403.

De Duve, C., Pressman, B.C., Gianetto, R., Wattiaux, R., and Appelmans, F. (1955). Tissue fractionation studies. 6. Intracellular distribution patterns of enzymes in rat-liver tissue. Biochem. J. *60*, 604–617.

Dean, R.A., Cox, J.H., Bellac, C.L., Doucet, A., Starr, A.E., and Overall, C.M. (2008). Macrophage-specific metalloelastase (MMP-12) truncates and inactivates ELR+ CXC chemokines and generates CCL2, -7, -8, and -13 antagonists: potential role of the macrophage in terminating polymorphonuclear leukocyte influx. Blood *112*, 3455–3464.

Delille, H.K., Bonekamp, N.A., and Schrader, M. (2006). Peroxisomes and disease - an overview. Int. J. Biomed. Sci. IJBS *2*, 308–314.

Denais, C.M., Gilbert, R.M., Isermann, P., McGregor, A.L., te Lindert, M., Weigelin, B., Davidson, P.M., Friedl, P., Wolf, K., and Lammerding, J. (2016). Nuclear envelope rupture and repair during cancer cell migration. Science *352*, 353–358.

DeNardo, D.G., Johansson, M., and Coussens, L.M. (2008). Immune cells as mediators of solid tumor metastasis. Cancer Metastasis Rev. *27*, 11–18.

Desai, R.A., Gao, L., Raghavan, S., Liu, W.F., and Chen, C.S. (2009). Cell polarity triggered by cell-cell adhesion via E-cadherin. J. Cell Sci. *122*, 905–911.

Desai, S.P., Bhatia, S.N., Toner, M., and Irimia, D. (2013). Mitochondrial localization and the persistent migration of epithelial cancer cells. Biophys. J. *104*, 2077–2088.

Dey, P. (2010). Cancer nucleus: Morphology and beyond. Diagn. Cytopathol. *38*, 382–390.

Di Lullo, G.A., Sweeney, S.M., Korkko, J., Ala-Kokko, L., and San Antonio, J.D. (2002). Mapping the ligand-binding sites and disease-associated mutations on the most abundant protein in the human, type I collagen. J. Biol. Chem. *277*, 4223–4231.

Dong, W., Cui, J., Yang, J., Li, W., Wang, S., Wang, X., Li, X., Lu, Y., and Xiao, W. (2015). Decreased expression of Rab27A and Rab27B correlates with metastasis and poor prognosis in colorectal cancer. Discov. Med. *20*, 357–367.

Dozynkiewicz, M.A., Jamieson, N.B., Macpherson, I., Grindlay, J., van den Berghe, P.V.E., von Thun, A., Morton, J.P., Gourley, C., Timpson, P., Nixon, C., et al. (2012). Rab25 and CLIC3 collaborate to promote integrin recycling from late endosomes/lysosomes and drive cancer progression. Dev. Cell *22*, 131–145.

Dumin, J.A., Dickeson, S.K., Stricker, T.P., Bhattacharyya-Pakrasi, M., Roby, J.D., Santoro, S.A., and Parks, W.C. (2001). Pro-collagenase-1 (matrix metalloproteinase-1) binds the alpha(2)beta(1) integrin upon release from keratinocytes migrating on type I collagen. J. Biol. Chem. *276*, 29368–29374.

Dumont, N., Liu, B., Defilippis, R.A., Chang, H., Rabban, J.T., Karnezis, A.N., Tjoe, J.A., Marx, J., Parvin, B., and Tlsty, T.D. (2013). Breast fibroblasts modulate early dissemination, tumorigenesis, and metastasis through alteration of extracellular matrix characteristics. Neoplasia N. Y. N *15*, 249–262.

Duong, T., Goud, B., and Schauer, K. (2012). Closed-form density-based framework for automatic detection of cellular morphology changes. Proc. Natl. Acad. Sci. U. S. A. *109*, 8382–8387.

Duriez, E., Masselon, C.D., Mesmin, C., Court, M., Demeure, K., Allory, Y., Malats, N., Matondo, M., Radvanyi, F., Garin, J., et al. (2017). Large-Scale SRM Screen of Urothelial Bladder Cancer Candidate Biomarkers in Urine. J. Proteome Res. *16*, 1617–1631.

Dykes, S.S., Gray, A.L., Coleman, D.T., Saxena, M., Stephens, C.A., Carroll, J.L., Pruitt, K., and Cardelli, J.A. (2016). The Arf-like GTPase Arl8b is essential for three-dimensional invasive growth of prostate cancer in vitro and xenograft formation and growth in vivo. Oncotarget.

Dykes, S.S., Gao, C., Songock, W.K., Bigelow, R.L., Woude, G.V., Bodily, J.M., and Cardelli, J.A. (2017). Zinc finger E-box binding homeobox-1 (Zeb1) drives anterograde lysosome trafficking and tumor cell invasion via upregulation of Na+/H+ Exchanger-1 (NHE1). Mol. Carcinog. *56*, 722–734.

Eagles, P.A., Johnson, L.N., and Van Horn, C. (1975). The distribution of Concanavalin A receptor sites on the membrane of chromaffin granules. J. Cell Sci. *19*, 33–54.

Earl, J., Rico, D., Carrillo-de-Santa-Pau, E., Rodríguez-Santiago, B., Méndez-Pertuz, M., Auer, H., Gómez, G., Grossman, H.B., Pisano, D.G., Schulz, W.A., et al. (2015a). The UBC-40 Urothelial Bladder Cancer cell line index: a genomic resource for functional studies. BMC Genomics *16*, 403.

Earl, J., Rico, D., Carrillo-de-Santa-Pau, E., Rodríguez-Santiago, B., Méndez-Pertuz, M., Auer, H., Gómez, G., Grossman, H.B., Pisano, D.G., Schulz, W.A., et al. (2015b). Erratum to:

The UBC-40 Urothelial Bladder Cancer Cell Line Index: a genomic resource for functional studies. BMC Genomics *16*, 1019.

Elkhatib, N., Bresteau, E., Baschieri, F., Rioja, A.L., van Niel, G., Vassilopoulos, S., and Montagnac, G. (2017). Tubular clathrin/AP-2 lattices pinch collagen fibers to support 3D cell migration. Science *356*.

Fennelly, C., and Amaravadi, R.K. (2017). Lysosomal Biology in Cancer. Methods Mol. Biol. Clifton NJ *1594*, 293–308.

Ferlay, J., Soerjomataram, I., Dikshit, R., Eser, S., Mathers, C., Rebelo, M., Parkin, D.M., Forman, D., and Bray, F. (2015). Cancer incidence and mortality worldwide: sources, methods and major patterns in GLOBOCAN 2012. Int. J. Cancer *136*, E359-386.

Fouad, Y.A., and Aanei, C. (2017). Revisiting the hallmarks of cancer. Am. J. Cancer Res. *7*, 1016–1036.

Friedl, P., and Alexander, S. (2011). Cancer invasion and the microenvironment: plasticity and reciprocity. Cell *147*, 992–1009.

Friedl, P., and Wolf, K. (2003). Tumour-cell invasion and migration: diversity and escape mechanisms. Nat. Rev. Cancer *3*, 362–374.

Friedl, P., Wolf, K., and Lammerding, J. (2011). Nuclear mechanics during cell migration. Curr. Opin. Cell Biol. *23*, 55–64.

Friedman, J.R., Dibenedetto, J.R., West, M., Rowland, A.A., and Voeltz, G.K. (2013). Endoplasmic reticulum-endosome contact increases as endosomes traffic and mature. Mol. Biol. Cell *24*, 1030–1040.

Fukumura, D., Xavier, R., Sugiura, T., Chen, Y., Park, E.C., Lu, N., Selig, M., Nielsen, G., Taksir, T., Jain, R.K., et al. (1998). Tumor induction of VEGF promoter activity in stromal cells. Cell *94*, 715–725.

Galluzzi, L., Baehrecke, E.H., Ballabio, A., Boya, P., Bravo-San Pedro, J.M., Cecconi, F., Choi, A.M., Chu, C.T., Codogno, P., Colombo, M.I., et al. (2017). Molecular definitions of autophagy and related processes. EMBO J.

Gálvez, B.G., Matías-Román, S., Yáñez-Mó, M., Sánchez-Madrid, F., and Arroyo, A.G. (2002). ECM regulates MT1-MMP localization with beta1 or alphavbeta3 integrins at distinct cell compartments modulating its internalization and activity on human endothelial cells. J. Cell Biol. *159*, 509–521.

Garg, S., Sharma, M., Ung, C., Tuli, A., Barral, D.C., Hava, D.L., Veerapen, N., Besra, G.S., Hacohen, N., and Brenner, M.B. (2011). Lysosomal trafficking, antigen presentation, and microbial killing are controlled by the Arf-like GTPase Arl8b. Immunity *35*, 182–193.

Gebhardt, C., Breitenbach, U., Richter, K.H., Fürstenberger, G., Mauch, C., Angel, P., and Hess, J. (2005). c-Fos-dependent induction of the small ras-related GTPase Rab11a in skin carcinogenesis. Am. J. Pathol. *167*, 243–253.

Glentis, A., Gurchenkov, V., and Vignjevic, D.M. Assembly, heterogeneity, and breaching of the basement membranes. - PubMed - NCBI.

Glunde, K., Guggino, S.E., Solaiyappan, M., Pathak, A.P., Ichikawa, Y., and Bhujwalla, Z.M. (2003). Extracellular acidification alters lysosomal trafficking in human breast cancer cells. Neoplasia N. Y. N *5*, 533–545.

Goldenring, J.R. (2013). A central role for vesicle trafficking in epithelial neoplasia: intracellular highways to carcinogenesis. Nat. Rev. Cancer *13*, 813–820.

Gomes, E.R., Jani, S., and Gundersen, G.G. (2005). Nuclear movement regulated by Cdc42, MRCK, myosin, and actin flow establishes MTOC polarization in migrating cells. Cell *121*, 451–463.

Greider, C.W., and Blackburn, E.H. (1985). Identification of a specific telomere terminal transferase activity in Tetrahymena extracts. Cell *43*, 405–413.

Greider, C.W., and Blackburn, E.H. (1989). A telomeric sequence in the RNA of Tetrahymena telomerase required for telomere repeat synthesis. Nature *337*, 331–337.

Grivennikov, S.I., Greten, F.R., and Karin, M. (2010). Immunity, inflammation, and cancer. Cell *140*, 883–899.

Grossier, J.-P., Goud, B., and Schauer, K. (2014a). Probabilistic density maps to study the spatial organization of endocytosis. Methods Mol. Biol. Clifton NJ *1174*, 117–138.

Grossier, J.-P., Xouri, G., Goud, B., and Schauer, K. (2014b). Cell adhesion defines the topology of endocytosis and signaling. EMBO J. *33*, 35–45.

Guardia, C.M., Farías, G.G., Jia, R., Pu, J., and Bonifacino, J.S. (2016). BORC Functions Upstream of Kinesins 1 and 3 to Coordinate Regional Movement of Lysosomes along Different Microtubule Tracks. Cell Rep. *17*, 1950–1961.

Gumbiner, B.M. (1996). Cell adhesion: the molecular basis of tissue architecture and morphogenesis. Cell *84*, 345–357.

H Rashed, M., Bayraktar, E., K Helal, G., Abd-Ellah, M.F., Amero, P., Chavez-Reyes, A., and Rodriguez-Aguayo, C. (2017). Exosomes: From Garbage Bins to Promising Therapeutic Targets. Int. J. Mol. Sci. *18*.

Hämälistö, S., and Jäättelä, M. (2016). Lysosomes in cancer-living on the edge (of the cell). Curr. Opin. Cell Biol. *39*, 69–76.

Hanahan, D., and Weinberg, R.A. (2000). The hallmarks of cancer. Cell *100*, 57–70.

Hanahan, D., and Weinberg, R.A. (2011). Hallmarks of cancer: the next generation. Cell *144*, 646–674.

Hare, S.H., and Harvey, A.J. (2017). mTOR function and therapeutic targeting in breast cancer. Am. J. Cancer Res. *7*, 383–404.

Harris, T.J.C., and Tepass, U. (2010). Adherens junctions: from molecules to morphogenesis. Nat. Rev. Mol. Cell Biol. *11*, 502–514.

Hasumi, H., Baba, M., Hasumi, Y., Huang, Y., Oh, H., Hughes, R.M., Klein, M.E., Takikita, S., Nagashima, K., Schmidt, L.S., et al. (2012). Regulation of mitochondrial oxidative metabolism by tumor suppressor FLCN. J. Natl. Cancer Inst. *104*, 1750–1764.

Hegerfeldt, Y., Tusch, M., Bröcker, E.-B., and Friedl, P. (2002). Collective cell movement in primary melanoma explants: plasticity of cell-cell interaction, beta1-integrin function, and migration strategies. Cancer Res. *62*, 2125–2130.

Hendrix, A., and De Wever, O. (2013). Rab27 GTPases distribute extracellular nanomaps for invasive growth and metastasis: implications for prognosis and treatment. Int. J. Mol. Sci. *14*, 9883–9892.

Heuser, J. (1989). Changes in lysosome shape and distribution correlated with changes in cytoplasmic pH. J. Cell Biol. *108*, 855–864.

Ho, J.R., Chapeaublanc, E., Kirkwood, L., Nicolle, R., Benhamou, S., Lebret, T., Allory, Y., Southgate, J., Radvanyi, F., and Goud, B. (2012a). Deregulation of Rab and Rab effector genes in bladder cancer. PloS One *7*, e39469.

Ho, J.R., Chapeaublanc, E., Kirkwood, L., Nicolle, R., Benhamou, S., Lebret, T., Allory, Y., Southgate, J., Radvanyi, F., and Goud, B. (2012b). Deregulation of Rab and Rab effector genes in bladder cancer. PloS One *7*, e39469.

Holthuis, J.C.M., and Levine, T.P. (2005). Lipid traffic: floppy drives and a superhighway. Nat. Rev. Mol. Cell Biol. *6*, 209–220.

Hoshino, D., Kirkbride, K.C., Costello, K., Clark, E.S., Sinha, S., Grega-Larson, N., Tyska, M.J., and Weaver, A.M. (2013). Exosome secretion is enhanced by invadopodia and drives invasive behavior. Cell Rep. *5*, 1159–1168.

Hotary, K.B., Allen, E.D., Brooks, P.C., Datta, N.S., Long, M.W., and Weiss, S.J. (2003). Membrane type I matrix metalloproteinase usurps tumor growth control imposed by the three-dimensional extracellular matrix. Cell *114*, 33–45.

Humphrey, P.A., Moch, H., Cubilla, A.L., Ulbright, T.M., and Reuter, V.E. (2016). The 2016 WHO Classification of Tumours of the Urinary System and Male Genital Organs-Part B: Prostate and Bladder Tumours. Eur. Urol. *70*, 106–119.

Huotari, J., and Helenius, A. (2011). Endosome maturation. EMBO J. *30*, 3481–3500.

Huynh, K.K., Eskelinen, E.-L., Scott, C.C., Malevanets, A., Saftig, P., and Grinstein, S. (2007). LAMP proteins are required for fusion of lysosomes with phagosomes. EMBO J. *26*, 313–324.

Ivaska, J., and Heino, J. (2011). Cooperation between integrins and growth factor receptors in signaling and endocytosis. Annu. Rev. Cell Dev. Biol. *27*, 291–320.

Johnson, D.E., Ostrowski, P., Jaumouillé, V., and Grinstein, S. (2016). The position of lysosomes within the cell determines their luminal pH. J. Cell Biol. *212*, 677–692.

Jongsma, M.L.M., Berlin, I., Wijdeven, R.H.M., Janssen, L., Janssen, G.M.C., Garstka, M.A., Janssen, H., Mensink, M., van Veelen, P.A., Spaapen, R.M., et al. (2016). An ER-Associated Pathway Defines Endosomal Architecture for Controlled Cargo Transport. Cell *166*, 152–166.

Jordens, I., Fernandez-Borja, M., Marsman, M., Dusseljee, S., Janssen, L., Calafat, J., Janssen, H., Wubbolts, R., and Neefjes, J. (2001). The Rab7 effector protein RILP controls lysosomal transport by inducing the recruitment of dynein-dynactin motors. Curr. Biol. CB *11*, 1680–1685.

Kajiho, H., Kajiho, Y., Frittoli, E., Confalonieri, S., Bertalot, G., Viale, G., Di Fiore, P.P., Oldani, A., Garre, M., Beznoussenko, G.V., et al. (2016). RAB2A controls MT1-MMP endocytic and E-cadherin polarized Golgi trafficking to promote invasive breast cancer programs. EMBO Rep. *17*, 1061–1080.

Kallunki, T., Olsen, O.D., and Jäättelä, M. (2013). Cancer-associated lysosomal changes: friends or foes? Oncogene *32*, 1995–2004.

Kapitein, L.C., Schlager, M.A., van der Zwan, W.A., Wulf, P.S., Keijzer, N., and Hoogenraad, C.C. (2010). Probing intracellular motor protein activity using an inducible cargo trafficking assay. Biophys. J. *99*, 2143–2152.

Keller, J.M., Collet, P., Bianchi, A., Huin, C., Bouillaud-Kremarik, P., Becuwe, P., Schohn, H., Domenjoud, L., and Dauça, M. (2000). Implications of peroxisome proliferator-activated receptors (PPARS) in development, cell life status and disease. Int. J. Dev. Biol. *44*, 429–442.

Klionsky, D.J., Abdalla, F.C., Abeliovich, H., Abraham, R.T., Acevedo-Arozena, A., Adeli, K., Agholme, L., Agnello, M., Agostinis, P., Aguirre-Ghiso, J.A., et al. (2012). Guidelines for the use and interpretation of assays for monitoring autophagy. Autophagy *8*, 445–544.

Klumperman, J., and Raposo, G. (2014). The complex ultrastructure of the endolysosomal system. Cold Spring Harb. Perspect. Biol. *6*, a016857.

Knollman, H., Godwin, J.L., Jain, R., Wong, Y.-N., Plimack, E.R., and Geynisman, D.M. (2015). Muscle-invasive urothelial bladder cancer: an update on systemic therapy. Ther. Adv. Urol. *7*, 312–330.

Knowles, M.A. (2008). Molecular pathogenesis of bladder cancer. Int. J. Clin. Oncol. *13*, 287–297.

Koblinski, J.E., Ahram, M., and Sloane, B.F. (2000). Unraveling the role of proteases in cancer. Clin. Chim. Acta Int. J. Clin. Chem. *291*, 113–135.

Koff, J.L., Ramachandiran, S., and Bernal-Mizrachi, L. (2015). A time to kill: targeting apoptosis in cancer. Int. J. Mol. Sci. *16*, 2942–2955.

Korolchuk, V.I., Saiki, S., Lichtenberg, M., Siddiqi, F.H., Roberts, E.A., Imarisio, S., Jahreiss, L., Sarkar, S., Futter, M., Menzies, F.M., et al. (2011). Lysosomal positioning coordinates cellular nutrient responses. Nat. Cell Biol. *13*, 453–460.

Krakhmal, N.V., Zavyalova, M.V., Denisov, E.V., Vtorushin, S.V., and Perelmuter, V.M. (2015). Cancer Invasion: Patterns and Mechanisms. Acta Naturae *7*, 17–28.

Krzewski, K., Gil-Krzewska, A., Nguyen, V., Peruzzi, G., and Coligan, J.E. (2013). LAMP1/CD107a is required for efficient perforin delivery to lytic granules and NK-cell cytotoxicity. Blood *121*, 4672–4683.

Labernadie, A., Kato, T., Brugués, A., Serra-Picamal, X., Derzsi, S., Arwert, E., Weston, A., González-Tarragó, V., Elosegui-Artola, A., Albertazzi, L., et al. (2017). A mechanically active heterotypic E-cadherin/N-cadherin adhesion enables fibroblasts to drive cancer cell invasion. Nat. Cell Biol. *19*, 224–237.

Labi, V., and Erlacher, M. (2015). How cell death shapes cancer. Cell Death Dis. *6*, e1675.

Lankat-Buttgereit, B., Fehmann, H.C., Hering, B.J., Bretzel, R.G., and Göke, B. (1994). Expression of the ras-related rab3a gene in human insulinomas and normal human pancreatic islets. Pancreas *9*, 434–438.

Leavesley, D.I., Ferguson, G.D., Wayner, E.A., and Cheresh, D.A. (1992). Requirement of the integrin beta 3 subunit for carcinoma cell spreading or migration on vitronectin and fibrinogen. J. Cell Biol. *117*, 1101–1107.

Lee, A.S. (2007). GRP78 induction in cancer: therapeutic and prognostic implications. Cancer Res. *67*, 3496–3499.

Li, X., Rydzewski, N., Hider, A., Zhang, X., Yang, J., Wang, W., Gao, Q., Cheng, X., and Xu, H. (2016). A molecular mechanism to regulate lysosome motility for lysosome positioning and tubulation. Nat. Cell Biol. *18*, 404–417.

Lin, C.W., Lin, J.C., and Prout, G.R. (1985). Establishment and characterization of four human bladder tumor cell lines and sublines with different degrees of malignancy. Cancer Res. *45*, 5070–5079.

Liu, Y.-J., Le Berre, M., Lautenschlaeger, F., Maiuri, P., Callan-Jones, A., Heuzé, M., Takaki, T., Voituriez, R., and Piel, M. (2015). Confinement and low adhesion induce fast amoeboid migration of slow mesenchymal cells. Cell *160*, 659–672.

Lodhi, I.J., and Semenkovich, C.F. (2014). Peroxisomes: a nexus for lipid metabolism and cellular signaling. Cell Metab. *19*, 380–392.

Lodillinsky, C., Infante, E., Guichard, A., Chaligné, R., Fuhrmann, L., Cyrta, J., Irondelle, M., Lagoutte, E., Vacher, S., Bonsang-Kitzis, H., et al. (2016). p63/MT1-MMP axis is required for in situ to invasive transition in basal-like breast cancer. Oncogene *35*, 344–357.

Luzio, J.P., Hackmann, Y., Dieckmann, N.M.G., and Griffiths, G.M. (2014). The biogenesis of lysosomes and lysosome-related organelles. Cold Spring Harb. Perspect. Biol. *6*, a016840.

Maaser, K., Wolf, K., Klein, C.E., Niggemann, B., Zänker, K.S., Bröcker, E.B., and Friedl, P. (1999). Functional hierarchy of simultaneously expressed adhesion receptors: integrin alpha2beta1 but not CD44 mediates MV3 melanoma cell migration and matrix reorganization within three-dimensional hyaluronan-containing collagen matrices. Mol. Biol. Cell *10*, 3067–3079.

Machado, E., White-Gilbertson, S., van de Vlekkert, D., Janke, L., Moshiach, S., Campos, Y., Finkelstein, D., Gomero, E., Mosca, R., Qiu, X., et al. (2015). Regulated lysosomal exocytosis mediates cancer progression. Sci. Adv. *1*, e1500603.

Macpherson, I.R., Rainero, E., Mitchell, L.E., van den Berghe, P.V.E., Speirs, C., Dozynkiewicz, M.A., Chaudhary, S., Kalna, G., Edwards, J., Timpson, P., et al. (2014). CLIC3 controls recycling of late endosomal MT1-MMP and dictates invasion and metastasis in breast cancer. J. Cell Sci. *127*, 3893–3901.

Marchesin, V., Castro-Castro, A., Lodillinsky, C., Castagnino, A., Cyrta, J., Bonsang-Kitzis, H., Fuhrmann, L., Irondelle, M., Infante, E., Montagnac, G., et al. (2015). ARF6-JIP3/4 regulate endosomal tubules for MT1-MMP exocytosis in cancer invasion. J. Cell Biol. *211*, 339–358.

Margiotta, A., Progida, C., Bakke, O., and Bucci, C. (2017). Rab7a regulates cell migration through Rac1 and vimentin. Biochim. Biophys. Acta *1864*, 367–381.

Marshall, C.J., Franks, L.M., and Carbonell, A.W. (1977). Markers of neoplastic transformation in epithelial cell lines derived from human carcinomas. J. Natl. Cancer Inst. *58*, 1743–1751.

Mathew, R., Karantza-Wadsworth, V., and White, E. (2007). Role of autophagy in cancer. Nat. Rev. Cancer *7*, 961–967.

Mathew, R., Karp, C.M., Beaudoin, B., Vuong, N., Chen, G., Chen, H.-Y., Bray, K., Reddy, A., Bhanot, G., Gelinas, C., et al. (2009). Autophagy suppresses tumorigenesis through elimination of p62. Cell *137*, 1062–1075.

Maxfield, F.R. (2014). Role of endosomes and lysosomes in human disease. Cold Spring Harb. Perspect. Biol. *6*, a016931.

Miesenböck, G., De Angelis, D.A., and Rothman, J.E. (1998). Visualizing secretion and synaptic transmission with pH-sensitive green fluorescent proteins. Nature *394*, 192–195.

Mollereau, B. (2013). Establishing links between endoplasmic reticulum-mediated hormesis and cancer. Mol. Cell. Biol. *33*, 2372–2374.

Monteiro, P., Rossé, C., Castro-Castro, A., Irondelle, M., Lagoutte, E., Paul-Gilloteaux, P., Desnos, C., Formstecher, E., Darchen, F., Perrais, D., et al. (2013). Endosomal WASH and exocyst complexes control exocytosis of MT1-MMP at invadopodia. J. Cell Biol. *203*, 1063–1079.

Moon, D.G., Lee, S.E., Oh, M.M., Lee, S.C., Jeong, S.J., Hong, S.K., Yoon, C.Y., Byun, S.S., Park, H.S., and Cheon, J. (2014). NVP-BEZ235, a dual PI3K/mTOR inhibitor synergistically potentiates the antitumor effects of cisplatin in bladder cancer cells. Int. J. Oncol. *45*, 1027–1035.

Morita, T., Shinohara, N., Honma, M., and Tokue, A. (1995). Establishment and characterization of a new cell line from human bladder cancer (JMSU1). Urol. Res. *23*, 143–149.

Mu, D., Cambier, S., Fjellbirkeland, L., Baron, J.L., Munger, J.S., Kawakatsu, H., Sheppard, D., Broaddus, V.C., and Nishimura, S.L. (2002). The integrin alpha(v)beta8 mediates epithelial homeostasis through MT1-MMP-dependent activation of TGF-beta1. J. Cell Biol. *157*, 493–507.

Muthuswamy, S.K., and Xue, B. (2012). Cell polarity as a regulator of cancer cell behavior plasticity. Annu. Rev. Cell Dev. Biol. *28*, 599–625.

Nakamura, S., and Yoshimori, T. (2017). New insights into autophagosome-lysosome fusion. J. Cell Sci. *130*, 1209–1216.

Näthke, I.S., Adams, C.L., Polakis, P., Sellin, J.H., and Nelson, W.J. (1996). The adenomatous polyposis coli tumor suppressor protein localizes to plasma membrane sites involved in active cell migration. J. Cell Biol. *134*, 165–179.

Nayak, S.K., O'Toole, C., and Price, Z.H. (1977). A cell line from an anaplastic transitional cell carcinoma of human urinary bladder. Br. J. Cancer *35*, 142–151.

Neeft, M., Wieffer, M., de Jong, A.S., Negroiu, G., Metz, C.H.G., van Loon, A., Griffith, J., Krijgsveld, J., Wulffraat, N., Koch, H., et al. (2005). Munc13-4 is an effector of rab27a and controls secretion of lysosomes in hematopoietic cells. Mol. Biol. Cell *16*, 731–741.

Nishimura, Y., Itoh, K., Yoshioka, K., Ikeda, K., and Himeno, M. (2002). A role for small GTPase RhoA in regulating intracellular membrane traffic of lysosomes in invasive rat hepatoma cells. Histochem. J. *34*, 189–213.

Odenthal, J., Takes, R., and Friedl, P. (2016). Plasticity of tumor cell invasion: governance by growth factors and cytokines. Carcinogenesis *37*, 1117–1128.

Ostenfeld, M.S., Jeppesen, D.K., Laurberg, J.R., Boysen, A.T., Bramsen, J.B., Primdal-Bengtson, B., Hendrix, A., Lamy, P., Dagnaes-Hansen, F., Rasmussen, M.H., et al. (2014). Cellular disposal of miR23b by RAB27-dependent exosome release is linked to acquisition of metastatic properties. Cancer Res. *74*, 5758–5771.

Ostrowski, M., Carmo, N.B., Krumeich, S., Fanget, I., Raposo, G., Savina, A., Moita, C.F., Schauer, K., Hume, A.N., Freitas, R.P., et al. (2010). Rab27a and Rab27b control different steps of the exosome secretion pathway. Nat. Cell Biol. *12*, 19-30; sup pp 1-13.

Parri, M., and Chiarugi, P. (2010). Rac and Rho GTPases in cancer cell motility control. Cell Commun. Signal. CCS *8*, 23.

Peinado, H., Portillo, F., and Cano, A. (2004). Transcriptional regulation of cadherins during development and carcinogenesis. Int. J. Dev. Biol. *48*, 365–375.

Petrosyan, A. (2015). Onco-Golgi: Is Fragmentation a Gate to Cancer Progression? Biochem. Mol. Biol. J. *1*.

Petrosyan, A., Holzapfel, M.S., Muirhead, D.E., and Cheng, P.-W. (2014). Restoration of compact Golgi morphology in advanced prostate cancer enhances susceptibility to galectin-1-induced apoptosis by modifying mucin O-glycan synthesis. Mol. Cancer Res. MCR *12*, 1704–1716.

Piao, S., and Amaravadi, R.K. (2015). Targeting the lysosome in cancer. Ann. N. Y. Acad. Sci.

Plutoni, C., Bazellières, E., and Gauthier-Rouvière, C. (2016). P-cadherin-mediated Rho GTPase regulation during collective cell migration. Small GTPases *7*, 156–163.

Poincloux, R., Lizárraga, F., and Chavrier, P. (2009). Matrix invasion by tumour cells: a focus on MT1-MMP trafficking to invadopodia. J. Cell Sci. *122*, 3015–3024.

Porter, A.P., Papaioannou, A., and Malliri, A. (2016). Deregulation of Rho GTPases in cancer. Small GTPases *7*, 123–138.

Pu, J., Schindler, C., Jia, R., Jarnik, M., Backlund, P., and Bonifacino, J.S. (2015). BORC, a multisubunit complex that regulates lysosome positioning. Dev. Cell *33*, 176–188.

Pu, J., Guardia, C.M., Keren-Kaplan, T., and Bonifacino, J.S. (2016). Mechanisms and functions of lysosome positioning. J. Cell Sci. *129*, 4329–4339.

Qadir, M.I., Parveen, A., and Ali, M. (2015). Cdc42: Role in Cancer Management. Chem. Biol. Drug Des. *86*, 432–439.

Raab, M., Gentili, M., de Belly, H., Thiam, H.R., Vargas, P., Jimenez, A.J., Lautenschlaeger, F., Voituriez, R., Lennon-Duménil, A.M., Manel, N., et al. (2016). ESCRT III repairs nuclear envelope ruptures during cell migration to limit DNA damage and cell death. Science *352*, 359–362.

Rabinovitz, I., and Mercurio, A.M. (1997). The integrin alpha6beta4 functions in carcinoma cell migration on laminin-1 by mediating the formation and stabilization of actin-containing motility structures. J. Cell Biol. *139*, 1873–1884.

Raiborg, C., Wenzel, E.M., Pedersen, N.M., Olsvik, H., Schink, K.O., Schultz, S.W., Vietri, M., Nisi, V., Bucci, C., Brech, A., et al. (2015). Repeated ER-endosome contacts promote endosome translocation and neurite outgrowth. Nature *520*, 234–238.

Rainero, E., Howe, J.D., Caswell, P.T., Jamieson, N.B., Anderson, K., Critchley, D.R., Machesky, L., and Norman, J.C. (2015). Ligand-Occupied Integrin Internalization Links Nutrient Signaling to Invasive Migration. Cell Rep.

Ramalho, J.S., Tolmachova, T., Hume, A.N., McGuigan, A., Gregory-Evans, C.Y., Huxley, C., and Seabra, M.C. (2001). Chromosomal mapping, gene structure and characterization of the human and murine RAB27B gene. BMC Genet. *2*, 2.

Rebouissou, S., Bernard-Pierrot, I., de Reyniès, A., Lepage, M.-L., Krucker, C., Chapeaublanc, E., Hérault, A., Kamoun, A., Caillault, A., Letouzé, E., et al. (2014). EGFR as a potential therapeutic target for a subset of muscle-invasive bladder cancers presenting a basal-like phenotype. Sci. Transl. Med. *6*, 244ra91.

Reck-Peterson, S.L. (2015). Dynactin revealed. Nat. Struct. Mol. Biol. *22*, 359–360.

van Rhijn, B.W., Lurkin, I., Radvanyi, F., Kirkels, W.J., van der Kwast, T.H., and Zwarthoff, E.C. (2001). The fibroblast growth factor receptor 3 (FGFR3) mutation is a strong indicator of superficial bladder cancer with low recurrence rate. Cancer Res. *61*, 1265–1268.

Rink, J., Ghigo, E., Kalaidzidis, Y., and Zerial, M. (2005). Rab conversion as a mechanism of progression from early to late endosomes. Cell *122*, 735–749.

Rizzo, R., Parashuraman, S., D'Angelo, G., and Luini, A. (2017). GOLPH3 and oncogenesis: What is the molecular link? Tissue Cell *49*, 170–174.

Rocha, N., Kuijl, C., van der Kant, R., Janssen, L., Houben, D., Janssen, H., Zwart, W., and Neefjes, J. (2009). Cholesterol sensor ORP1L contacts the ER protein VAP to control Rab7-RILP-p150 Glued and late endosome positioning. J. Cell Biol. *185*, 1209–1225.

Rodríguez, A., Webster, P., Ortego, J., and Andrews, N.W. (1997). Lysosomes behave as Ca2+-regulated exocytic vesicles in fibroblasts and epithelial cells. J. Cell Biol. *137*, 93–104.

Rosa-Ferreira, C., and Munro, S. (2011). Arl8 and SKIP act together to link lysosomes to kinesin-1. Dev. Cell *21*, 1171–1178.

van Roy, F. (2014). Beyond E-cadherin: roles of other cadherin superfamily members in cancer. Nat. Rev. Cancer *14*, 121–134.

Salogiannis, J., Egan, M.J., and Reck-Peterson, S.L. (2016). Peroxisomes move by hitchhiking on early endosomes using the novel linker protein PxdA. J. Cell Biol. *212*, 289–296.

Schauer, K., Duong, T., Bleakley, K., Bardin, S., Bornens, M., and Goud, B. (2010a). Probabilistic density maps to study global endomembrane organization. Nat. Methods *7*, 560–566.

Schauer, K., Duong, T., Bleakley, K., Bardin, S., Bornens, M., and Goud, B. (2010b). Probabilistic density maps to study global endomembrane organization. Nat. Methods *7*, 560–566.

Schiefermeier, N., Scheffler, J.M., de Araujo, M.E.G., Stasyk, T., Yordanov, T., Ebner, H.L., Offterdinger, M., Munck, S., Hess, M.W., Wickström, S.A., et al. (2014). The late endosomal p14-MP1 (LAMTOR2/3) complex regulates focal adhesion dynamics during cell migration. J. Cell Biol. *205*, 525–540.

Scott, K.L., Kabbarah, O., Liang, M.-C., Ivanova, E., Anagnostou, V., Wu, J., Dhakal, S., Wu, M., Chen, S., Feinberg, T., et al. (2009). GOLPH3 modulates mTOR signalling and rapamycin sensitivity in cancer. Nature *459*, 1085–1090.

Settembre, C., Zoncu, R., Medina, D.L., Vetrini, F., Erdin, S., Erdin, S., Huynh, T., Ferron, M., Karsenty, G., Vellard, M.C., et al. (2012). A lysosome-to-nucleus signalling mechanism senses and regulates the lysosome via mTOR and TFEB. EMBO J. *31*, 1095–1108.

Simons, M., and Raposo, G. (2009). Exosomes--vesicular carriers for intercellular communication. Curr. Opin. Cell Biol. *21*, 575–581.

Singh, R.K., Liao, W., Tracey-White, D., Recchi, C., Tolmachova, T., Rankin, S.M., Hume, A.N., and Seabra, M.C. (2012). Rab27a-mediated protease release regulates neutrophil recruitment by allowing uropod detachment. J. Cell Sci. *125*, 1652–1656.

Solomon, M., and Muro, S. (2017). Lysosomal enzyme replacement therapies: Historical development, clinical outcomes, and future perspectives. Adv. Drug Deliv. Rev.

Sounni, N.E., Dehne, K., van Kempen, L., Egeblad, M., Affara, N.I., Cuevas, I., Wiesen, J., Junankar, S., Korets, L., Lee, J., et al. (2010). Stromal regulation of vessel stability by MMP14 and TGFbeta. Dis. Model. Mech. *3*, 317–332.

Southgate, J., Hutton, K.A., Thomas, D.F., and Trejdosiewicz, L.K. (1994). Normal human urothelial cells in vitro: proliferation and induction of stratification. Lab. Investig. J. Tech. Methods Pathol. *71*, 583–594.

Steffan, J.J., Snider, J.L., Skalli, O., Welbourne, T., and Cardelli, J.A. (2009). Na+/H+ exchangers and RhoA regulate acidic extracellular pH-induced lysosome trafficking in prostate cancer cells. Traffic Cph. Den. *10*, 737–753.

Steffan, J.J., Williams, B.C., Welbourne, T., and Cardelli, J.A. (2010). HGF-induced invasion by prostate tumor cells requires anterograde lysosome trafficking and activity of Na+-H+ exchangers. J. Cell Sci. *123*, 1151–1159.

Steffan, J.J., Dykes, S.S., Coleman, D.T., Adams, L.K., Rogers, D., Carroll, J.L., Williams, B.J., and Cardelli, J.A. (2014). Supporting a role for the GTPase Rab7 in prostate cancer progression. PloS One *9*, e87882.

Steffen, A., Le Dez, G., Poincloux, R., Recchi, C., Nassoy, P., Rottner, K., Galli, T., and Chavrier, P. (2008). MT1-MMP-dependent invasion is regulated by TI-VAMP/VAMP7. Curr. Biol. CB *18*, 926–931.

Stenmark, H. (2009). Rab GTPases as coordinators of vesicle traffic. Nat. Rev. Mol. Cell Biol. *10*, 513–525.

Tachibana, M., Miyakawa, A., Nakashima, J., Murai, M., Nakamura, K., Kubo, A., and Hata, J.I. (1997). Constitutive production of multiple cytokines and a human chorionic

gonadotrophin beta-subunit by a human bladder cancer cell line (KU-19-19): possible demonstration of totipotential differentiation. Br. J. Cancer *76*, 163–174.

Tanaka, Y., Kanai, Y., Okada, Y., Nonaka, S., Takeda, S., Harada, A., and Hirokawa, N. (1998). Targeted disruption of mouse conventional kinesin heavy chain, kif5B, results in abnormal perinuclear clustering of mitochondria. Cell *93*, 1147–1158.

Taub, N., Teis, D., Ebner, H.L., Hess, M.W., and Huber, L.A. (2007). Late endosomal traffic of the epidermal growth factor receptor ensures spatial and temporal fidelity of mitogen-activated protein kinase signaling. Mol. Biol. Cell *18*, 4698–4710.

Théry, M. (2010). Micropatterning as a tool to decipher cell morphogenesis and functions. J. Cell Sci. *123*, 4201–4213.

Théry, M., Racine, V., Piel, M., Pépin, A., Dimitrov, A., Chen, Y., Sibarita, J.-B., and Bornens, M. (2006a). Anisotropy of cell adhesive microenvironment governs cell internal organization and orientation of polarity. Proc. Natl. Acad. Sci. U. S. A. *103*, 19771–19776.

Théry, M., Pépin, A., Dressaire, E., Chen, Y., and Bornens, M. (2006b). Cell distribution of stress fibres in response to the geometry of the adhesive environment. Cell Motil. Cytoskeleton *63*, 341–355.

Theveneau, E., and Mayor, R. (2012). Cadherins in collective cell migration of mesenchymal cells. Curr. Opin. Cell Biol. *24*, 677–684.

Thiery, J.P., and Sleeman, J.P. (2006). Complex networks orchestrate epithelial-mesenchymal transitions. Nat. Rev. Mol. Cell Biol. *7*, 131–142.

Thiery, J.P., Acloque, H., Huang, R.Y.J., and Nieto, M.A. (2009). Epithelial-mesenchymal transitions in development and disease. Cell *139*, 871–890.

Thuault, S., Comunale, F., Hasna, J., Fortier, M., Planchon, D., Elarouci, N., De Reynies, A., Bodin, S., Blangy, A., and Gauthier-Rouvière, C. (2016). The RhoE/ROCK/ARHGAP25 signaling pathway controls cell invasion by inhibition of Rac activity. Mol. Biol. Cell *27*, 2653–2661.

Tu, C., Ortega-Cava, C.F., Chen, G., Fernandes, N.D., Cavallo-Medved, D., Sloane, B.F., Band, V., and Band, H. (2008). Lysosomal cathepsin B participates in the podosome-mediated extracellular matrix degradation and invasion via secreted lysosomes in v-Src fibroblasts. Cancer Res. *68*, 9147–9156.

Tubiana, M. (2008). [Generalities about carcinogenesis]. C. R. Biol. *331*, 114–125.

Uetrecht, A.C., and Bear, J.E. (2009). Golgi polarity does not correlate with speed or persistence of freely migrating fibroblasts. Eur. J. Cell Biol. *88*, 711–717.

Valadi, H., Ekström, K., Bossios, A., Sjöstrand, M., Lee, J.J., and Lötvall, J.O. (2007). Exosome-mediated transfer of mRNAs and microRNAs is a novel mechanism of genetic exchange between cells. Nat. Cell Biol. *9*, 654–659.

Valdés, F., Alvarez, A.M., Locascio, A., Vega, S., Herrera, B., Fernández, M., Benito, M., Nieto, M.A., and Fabregat, I. (2002). The epithelial mesenchymal transition confers resistance to the apoptotic effects of transforming growth factor Beta in fetal rat hepatocytes. Mol. Cancer Res. MCR *1*, 68–78.

Varley, C.L., Stahlschmidt, J., Lee, W.-C., Holder, J., Diggle, C., Selby, P.J., Trejdosiewicz, L.K., and Southgate, J. (2004). Role of PPARgamma and EGFR signalling in the urothelial terminal differentiation programme. J. Cell Sci. *117*, 2029–2036.

Vihervaara, T., Uronen, R.-L., Wohlfahrt, G., Björkhem, I., Ikonen, E., and Olkkonen, V.M. (2011). Sterol binding by OSBP-related protein 1L regulates late endosome motility and function. Cell. Mol. Life Sci. CMLS *68*, 537–551.

Vogelstein, B., Papadopoulos, N., Velculescu, V.E., Zhou, S., Diaz, L.A., and Kinzler, K.W. (2013). Cancer genome landscapes. Science *339*, 1546–1558.

Wallace, D.C. (2012). Mitochondria and cancer. Nat. Rev. Cancer *12*, 685–698.

Wang, T., and Hong, W. (2002). Interorganellar regulation of lysosome positioning by the Golgi apparatus through Rab34 interaction with Rab-interacting lysosomal protein. Mol. Biol. Cell *13*, 4317–4332.

Wang, S., Ma, Z., Xu, X., Wang, Z., Sun, L., Zhou, Y., Lin, X., Hong, W., and Wang, T. (2014). A role of Rab29 in the integrity of the trans-Golgi network and retrograde trafficking of mannose-6-phosphate receptor. PloS One *9*, e96242.

Warburg, O. (1956). On respiratory impairment in cancer cells. Science *124*, 269–270.

Webster, M., Witkin, K.L., and Cohen-Fix, O. (2009). Sizing up the nucleus: nuclear shape, size and nuclear-envelope assembly. J. Cell Sci. *122*, 1477–1486.

Wheeler, D.B., Zoncu, R., Root, D.E., Sabatini, D.M., and Sawyers, C.L. (2015). Identification of an oncogenic RAB protein. Science *350*, 211–217.

White, E. (2015). The role for autophagy in cancer. J. Clin. Invest. *125*, 42–46.

Wilbur, M.A., Shih, I.-M., Segars, J.H., and Fader, A.N. (2017). Cancer Implications for Patients with Endometriosis. Semin. Reprod. Med. *35*, 110–116.

Williams, K.C., and Coppolino, M.G. (2011). Phosphorylation of membrane type 1-matrix metalloproteinase (MT1-MMP) and its vesicle-associated membrane protein 7 (VAMP7)-dependent trafficking facilitate cell invasion and migration. J. Biol. Chem. *286*, 43405–43416.

Wodarz, A., and Näthke, I. (2007). Cell polarity in development and cancer. Nat. Cell Biol. *9*, 1016–1024.

Wu, X., Rao, K., Bowers, M.B., Copeland, N.G., Jenkins, N.A., and Hammer, J.A. (2001). Rab27a enables myosin Va-dependent melanosome capture by recruiting the myosin to the organelle. J. Cell Sci. *114*, 1091–1100.

Yadav, R.K., Chae, S.-W., Kim, H.-R., and Chae, H.J. (2014). Endoplasmic reticulum stress and cancer. J. Cancer Prev. *19*, 75–88.

Zink, D., Fischer, A.H., and Nickerson, J.A. (2004a). Nuclear structure in cancer cells. Nat. Rev. Cancer *4*, 677–687.

Zink, D., Fischer, A.H., and Nickerson, J.A. (2004b). Nuclear structure in cancer cells. Nat. Rev. Cancer *4*, 677–687.

Zong, W.-X., Rabinowitz, J.D., and White, E. (2016). Mitochondria and Cancer. Mol. Cell *61*, 667–676.

(2017). WHO | Cancer.

APPENDIX

Article in preparation

Appendix

Title: Bladder cancer progression is characterized by peripheral positioning of late endosomes / lysosomes

Short running title: Peripheral late endosome/lysosomes support invasiveness

Camilla De Barros Santos[1,2],
Bruno Latgé[1,2],
François Radvanyi[1,2],
Bruno Goud[1,2],
Kristine Schauer[1,2]

[1] Institut Curie, PSL Research University, Molecular Mechanisms of Intracellular Transport group, 75248 Paris Cedex 05, France
[2] Centre National de la Recherche Scientifique, Unité Mixte de Recherche 144, 75005 Paris, France
[3] IFOM, the FIRC Institute of Molecular Oncology, 20139 Milan, Italy
Contact: Correspondence should be addressed to Kristine Schauer (kristine.schauer@curie.fr).

Keywords Lysosome positioning, Lamp1, invasion, density maps

Abstract

Alterations of cell morphology are a hallmark of cancer. Yet, sub-cellular changes of organelles remain a black box. Systematic studies on intracellular organelles are difficult, because *in vivo* approaches are limited by the access of the samples and the lack of subcellular resolution and *in vitro* cultured cells display a dynamic shape and strong morphological cell-to-cell variation. Employing innovative micro-fabrication techniques in combination with quantitative, probabilistic mapping of cell organelles we found that cancer progression correlated well with a gradual peripheral positioning of lysosomes. Moreover, we found that displacing lysosomes experimentally to cell periphery accelerates 3D cell invasion, indicating that lysosomal homeostasis potentially plays an important role in malignancy.

Introduction

Malignant transformation is characterized by major alterations in cell morphology. (Wodarz and Nathke 2007). For instance, changes in the size and shape of the nucleus have been associated with cell transformation and are used as a diagnostic criterion for cancer (Capell and Collins, 2006; Chow et al., 2012; Webster et al., 2009; Zink et al., 2004) . Moreover, the loss of cell-polarity such as seen in Epithelial-Mesenchymal Transition (EMT) have been well-described (Thiery et al., 2009). However, little is known about which alterations are found in cancer cells on the sub-cellular, organelle level. No systematic studies on the organization of intracellular organelles have been performed, because, on the one hand, *in vivo* approaches are limited by the access of the samples and perturbation, and on the other hand, *in vitro* cultured cells display a dynamic shape and strong morphological cell-to-cell variations.

To investigate the impact of organelle organization on cancer progression, we have focused on bladder cancer that is the fourth most common cancer in men and ninth most common in women in the western world (Burger et al., 2013). The bladder cancer model is interesting, because bladder carcinomas are heterogeneous showing great diversity that is well represented in available cancer-derived cell lines (Earl et al., 2015b): Non-muscle-invasive bladder cancers (NMIBC) can be divided into two distinct classes by their appearance that correlates with cancer progression. Papillary cancers are non-invasive (stage Ta) show low-grades of aggressive behavior (G1/G2), correlating with 10%-15% probability to progress into invasive tumors), but have a high recurrence rate (60%). Carcinoma *in situ* (CIS) shows flat lesions and high-grade of aggressive behavior (G3), often progressing from non-invasive stage Tis to T1 (invasion of basal membrane) (according to The Union for International Cancer Control TNM system). Muscle-invasive bladder cancers (MIBC) are classified in stages T2, in which the invasion reaches the muscle tissue, T3 in which invasion reaches the adipose tissue and T4 which is characterized by the dissemination into nearby organs (Benhamou et al., 2016; Ho et al., 2012a). Molecular classification of MIBC have identified luminal-like and basal-like (23,5% of MIBC) subtypes whose transcription signatures correspond to luminal and basal normal bladder epithelial cells (Rebouissou et al., 2014; Choi et al. 2014). Interestingly, the luminal-like subgroup presents fibroblast growth factor receptor 3 (FGFR3) overexpression and mutations (Choi et al., 2014). Because activating mutations of FGFR3 is the most common genetic alteration in papillary NMIBC (Billerey et al., 2001; Knowles, 2008) this indicates that luminal-like subgroup originates from papillary NMIBC (Choi et al., 2014). The basal-like subgroup present overexpression of the epidermal growth factor receptor (EGFR) pathway

(Rebouissou et al. 2014) as well as biomarkers characteristic of EMT and stem cells (Choi et al. 2014) and is associated with squamous differentiation, high grades and stages of bladder cancer progression, leading to poor survival (Rebouissou et al., 2014).

Here we have employed micro-patterning and single cell analysis to investigate the intracellular alterations of different urothelial carcinoma cell lines that represent bladder tumors of different grades and stages. This allowed us to study intracellular alterations associated with the development and progression of bladder tumors under laboratory conditions.

Results

Comparative analysis of intracellular organelles revels intracellular alterations of late endosomes/lysosomes during bladder cancer progression

We hypothesized that intracellular organization can change as a result of tumorigenesis. To investigate the intracellular alterations during cancer progression under laboratory conditions, we focused on a collection of bladder tumor cell lines that derive from tumors of different grades and stages of disease progression and control normal human urothelium (NHU) cells. We analyzed the following well-characterized urothelial carcinoma cell lines 1) MGH-U3 from papillary, non-invasive transitional cell carcinoma representing Stage Ta and Grade G1 that contains a mutation in FGFR3 (Lin CW et al., 1985) 2) RT112 from papillary, non-invasive transitional cell carcinoma representing Stage Ta and Grade G2 (Marshall CJ et al., 1977) 3) KU19-19 from invasive transitional cell carcinoma representing Stage T3 and Grade G3 (Tachibana M et al., 1997) and 4) JMSU1 from malignant ascitic fluid from a patient with invasive transitional cell carcinoma representing Stage T4 and Grade G3 (Morita T et al., 1995) (Supplementary Figure 1). These cell lines were chosen, because they represent different grades and stages of malignancy and were reported to show close correlation in behavior and morphology between culture conditions and the original tumor. To be able to test our hypothesis and to compare the phenotypically different bladder cancer cells, we cultured them on identical crossbow-shaped patterns of extra-cellular matrix. Micropatterns normalize cells to the same, comparable shape and impair their migration without interfering with their cell cycle (Théry et al., 2006a). All tested cells were fully spread as judged by actin cytoskeleton staining (Figure 1A) revealing that all cells adopted well to the micropatterns. It is well documented that nucleus size changes during cell

transformation (Capell and Collins, 2006; Chow et al., 2012; Webster et al., 2009; Zink et al., 2004b). We thus first analyzed average nucleus size in micropatterned cells. We found that the volume of the nucleus indeed increased with the stage of disease progression (Figure 1B,C), confirming that cells grown on micropatterns maintain their cancer-related characteristics. Next, we used well-defined markers of intracellular organelles to visualize and compare different compartments by immunofluorescence. Interestingly, although many changes were apparent, we found strong differences in the late endosomes/lysosomes (LEL) compartment, which was clustered in NHU cells and low stage cell lines and scattered in the cytoplasm in high stage cell lines (Figure 1D). To further quantify and compare the spatial positioning of LEL in many cells we used probabilistic density maps that represent cellular areas containing the highest concentration of analyzed structures (Schauer et al. 2010). Plotting the 50% density map of LEL revealed the smallest 3D volume in which half LEL were found (Figure 1E). Density maps confirmed that lysosome positioning was central in NHU and low-stage, low-grade bladder cancer cell line (MGH-U3, TaG1), but peripheral in high-stage, high-grade bladder cell lines (T3G3, T4G3). In addition to a visual summary, density maps were used to statistically compare positioning of LEL (Duong et al. 2012) Table 1. Interestingly, we found that LEL positioning changed according to the grade of aggressive behavior by which cells were classified (Table 1). Analysis of the average number of LEL per cell revealed a significant increase of lysosomes in G1 and T4G3 cells (Figure 1F). The average volume of LEL was significantly increased in all cell lines (Figure 1G). We monitored LEL positioning in several additional cell lines, representing grades G1 and G3 and confirmed our results that peripheral LEL positioning correlated with cancer grades (Supplementary Figure 1B,C). Together this analysis indicated that LEL positioning could be a novel hallmark of bladder cancer progression.

Alterations in the late endosome/lysosomal compartment in bladder cancer cell lines are also evident in classical cell culture conditions

To verify that LEL positioning changes were not induced by micropatterning, we analyzed LEL in non-patterned bladder cell lines, employing classical cell culture conditions (Figure 2A). We analyzed the numbers of LEL that were found in each third of the area between the nucleus and the plasma membrane. In agreement with

our density map analysis, we found that in MGH-U3 (TaG1) cells 65 % the LEL were perinuclear and about 10% were peripheral (Figure 2B). LEL positioning was significantly different from MGH-U3 cells in RT112 (TaG2), KU19-19 (T3G3) and JMSU1 (T4G3) cells under classical culture conditions. Strikingly, the percentage of peripheral LEL positioning significantly increased from TaG1 to T4G3, JMSU1 showing about 30% of peripheral LEL. Finally, because LEL have been implicated in the secretion of proteases (Kallunki et al., 2013; Steffan et al., 2010), we tested extracellular activity of MMP1 and MMP14 (MMPs). We found that MMPs activity was higher in RT112 (TaG2) and KU19-19 (T3) cells than in MGH-U3 (TaG1) cells, however this was not significant. Contrary, JMSU1 (T4) cells showed significantly higher MMPs activity than MGH-U3 (TaG1) and RT112 (TaG2) cells, indicating that MMPs activity somehow correlated with the stage of cell lines.

Changes of LEL positioning to the cell periphery increase invasion of MGH-U3 (TaG1) cells.

To investigate whether LEL positioning only correlates with cancer grade or if LEL positioning regulates cancer-related behavior, we tested the role of LEL positioning changes in invasion, a hallmark of cancer cells. We employed an invasion assay based on collagen I matrix invasion from cell aggregates called spheroids. MGH-U3 cells were deposited on a convex agarose well to form spheroids for three days. Then, spheroids were transfected with siRNA targeting known regulators of LEL positioning and embedded in 2 mg/ml collagen matrix. Spheroids were observed for 6 consecutive days to monitor invasion that was characterized by the escape of cells from spheroids (Supplementary Figure 3). Because LEL are perinuclear in MHG-U3 cells, we aimed at changing LEL positioning towards the cell periphery. Thus, we tested whether MGH-U3 cells became more invasive when showing more peripheral LEL. We knocked down the small GTPases Rab7, a general regulator of LEL movement that predominately regulates centripetal movement of LEL (Jordens et al., 2001) and Rab27 that was shown to be downregulated in high stages bladder cancer cells (Ho et al., 2012a) and regulates positioning of late endosomes and the secretion of exosomes (Hendrix and De Wever, 2013). Additionally, we targeted RNF26, a protein found at the endoplasmic reticulum that mediates ubiquitin ligation and has recently been shown to retain LEL at the perinuclear region (Jongsma et al., 2016). Gene silencing substantially decreased Rab7 protein levels and RNF26 mRNA levels to 15% and 40% of the control (siLUC), respectively in MGH-U3 cells (Figure 3A). Under all conditions, LEL were found more at the cell periphery as

judged by the 50 % probability contour of LEL density maps (Figure 3B). Depletion of all genes significantly increased the number of invading spheroids in the six days of observation: whereas only 30% of MGH-U3 spheroids were invasive, gene silencing of Rab7 and Rab27 increased this number to over 50% (60%, 85% and 65%, respectively) (Figure 3C). Cells depleted for Rab7, Rab27 or RNF26 invaded significantly earlier than control (siLUC) cells (Figure 3D). Together, these results indicated that LEL movement to the cell periphery facilitated 3D invasion of MGH-U3 cells.

Changes of LEL positioning in RT112 cells predicts invasion behavior

Next, we investigated LEL positioning changes in RT112 (TaG2) cells. Because RT112 cells contain about 50 % of LEL that are not perinuclear, we aimed at changing LEL positioning towards both, the cell periphery and the cell center. We tested whether RT112 cells became more or less invasive when showing more or less peripheral LEL, respectively. In addition to Rab7, Rab27 and RNF26 we knocked down the small GTPase ADP-rybosylation factor like protein 8B (Arl8B) and its effector the microtubule +end motor kinesin-1 Kif5B. Arl8B recruits Kif5B in order to promote movement towards the cell periphery of LEL (Pu et al. 2016), thus knock down of Arl8B leads to clustering of LEL at the cell center. Gene silencing substantially decreased protein or RNA levels of all tested proteins (Figure 4A). As expected, sine silencing of Rab7, Rab27 and RNF26 moved LEL to the cell periphery, whereas gene silencing of Arl8b and Kif5B moved LEL to the cell center as judged by the 50 % probability contour of LEL density maps (Figure 4B). According their classification as G2, RT112 cells were more aggressive than G1 MGH-U3 cells and 80 % of tested spheroids were invasive in the six days of observation (Figure 4C). The invasive behavior also correlated with the more peripheral positioning of LEL in RT112 than MGH-U3 cells. Knock down of Rab7 or Rab27 moderately increased invasion to 85 % of spheroids (Figure 4C) but led to a significantly earlier invasion than control (siLUC) cells (Figure 4D). Depletion of RNF26 increased invasion to 100 % of spheroids (Figure 4C) without accelerating invasion (Figure 4D). Strikingly, depletion of Arl8B or Kif5B significantly decreased the number of invading spheroids to about 60% (Figure 4C). Additionally, cells depleted for Arl8B or Kif5B invaded slower than siLUC control cells (Figure 4D). These results indicated that lysosome positioning controls invasion behavior of RT112 cells.

Secretion of MMP

Finally, we addressed whether lysosome positioning impacted secretion of MMPs.

Discussion

Here, we investigated for the first time intracellular changes that can be found in urothelial carcinoma cell lines that represent bladder tumors of different grades and stages. Because bladder carcinomas show great diversity, giving rise to many morphologically distinct cells, we employed normalized cell culture condition on adhesive micropatterns that are getting popular and that allow fast and rigorous quantification. Analyzing the size of the nucleus on micropatterned cells, we evidenced that the volume of the nucleus increased with the stage of bladder cancer that is consistent with previous results (Dey, 2010; Zink et al., 2004a). Moreover, the average volume of LEL and their average number per cell in micropatterned cells was comparable to those measured in classical cell culture conditions for all cell lines tested. Together these results indicate that culture conditions on micropatterns are valid to study intracellular alterations in cancer cells.

Role of LEL in cancer disease

We found unprecedented changes in the positioning of LEL during bladder cancer progression. The lysosomal compartment has been reported to shows acidification defects and a changed lysosome-cytosol pH-gradient in cancer (Fehrenbacher and Jaattela 2005; Ndolo et al. 2012). The important role of lysosomal proteases in cancer progression is well documented: the aspartate and cysteine protease activities of cathepsin D and cathepsin B, respectively, are increased in most solid cancers (Dykes et al., 2016; Machado et al., 2015; Steffan et al., 2014). Membrane-type I MMP (MT1-MMP, also known as MMP14) are also significantly unregulated in invasive breast cancer, and correlate with higher-grade tumors (Lodillinsky et al., 2016). The secreted proteases participate in the degradation of the extracellular matrix, which favors cell invasion, tumor growth and angiogenesis (Fennelly and Amaravadi, 2017) and exacerbated lysosomal exocytosis of proteases increases the invasiveness phenotype of cancer cells (Machado et al., 2015). Our results further support that lysosomal homeostasis potentially plays an important role in malignancy and peripheral lysosome positioning could potentially be relevant in lysosomal secretion. Because enhanced secretion from lysosomes also leads to acidification of the extracellular milieu and acidification is a general feature of the tumor

microenvironment, lysosome positioning changes could play a role in other cancer types.

LEL positioning changes and invasion

Besides major interest in cancer research and high investigation, the importance of positioning changes of the LEL compartment in cancer is however emerging. Steffan et al. have reported that lysosomes are more peripheral in prostate cancer due to acidification of the extracellular milieu that is a common feature of the tumor microenvironment and has been implicated in enhanced tumor invasion (Steffan et al., 2009). Yet, it was shown that lysosomes are distributed to the cell periphery due to acidification of the microenvironment in tumors (Glunde et al., 2003; Steffan et al., 2009)(Glunde et al. 2003; Steffan et al. 2009). These peripheral lysosomes induces filopodia formation and tumor invasion, in breast cancer cells (Glunde et al., 2003). Furthermore, peripheral lysosomes in response to low pH in prostate cancer cells, secrete more cathepsin B, which increases tumor invasion (Steffan et al., 2010). Interestingly, several functions of LEL are regulated by intracellular positioning, such as proteolysis (Johnson et al., 2016), migration (Margiotta et al., 2017; Schiefermeier et al., 2014) and cholesterol transport (Rocha et al., 2009). Indeed, the Cardelli lab has shown that proteins and mechanisms implicated in lysosome positioning are deregulated in cancer progression, both *in vitro* and *in vivo* (Dykes et al., 2016, 2017, Steffan et al., 2009, 2010). In prostate cancer cells, depleted of Rab7 leads to the translocation of LEL to the cell periphery, increases the secretion of the cathepsin-B, and increase of invasion (Steffan et al. 2010). Additionally, in 2014, they showed evidence that Rab7 is a tumor suppressor, *in vivo:* tumors derived from Rab7-silenced cells grew larger due to increased proliferation and invasion of cancer cells, and decreased apoptotic rates (Steffan et al. 2014). Conversely, when the Rab7 effector RILP was overexpressed the lysosomes were clustered at the perinuclear region and the invasion was decreased (Steffan et al. 2010). Arl8b was recently implicated in cancer progression in prostate cancer cells. The knock-down of Arl8b prevented the anterograde transport of lysosomes, which decreases the secretion of proteases, thus impairing cell invasion in 3D matrix. Moreover, depleted Arl8b cells did not grow as xenograft tumors *in vivo* (Dykes et al. 2016).

Moreover, it has been noted that peripheral lysosomes reveal a higher pH and are compromised in their degradation capacity (Johnson et al., 2016), thus signaling receptors are more active in cells with peripheral lysosomes. Contrary, central

lysosomes increase degradation of growth factor receptors and thus decrease downstream signaling (Hoepfner et al. 2005; Taub et al. 2007). The epidermal growth factor receptor (EGFR) signaling pathway is often altered in different cancer types (Baumdick et al., 2015) and about 40 to 60% of bladder cancers present an overexpression of EGFR (Ahmad et al., 2012). It would be interesting to investigate whether LEL positioning changes control attenuation of EGFR signaling.

Rab27 is a well-known regulator of late endosome positioning (Ostrowski et al., 2010). Additionally, inhibition of Rab27a significantly reduced the growth of metastatic mammary adenocarcinoma 4T1 in mice, and reduced its ability to metastasize. Contrary, the growth and spreading of the nonmetastatic mammary tumor type, TS/A, were not impaired by Rab27a inhibition (Bobrie et al., 2012). Additionally, it has been shown that Rab27b overexpression is implicated in the increase of invasion, proliferation and acidification of extra-cellular matrix *in vitro*, and increased tumor volume and weight *in vivo* (Hendrix and De Wever, 2013). Interestingly, in bladder cancer, the deregulation of Rab27 and its effector proteins are associated with muscle-invasive tumors in both Ta and Cis pathways, and could be linked to the loss of differentiation markers of these tumors (Ho et al., 2012a).

Could LEL positioning integrate the many changes of tumor cells into a limited number of phenotypes?

The genetic and epigenetic changes occurring during cancer development lead to major changes in the transcriptome and proteome profiles of cells and thus to alterations in multiple signaling pathways, intracellular trafficking and metabolism. Although the pathways triggering cancer are complex, the resulting phenotypes of tumor cells are few, defined by proliferation, migration and invasion. A pertinent question is thus, at which level the multifold transformations are integrated giving rise to relatively restricted cellular phenotypes? We propose that regulation of LEL positioning downstream of different intracellular trafficking pathways could integrate many changes of tumor cells into a limited number of phenotypes that confer competitive advantages to transformed cells. We show that positioning changes due to different pathways impact invasion. LEL emerge as a logistic epicenter in cells. In addition to their classical role as final acidic degradation compartments in eukaryotic cells, lysosomes are responsible for the intracellular recycling of macromolecules and organelles delivered to them by endocytosis and autophagy. Additionally, lysosomes have been associated with signal regulation (Hoepfner et al. 2005; Taub et al. 2007), secretion of proteinases (Koblinski et al., 2000; Steffan et al., 2014; Tu et al., 2008), nutrient sensing (Rocha et al. 2009; Korolchuk et al. 2011) and cell

migration (Dozynkiewicz et al., 2012; Pu et al., 2015; Schiefermeier et al., 2014), all functions that are deregulated in cancer. Lysosomes have been implicated in more than 50 inherited lysosomal storage disorders and neurodegenerative diseases, their alterations in cancer opens a new horizon of lysosomal contribution to cancer-related pathologies.

The deeper understanding of the very complex cancer disease is one of the greatest challenges currently attacked by many scientists worldwide. This study allowed an unprecedented, detailed investigation of intracellular morphology changes that take place during transformation, providing great potential to identify key biological processes underlying cancer pathogenesis that is important for the rational design of more effective and less toxic therapeutic strategies.

Material and Methods

Cells and reagents

Bladder cancer cells lines MGH-U3, RT112, KU19-91, JMSU1, RT4, T24 and TCCSup were grown in RPMI medium (Life Technologies, Carlsbad, CA, USA), supplemented with 10% Fetal Bovine Serum (FBS; Eurobio, Courtaboeuf, France), and Normal human urothelium (NHU) cells were grown in KSFMC medium in a humidified atmosphere containing 5% CO_2.. During invasion assays 1% Penicillin-Streptomycin (Life Technologies) was added to the medium. For micropatterned experiments, HEPES was from Life Technologies, Fibronectin from Sigma-Aldrich (St. Louis, MO, USA), fibrinogen–Cy5 from Invitrogen, and Poly-L-Lysine(20)-grafted[3.5]-Polyethyleneglycol(2) (PLL-g-PEG) from SuSoS (Dübendorf, Switzerland). The PLL-g-PEG was used at a final concentration of 0.1 $mg.mL^{-1}$ in 10 mM HEPES (pH 7,3) solution. Mouse monoclonal antibodies against Lamp1/CD107a and Rab7, was bought BP Pharmingen™ (Material number 555798) and Cell Signaling, respectevely. Rabbit polyclonal antibody against Kif5B was from Santa Cruz Biotechnology (UKHC, Santa Cruz). Human monoclonal antibody F2C-hFc against α-tubulin was produced by the Recombinant Protein and Antibody Platform of the Institut Curie. FluoProbes 547H (557/572nm) coupled Phalloïdin was from Interchim. Nuclei were marked using 0.2 $\mu g.ml^{-1}$ 4',6-diamidino-2-phenylindole (DAPI; Sigma-Aldrich).

Cell transfection

Cells (200 000) were transfected in 6 well plate with 25 $pmol.mL^{-1}$ siRNA (Sigma-Aldrich, see table 2) using Lipofectamine RNAiMAX Transfection Reagent (5 $\mu L.mL^{-1}$; Life Technologies). Cells were incubated 72 h prior further manipulations. Efficiency of siRNA gene silencing was verified by performing real time PCR on cell mRNA or Western Blot on cell lysate after three days of transfection. Controls were performed with siRNA targeting Luciferase. Rab7, RNF26 and KIF5B gene silencing was performed using the 2 siRNA independently and results were pooled for plotting. In invasion assays, the siRNA was added in the collagen mix that surrounds the cell aggregate.

Gene	Sequence
Luciferase	5’-CGTACGCGGAATACTTCGA-3’
Luciferase	5’-CGTACGCGGAATACTTCGA-3’
Rab7-5	5’-CACGTAGGCCTTCAACACAAT-3’
Rab7-6	5’-CTGCTGCGTTCTGGTATTTGA-3’
Rab27a	
RNF26-1	5’-GAGAGGAUGUCAUGCGGCU-3’
RNF26-2	5’-GCAGAUCAGAGGCAGAAGA-3’
Arl8b	5’- GAUAGAAGCUUCCCGAAAU-3’
KIF5B#2	5’-GCACATCTCAAGAGCAAGT-3’
KIF5B#3	5’-AACGTTGCAAGCAGTTAGAAA-3’

<u>Table 2:</u> siRNA sequences

cDNA	Forward	Reverse
GAPDH	5’-TGCACCACCAACTGCTTAGC-3’	5’-GGCATGGACTGTGGTCATGAG-3’
Arl8b	5’-AAGCATGTGGGAGCGGTAT-3’	5’-CGATCTGCAGCATCTATCATGT-3’
RNF26	5’-AGCCTGGTGGCTTATGTGAT-3’	5’-AGGTTCTGAGTGCCGATGAG-3’

Table3: RT-PCR primers

Micropatterned coverslips preparation and cell seeding

Micropattern production was as previously described (Azioune et al., 2009b) using photo-lithography methods. Briefly, coverslips were coated with PLL-g-PEG and spatially controlled areas were exposed to deep UV during 5 min using a photomask. Crossbows (37 µm diameter, 7 µm thick) were therefore photo-printed. Prior to cell seeding, the patterned substrates were incubated for 1h with fibronectin (Sigma-Aldrich) at a concentration of 50 $mg.mL^{-1}$ and concanavalin A (Sigma-Aldrich) at a concentration of 5 µg/ml for the crossbow patterning. The fibronectin mixture was supplemented with 10 $mg.mL^{-1}$ fibrinogen–Cy5 (Invitrogen) to stain micropatterns. Cells were seeded on micropatterns in RPMI medium supplemented with 10 mM HEPES for 4 h prior the experiment.

Immunofluorescence, image acquisition and analysis

For immunofluorescence staining, formaldehyde-fixed cells were washed three times

with PBS and permeabilized in PBS/0.2% BSA/0.05% saponin. Cells were then incubated with a primary antibody for 1 h, washed in PBS and incubated with Alexa Fluor 488- or Cy3- coupled secondary antibodies (Jackson ImmunoResearch). Slices were mounted in Mowiol (Sigma-Aldrich). Z images from fixed and immunolabelled cells were acquired with an inverted widefield Deltavision Core Microscope (Applied Precision) equipped with highly sensitive cooled interlined charge-coupled device (CCD) camera (CoolSnap Hq2,Photometrics). Z-dimension series were acquired every 0.5 µm.

For each experiment, several tens of cells were imaged and aligned using the coordinates of the center and the angle of rotation of the micropattern (determined on ImageJ (Bethesda, MD, USA) as previously described (Grossier et al., 2014b; Schauer et al., 2010b). To extract the 3D spatial coordinates of intracellular structures, images were segmented with the multidimensional image analysis (MIA) interface on MetaMorph (Molecular Devices, Sunnyvale, CA, USA) based on wavelet decomposition. Circular distribution of the vector nucleus centroid-centrosome was potted using the R function rose.diag() and the maximum contour represent 25% of the cells.

Kernel density estimation

The coordinates of the segmented structures were processed for density estimation programmed in the ks library in the R programming language (R Development Core Team, 2013) (Schauer et al., 2010b): the probability density function *f* for each data sample of *n* coordinates $X_1, X_2, \ldots, X_n$ was estimated. We used a non-parametric, unbinned kernel density estimator. At each of the data points, a kernel function *K* was centered. The kernel functions were then summed to form the kernel density estimator $\hat{f}$:

$$\hat{f}_H(x) = \frac{1}{n}\sum_{i=1}^{n} K_H(x - X_i),$$

in which K_H is the Gaussian kernel with mean zero and variance matrix *H*. To estimate *H* (also known as the bandwidth), we used the plug-in selector in the ks library that has been shown to be reliable for 2D and 3D spatial distributions. For visualizing kernel density estimates, we used probability contours and the extension libraries mvtnorm, rgl, and miscd.

Invasion assay, acquisition and analysis

Cells were trypsinized and 10^4 cells/ml were ressuspended in RPMI medium

containing 10% FBS and 1% Penicillin-Streptomycin (Life Technologies). Then 100 µl of cell suspension was plated in 48-well plates coated with 1% agarose (Life Technologies) and incubated for 3 days (Figure 43). In each well, a spheroid was formed from 10^3 cells. Next, the spheroids were plated on Lab-Tek chambers (Sigma), in a mixture of collagen I from rat tail (Corning) at a final concentration of 2 $mg.ml^{-1}$, PBS, sodium hydroxide (NaOH) and serum-free medium. For siRNA experiments, the medium was replaced with the transfection mixture (Opti-MEM medium from Life Technologies, Lipofectamin RNAiMAX and siRNA). For inducible cargo trafficking assays, 1 µM of A/C heterodimerizer (Clontech, California-USA) was added in the collagen mixture and in the culture medium. The spheroids were monitored for 6 consecutive days by using an inverted Leica microscope (Wetzlar, Alemanha) equipped with camera device using 4x objective.

Matrix metalloproteinases activity

MMPs activity was tested following the manufacturer's protocol of the fluorimetric SensoLyte® 520 generic MMP activity assay (AnaSpec). Briefly, cell supernatant was centrifuged to eliminate floating cells. Then, samples were incubated with APMA (4-aminophenylmercuric acetate) for 3 hours at 37°C to target MMP1 and MMP14. Then, the MMP substrate containing 5-FAM/QXL™520 FRET peptide was incubated 1 hour at RT prior to measurement of fluorescence signal (450 nm excitation and 520 nm emission).

Statistical analysis

For each experiment, a large number of cells were monitored from 3 to 6 independent experiments. Bilateral Student t-tests were performed on averages to access the significance of difference. Additionally, to compare the global distribution of cell population, χ^2 tests were performed (R function "chi-square()"). In this case, results from independent experiments were individually compared and combined for representation and statistical analysis.

Acknowledgements

We greatly acknowledge Danijela Vignjevic and her team for help with invasion assays and for providing materials: The authors greatly acknowledge the Cell and Tissue Imaging Facility (PICT-IBiSA @Burg and @Pasteur) and Nikon Imaging Center, Institut Curie (Paris), member of the French National Research Infrastructure France-BioImaging (ANR10-INBS-04). We thank Tarn Duong for advices on

statistical analysis and kernel density estimation. This project was supported by grants from Capes/ Ciência sem Fronteiras/ Process {9121137}, ARC, SIRIC, Agence Nationale de la Recherche (#2010 BLAN 122902), the Centre National de la Recherche Scientifique and Institut Curie. The Goud team is members of Labex CelTisPhyBio (11-LBX-0038) and Idex Paris Sciences et Lettres (ANR-10-IDEX-0001-02 PSL). The authors declare no conflict of interest.

References

Ahmad, I., Sansom, O.J., and Leung, H.Y. (2012). Exploring molecular genetics of bladder cancer: lessons learned from mouse models. Dis. Model. Mech. *5*, 323–332.

Azioune, A., Storch, M., Bornens, M., Théry, M., and Piel, M. (2009). Simple and rapid process for single cell micro-patterning. Lab. Chip *9*, 1640–1642.

Baumdick, M., Brüggemann, Y., Schmick, M., Xouri, G., Sabet, O., Davis, L., Chin, J.W., and Bastiaens, P.I. (2015). EGF-dependent re-routing of vesicular recycling switches spontaneous phosphorylation suppression to EGFR signaling. eLife *4*.

Benhamou, S., Bonastre, J., Groussard, K., Radvanyi, F., Allory, Y., and Lebret, T. (2016). A prospective multicenter study on bladder cancer: the COBLAnCE cohort. BMC Cancer *16*, 837.

Billerey, C., Chopin, D., Aubriot-Lorton, M.H., Ricol, D., Gil Diez de Medina, S., Van Rhijn, B., Bralet, M.P., Lefrere-Belda, M.A., Lahaye, J.B., Abbou, C.C., et al. (2001). Frequent FGFR3 mutations in papillary non-invasive bladder (pTa) tumors. Am. J. Pathol. *158*, 1955–1959.

Bobrie, A., Krumeich, S., Reyal, F., Recchi, C., Moita, L.F., Seabra, M.C., Ostrowski, M., and Théry, C. (2012). Rab27a supports exosome-dependent and -independent mechanisms that modify the tumor microenvironment and can promote tumor progression. Cancer Res. *72*, 4920–4930.

Burger, M., Catto, J.W.F., Dalbagni, G., Grossman, H.B., Herr, H., Karakiewicz, P., Kassouf, W., Kiemeney, L.A., La Vecchia, C., Shariat, S., et al. (2013). Epidemiology and risk factors of urothelial bladder cancer. Eur. Urol. *63*, 234–241.

Capell, B.C., and Collins, F.S. (2006). Human laminopathies: nuclei gone genetically awry. Nat. Rev. Genet. *7*, 940–952.

Choi, W., Porten, S., Kim, S., Willis, D., Plimack, E.R., Hoffman-Censits, J., Roth, B., Cheng, T., Tran, M., Lee, I.-L., et al. (2014). Identification of distinct basal and luminal subtypes of muscle-invasive bladder cancer with different sensitivities to frontline chemotherapy. Cancer Cell *25*, 152–165.

Chow, K.-H., Factor, R.E., and Ullman, K.S. (2012). The nuclear envelope environment and its cancer connections. Nat. Rev. Cancer *12*, 196–209.

Dey, P. (2010). Cancer nucleus: Morphology and beyond. Diagn. Cytopathol. *38*, 382–390.

Dozynkiewicz, M.A., Jamieson, N.B., Macpherson, I., Grindlay, J., van den Berghe, P.V.E., von Thun, A., Morton, J.P., Gourley, C., Timpson, P., Nixon, C., et al. (2012). Rab25 and CLIC3 collaborate to promote integrin recycling from late endosomes/lysosomes and drive cancer progression. Dev. Cell *22*, 131–145.

Dykes, S.S., Gray, A.L., Coleman, D.T., Saxena, M., Stephens, C.A., Carroll, J.L., Pruitt, K., and Cardelli, J.A. (2016). The Arf-like GTPase Arl8b is essential for three-dimensional invasive growth of prostate cancer in vitro and xenograft formation and growth in vivo. Oncotarget.

Dykes, S.S., Gao, C., Songock, W.K., Bigelow, R.L., Woude, G.V., Bodily, J.M., and Cardelli, J.A. (2017). Zinc finger E-box binding homeobox-1 (Zeb1) drives anterograde lysosome trafficking and tumor cell invasion via upregulation of Na+/H+ Exchanger-1 (NHE1). Mol. Carcinog. *56*, 722–734.

Earl, J., Rico, D., Carrillo-de-Santa-Pau, E., Rodríguez-Santiago, B., Méndez-Pertuz, M., Auer, H., Gómez, G., Grossman, H.B., Pisano, D.G., Schulz, W.A., et al. (2015). Erratum to:

The UBC-40 Urothelial Bladder Cancer Cell Line Index: a genomic resource for functional studies. BMC Genomics *16*, 1019.

Fennelly, C., and Amaravadi, R.K. (2017). Lysosomal Biology in Cancer. Methods Mol. Biol. Clifton NJ *1594*, 293–308.

Glunde, K., Guggino, S.E., Solaiyappan, M., Pathak, A.P., Ichikawa, Y., and Bhujwalla, Z.M. (2003). Extracellular acidification alters lysosomal trafficking in human breast cancer cells. Neoplasia N. Y. N *5*, 533–545.

Grigoriev, I., Splinter, D., Keijzer, N., Wulf, P.S., Demmers, J., Ohtsuka, T., Modesti, M., Maly, I.V., Grosveld, F., Hoogenraad, C.C., et al. (2007). Rab6 regulates transport and targeting of exocytotic carriers. Dev. Cell *13*, 305–314.

Grossier, J.-P., Xouri, G., Goud, B., and Schauer, K. (2014). Cell adhesion defines the topology of endocytosis and signaling. EMBO J. *33*, 35–45.

Hendrix, A., and De Wever, O. (2013). Rab27 GTPases distribute extracellular nanomaps for invasive growth and metastasis: implications for prognosis and treatment. Int. J. Mol. Sci. *14*, 9883–9892.

Ho, J.R., Chapeaublanc, E., Kirkwood, L., Nicolle, R., Benhamou, S., Lebret, T., Allory, Y., Southgate, J., Radvanyi, F., and Goud, B. (2012). Deregulation of Rab and Rab effector genes in bladder cancer. PloS One *7*, e39469.

Johnson, D.E., Ostrowski, P., Jaumouillé, V., and Grinstein, S. (2016). The position of lysosomes within the cell determines their luminal pH. J. Cell Biol. *212*, 677–692.

Jongsma, M.L.M., Berlin, I., Wijdeven, R.H.M., Janssen, L., Janssen, G.M.C., Garstka, M.A., Janssen, H., Mensink, M., van Veelen, P.A., Spaapen, R.M., et al. (2016). An ER-Associated Pathway Defines Endosomal Architecture for Controlled Cargo Transport. Cell *166*, 152–166.

Jordens, I., Fernandez-Borja, M., Marsman, M., Dusseljee, S., Janssen, L., Calafat, J., Janssen, H., Wubbolts, R., and Neefjes, J. (2001). The Rab7 effector protein RILP controls lysosomal transport by inducing the recruitment of dynein-dynactin motors. Curr. Biol. CB *11*, 1680–1685.

Kallunki, T., Olsen, O.D., and Jäättelä, M. (2013). Cancer-associated lysosomal changes: friends or foes? Oncogene *32*, 1995–2004.

Knowles, M.A. (2008). Molecular pathogenesis of bladder cancer. Int. J. Clin. Oncol. *13*, 287–297.

Koblinski, J.E., Ahram, M., and Sloane, B.F. (2000). Unraveling the role of proteases in cancer. Clin. Chim. Acta Int. J. Clin. Chem. *291*, 113–135.

Lodillinsky, C., Infante, E., Guichard, A., Chaligné, R., Fuhrmann, L., Cyrta, J., Irondelle, M., Lagoutte, E., Vacher, S., Bonsang-Kitzis, H., et al. (2016). p63/MT1-MMP axis is required for in situ to invasive transition in basal-like breast cancer. Oncogene *35*, 344–357.

Machado, E., White-Gilbertson, S., van de Vlekkert, D., Janke, L., Moshiach, S., Campos, Y., Finkelstein, D., Gomero, E., Mosca, R., Qiu, X., et al. (2015). Regulated lysosomal exocytosis mediates cancer progression. Sci. Adv. *1*, e1500603.

Margiotta, A., Progida, C., Bakke, O., and Bucci, C. (2017). Rab7a regulates cell migration through Rac1 and vimentin. Biochim. Biophys. Acta *1864*, 367–381.

Ostrowski, M., Carmo, N.B., Krumeich, S., Fanget, I., Raposo, G., Savina, A., Moita, C.F., Schauer, K., Hume, A.N., Freitas, R.P., et al. (2010). Rab27a and Rab27b control different steps of the exosome secretion pathway. Nat. Cell Biol. *12*, 19-30; sup pp 1-13.

Pu, J., Schindler, C., Jia, R., Jarnik, M., Backlund, P., and Bonifacino, J.S. (2015). BORC, a multisubunit complex that regulates lysosome positioning. Dev. Cell *33*, 176–188.

Rebouissou, S., Bernard-Pierrot, I., de Reyniès, A., Lepage, M.-L., Krucker, C., Chapeaublanc, E., Hérault, A., Kamoun, A., Caillault, A., Letouzé, E., et al. (2014). EGFR as a potential therapeutic target for a subset of muscle-invasive bladder cancers presenting a basal-like phenotype. Sci. Transl. Med. *6*, 244ra91.

Rocha, N., Kuijl, C., van der Kant, R., Janssen, L., Houben, D., Janssen, H., Zwart, W., and Neefjes, J. (2009). Cholesterol sensor ORP1L contacts the ER protein VAP to control Rab7-RILP-p150 Glued and late endosome positioning. J. Cell Biol. *185*, 1209–1225.

Schauer, K., Duong, T., Bleakley, K., Bardin, S., Bornens, M., and Goud, B. (2010). Probabilistic density maps to study global endomembrane organization. Nat. Methods *7*, 560–566.

Schiefermeier, N., Scheffler, J.M., de Araujo, M.E.G., Stasyk, T., Yordanov, T., Ebner, H.L., Offterdinger, M., Munck, S., Hess, M.W., Wickström, S.A., et al. (2014). The late endosomal p14-MP1 (LAMTOR2/3) complex regulates focal adhesion dynamics during cell migration. J. Cell Biol. *205*, 525–540.

Splinter, D., Tanenbaum, M.E., Lindqvist, A., Jaarsma, D., Flotho, A., Yu, K.L., Grigoriev, I., Engelsma, D., Haasdijk, E.D., Keijzer, N., et al. (2010). Bicaudal D2, dynein, and kinesin-1 associate with nuclear pore complexes and regulate centrosome and nuclear positioning during mitotic entry. PLoS Biol. *8*, e1000350.

Steffan, J.J., Snider, J.L., Skalli, O., Welbourne, T., and Cardelli, J.A. (2009). Na+/H+ exchangers and RhoA regulate acidic extracellular pH-induced lysosome trafficking in prostate cancer cells. Traffic Cph. Den. *10*, 737–753.

Steffan, J.J., Williams, B.C., Welbourne, T., and Cardelli, J.A. (2010). HGF-induced invasion by prostate tumor cells requires anterograde lysosome trafficking and activity of Na+-H+ exchangers. J. Cell Sci. *123*, 1151–1159.

Steffan, J.J., Dykes, S.S., Coleman, D.T., Adams, L.K., Rogers, D., Carroll, J.L., Williams, B.J., and Cardelli, J.A. (2014). Supporting a role for the GTPase Rab7 in prostate cancer progression. PloS One *9*, e87882.

Théry, M., Racine, V., Piel, M., Pépin, A., Dimitrov, A., Chen, Y., Sibarita, J.-B., and Bornens, M. (2006). Anisotropy of cell adhesive microenvironment governs cell internal organization and orientation of polarity. Proc. Natl. Acad. Sci. U. S. A. *103*, 19771–19776.

Thiery, J.P., Acloque, H., Huang, R.Y.J., and Nieto, M.A. (2009). Epithelial-mesenchymal transitions in development and disease. Cell *139*, 871–890.

Tu, C., Ortega-Cava, C.F., Chen, G., Fernandes, N.D., Cavallo-Medved, D., Sloane, B.F., Band, V., and Band, H. (2008). Lysosomal cathepsin B participates in the podosome-mediated extracellular matrix degradation and invasion via secreted lysosomes in v-Src fibroblasts. Cancer Res. *68*, 9147–9156.

Webster, M., Witkin, K.L., and Cohen-Fix, O. (2009). Sizing up the nucleus: nuclear shape, size and nuclear-envelope assembly. J. Cell Sci. *122*, 1477–1486.

Zink, D., Fischer, A.H., and Nickerson, J.A. (2004a). Nuclear structure in cancer cells. Nat. Rev. Cancer *4*, 677–687.

Zink, D., Fischer, A.H., and Nickerson, J.A. (2004b). Nuclear structure in cancer cells. Nat. Rev. Cancer *4*, 677–687.

Supplementary methods

Cell lines: British Journal of Cancer. 1970;24:746-54.) T24 G3 (Bubenik J, Baresova M, Viklicky V, Jakoubkova J, Sainerova H, Donner J. Established cell line of urinary bladder carcinoma (T24) containing tumour-specific antigen. Int J Cancer. 1973;11:765-73.) TCCSUP G4 (Nayak SK, O'Toole C, Price ZH. A cell line from an anaplastic transitional cell carcinoma of human urinary bladder. Br J Cancer. 1977;35:142-51.)

Figure legends

Figure 1: Alterations of bladder cells on subcellular level. (A) All analyzed cells well spread on micropatterns as judged by actin stained by Phalloidin. (B) Representative image of nuclei labeled with DAPI showing increase in nuclear size in cells representing higher grades of bladder cancer. (C). Quantification of nuclear size based on segmentation data from nucleus staining. Data was based on more than 140 cells and each nucleus was represented by one point coordinate. (D) Representative normalized single cell fluorescently stained for LEL using anti-Lamp1 antibody for each analyzed bladder cell type. (E) 50% contour of the 3D density maps quantifying LEL distribution (in turquoise), compared to NHU control cells (in white). LEL distribution is gradually more peripheral in bladder cancer cells. N is the number of cells. (F) Average number of LEL per cell. Significant decrease in number of lysosomes in MGHU-3 (TaG1) and JMSU1 (T4) cells. (G) Average volume of LEL. Significant increase of volume in all analyzed cells compared with NHU cells. Red lines represent median. ns, $p>0.5$ and ***, $p<0.001$in a Student's t-test. Scale bar 10µm.

Supplementary figure 1: Bladder cells. (A) Morphological differences between NHU control cells and bladder cancer cells in classical cell culture. Scale bar 50 µm. (B) Representative normalized single cell fluorescently stained for LEL using anti-Lamp1 antibody for of supplementary grade 3 cell lines. (C) 50% contour of the 3D density maps quantifying LEL distribution (in turquoise), compared to NHU control cells (in white). LEL distribution is more peripheral in additional grade 3 bladder cancer cell lines. N is the number of cells.

Figure 2: Alterations of LEL compartment in classical *in vitro* culture. (A) Representative unconstrained single cell image fluorescently stained for LEL (Lamp1), nucleus (DAPI) and actin cytoskeleton (Phalloidin) for each bladder cancer cell line. Scale bar 10µm. B. Distribution of LEL in unconstrained cells was divided in 3 regions: perinuclear (white), intermediate (gray) and peripheral (red). Lysosome peripheral dispersion is gradually increased depending on the bladder cancer cell grade. Analysis based in > 60 cells. ***, $p<0.001$in a Student's t-test.

Figure 3: Changes of LEL positioning to the cell periphery increase invasion of MGHU3 (TaG1) cells. (A) Quantification of Rab7 and RNF26 depletion from cell lysate Western Blot analysis and mRNA levels in RT-PCR, respectively.(B) 50%

contour of the 3D density maps quantifying lysosome distribution in depleted cells (in turquoise), compared to control cells treated with siLUC (in white). Lysosome distribution is more peripheral after depletion of Rab7 and Rab27. (C) Number of invasive spheroids. A strong increase of invasive spheroids is observed in depleted MGHU3 (TaG1) cells. (D) Median day of invasion. A significant acceleration of invasion in Rab27 depleted cells. Error bars from > 6 experiment.

Figure 4: Changes of LEL positioning in RT112 (TaG2) cells predict invasion behavior. (A) Quantification of depletion of Rab7 from cell lysate by Western Blot analysis and RNF26 and Arl8b by RT-PCR.(B) 50% contour of the 3D density maps quantifying LEL distribution in depleted cells (in turquoise), compared to control cells treated with siLUC (in white). LEL distribution is more peripheral after depletion of Rab7 and Rab27. Conversely, LEL are distributed to the cell center in Arl8b depleted cells. (C) Number of invasive spheroids. Rab7 and Rab27 silencing does not have an impact on number of invasive spheroids. 100% of RNF26 depleted spheroids invaded within 6 days. (D) Median day of invasion. A significant acceleration of invasion in Rab7 depleted cells. Error bars from > 6 experiment. **, $p<0.01$ in a Student's t-test.

Table 1: Statistical differences between density maps. P-values correspond to differences between lysosome density maps of analyzed bladder cancer cells and NHU control cells based on nonparametric and asymptotically comparison of kernel distribution. Larger differences are represented by higher p-values.

Figure 1

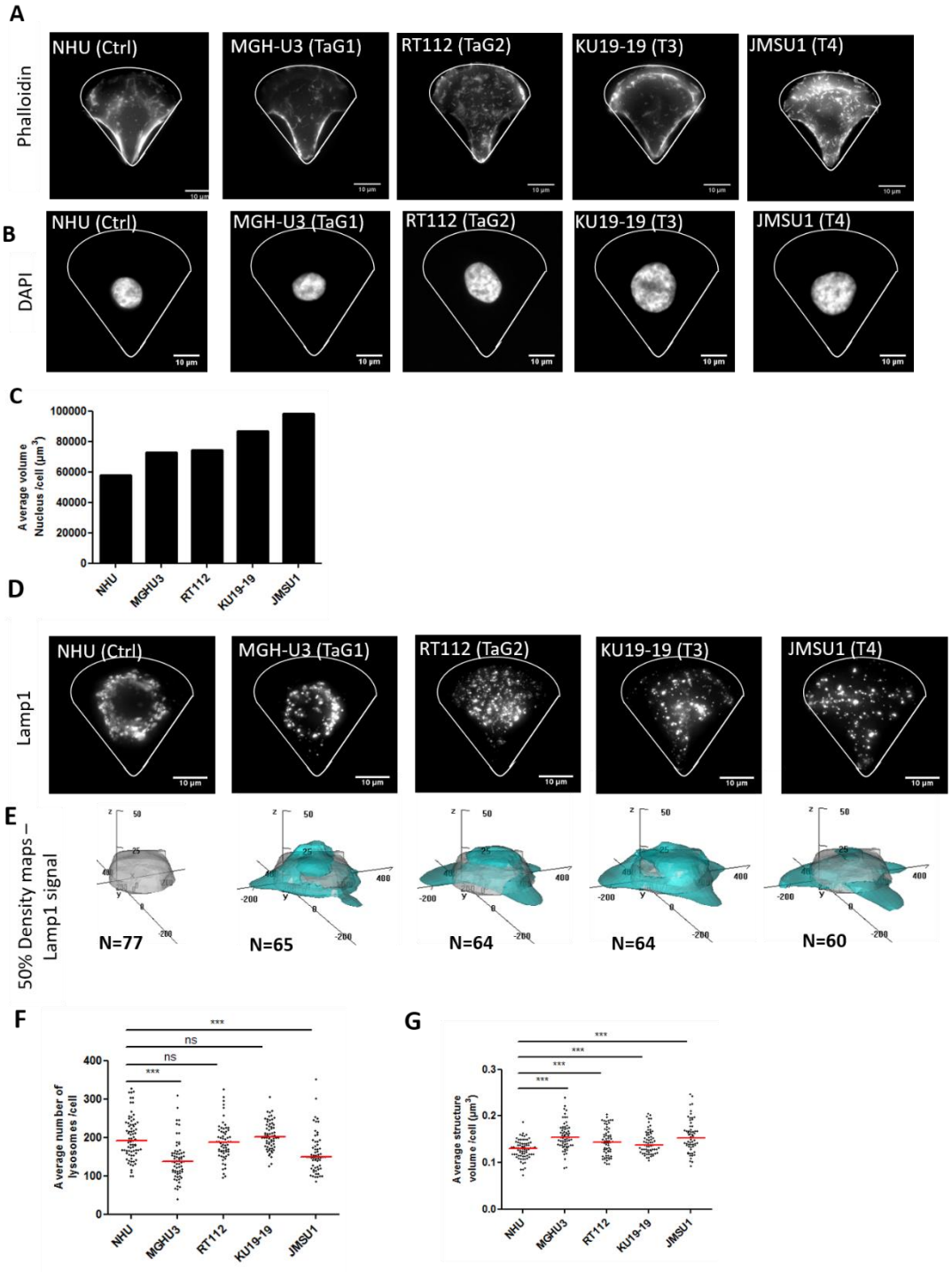
A
Phalloidin
NHU (Ctrl)
MGH-U3 (TaG1)
RT112 (TaG2)
KU19-19 (T3)
JMSU1 (T4)
B
DAPI
NHU (Ctrl)
MGH-U3 (TaG1)
RT112 (TaG2)
KU19-19 (T3)
JMSU1 (T4)
C
Average volume Nucleus /cell (µm³)
100000
80000
60000
40000
20000
0
NHU
MGHU3
RT112
KU19-19
JMSU1
D
Lamp1
NHU (Ctrl)
MGH-U3 (TaG1)
RT112 (TaG2)
KU19-19 (T3)
JMSU1 (T4)
E
50% Density maps – Lamp1 signal
N=77
N=65
N=64
N=64
N=60
F
Average number of lysosomes /cell
ns
ns
***
***
400
300
200
100
0
NHU
MGHU3
RT112
KU19-19
JMSU1
G
Average structure volume /cell (µm³)
***
***
***
***
0.3
0.2
0.1
0.0
NHU
MGHU3
RT112
KU19-19
JMSU1

Figure 2

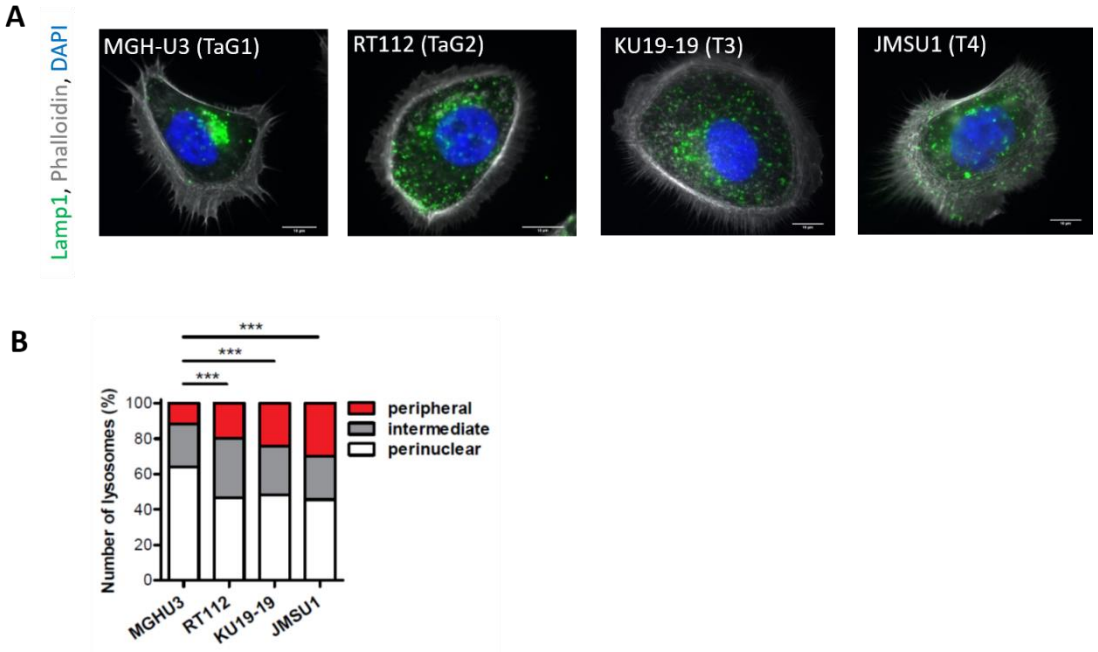
A
Lamp1, Phalloidin, DAPI
MGH-U3 (TaG1)
RT112 (TaG2)
KU19-19 (T3)
JMSU1 (T4)
B
***
***
***
Number of lysosomes (%)
100
80
60
40
20
0
peripheral
intermediate
perinuclear
MGHU3
RT112
KU19-19
JMSU1

Figure 3

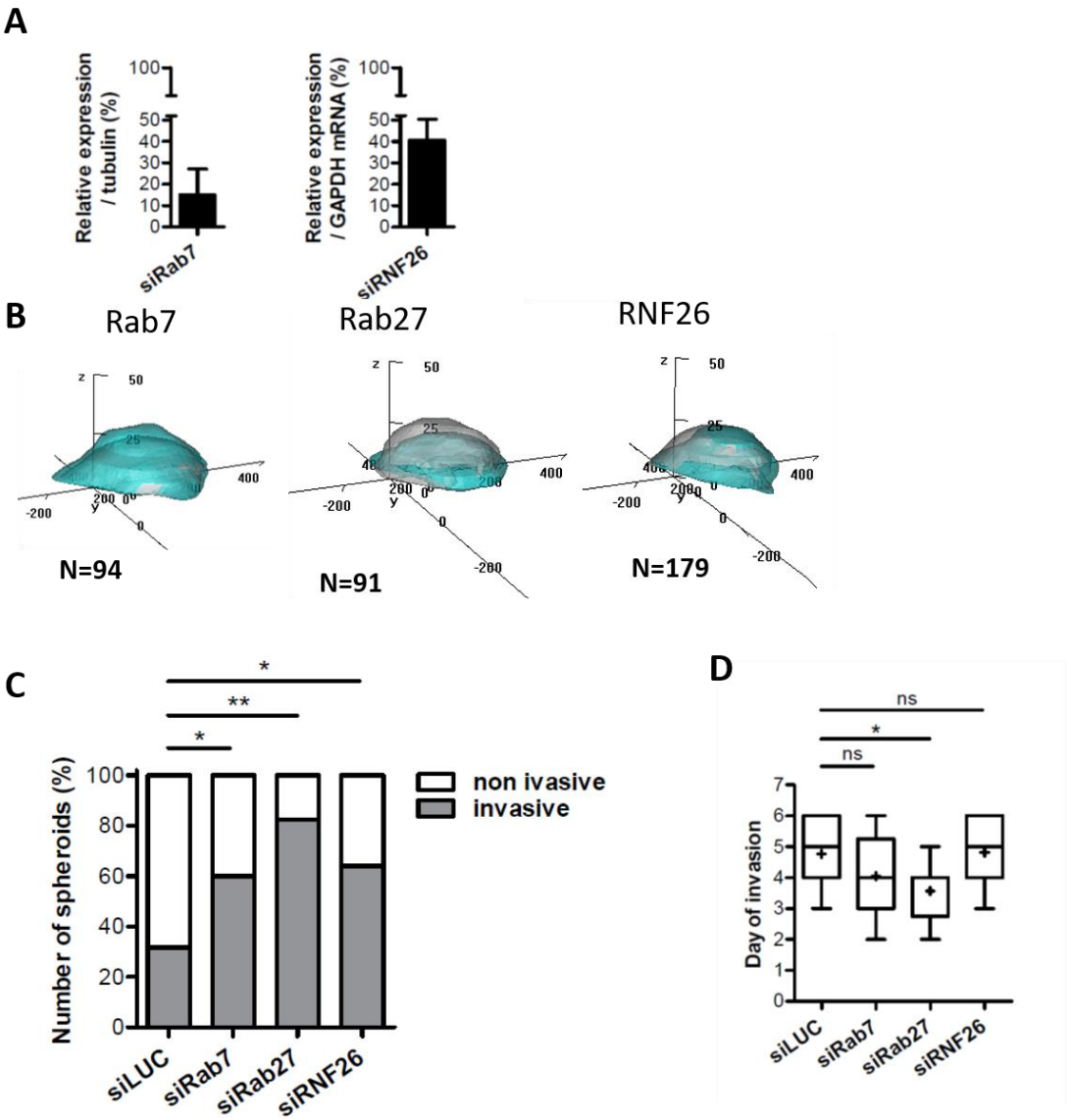
A
Relative expression / tubulin (%)
siRab7
Relative expression / GAPDH mRNA (%)
siRNF26
B
Rab7
Rab27
RNF26
N=94
N=91
N=179
C
Number of spheroids (%)
non ivasive
invasive
siLUC
siRab7
siRab27
siRNF26
D
Day of invasion
ns
*
**

Figure 4

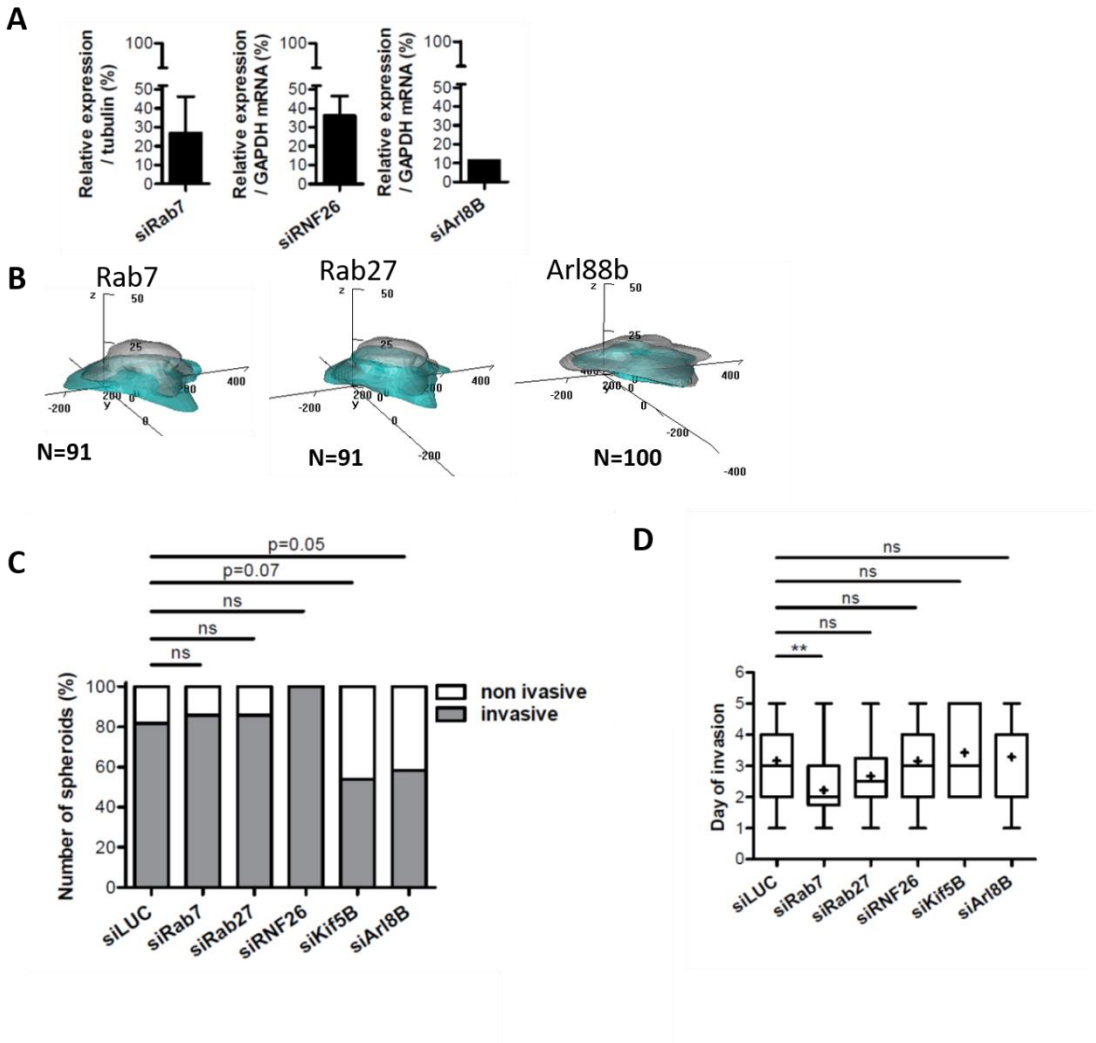
A
Relative expression / tubulin (%)
Relative expression / GAPDH mRNA (%)
Relative expression / GAPDH mRNA (%)
siRab7
siRNF26
siArl8B
B
Rab7
Rab27
Arl88b
N=91
N=91
N=100
C
p=0.05
p=0.07
ns
ns
ns
Number of spheroids (%)
non ivasive
invasive
siLUC
siRab7
siRab27
siRNF26
siKif5B
siArl8B
D
ns
ns
ns
ns
**
Day of invasion
siLUC
siRab7
siRab27
siRNF26
siKif5B
siArl8B

Supplementary Figure 1

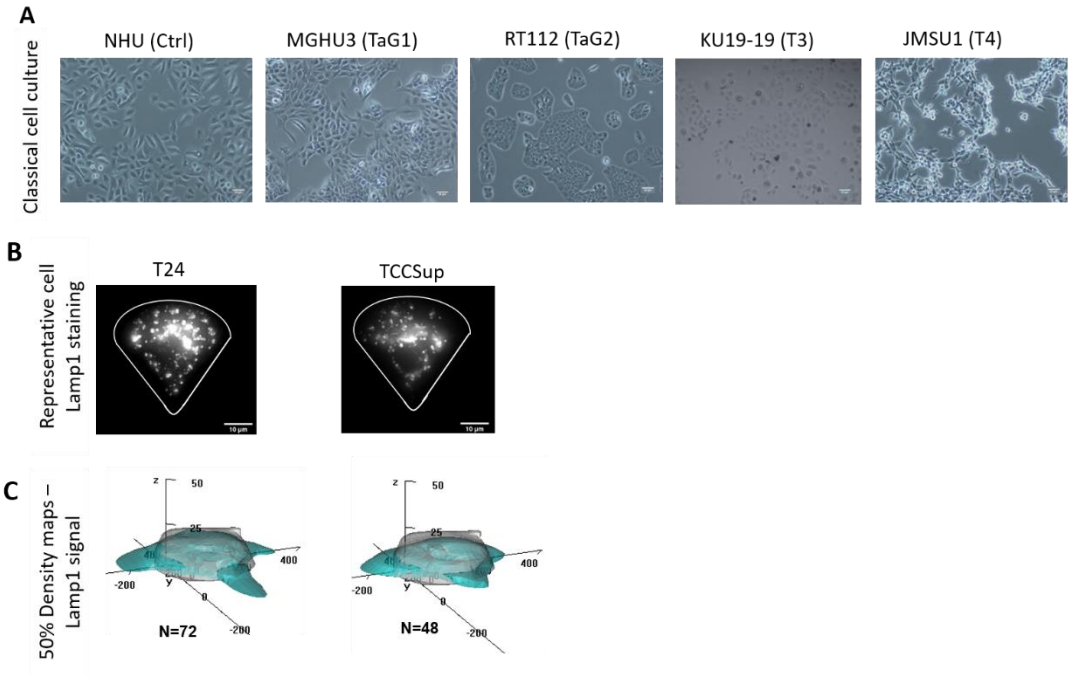

Table 1

Cell line	p-value
MGHU3 (TaG1)	3,51E-32
RT112 (TaG2)	3,51E-60
KU19-19 (T3)	1,16E-241
JMSU1 (T4)	4,34E-48
T24 (G3)	1,09E-114
TCCSup (G3)	1,30E-99